FLOW STRUCTURE OF THE CIRCULAR WEDGE SHAPED JET

BY

MASUD AHMED SELIM

Thesis submitted to the Department of Mechanical Engineering
in partial fulfilment of the requirements of the degree of
Master of Science
in
Mechanical Engineering.

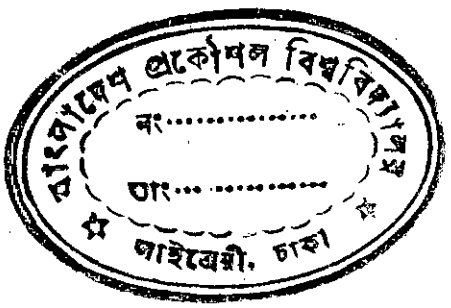

August , 1988.

BANGLADESH UNIVERSITY OF ENGINEERING AND TECHNOLOGY, DHAKA-1000
BANGLADESH.

FLOW STRUCTURE OF THE CIRCULAR WEDGE SHAPED JET

A Thesis

By

Masud Ahmed Selim

Approved as to style and content :

M. A. Taher Ali

Dr. M. A. Taher Ali
Professor,
Dept. of Mechanical Engg.,
BUET, Dhaka.

Chairman

Dr. Dipak Kanti Das
Professor & Head
Dept. of Mechanical Engg.,
BUET, Dhaka.

Member

mqalam.

Dr. Md. Quamrul Islam
Associate Professor
Dept. of Mechanical Engg.,
BUET, Dhaka.

Member

Dr. M. A. Hannan
Professor
Dept. of Water Resources Engg.,
BUET, Dhaka.

Member (External)

CERTIFICATE OF RESEARCH

This is to certify that the work presented in this thesis is the outcome of the investigation carried out by the candidate under the supervision of Dr. M. A. Taher Ali in the Department of Mechanical Engineering at Bangladesh University of Engineering & Technology, Dhaka.

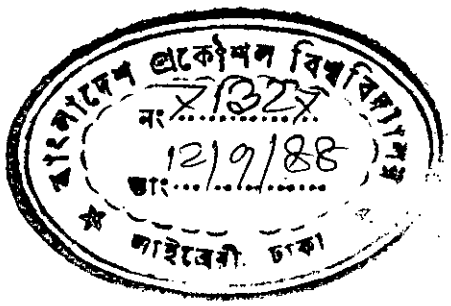

M. A. Taher Ali
Supervisor

M. A. Selim
Candidate

ABSTRACT

With a view to resolving some controversies regarding the turbulent mixing layer structure, the characteristic measures of axisymmetric free shear layer and asymmetric free shear layer were investigated. In the present work the effect of initial conditions on axisymmetric free shear layer was investigated. Here initial displacement thickness and Reynolds number were taken as characteristic identifiers of initial condition. Asymmetric free shear layer was investigated by using circular wedge shaped nozzle at different Reynolds number. The effect of changing Reynolds number at the exit has been studied and mean velocity and turbulence intensity of the three axes of circular wedge shaped jet and those of axisymmetric jets were compared. In this investigation 1/16 inch United sensor (U.S.A) pitot static tube along with Furnace Control (U.K) pressure transducer and Keithly(U.S.A) data logger were used for measuring mean velocities and constant temperature hot-wire (DISA 56C00 system) anemometer was applied for measuring turbulence intensities. Photographs of oscilloscope traces were also taken to analyse the pattern of change of turbulent intensities. In the present investigation of the different exit initial conditions of the jet flow, it was found that the thickness of initial boundary layer supressed the peak value of turbulence intensities and increased the spread rate of the jet. Self preservation characteristics of the axisymmetric jets are found to be independent of Reynolds number and initial boundary layer thickness. It was found that asymmetry in the jet flow in one axis had little effect on mean velocity in other axes but suppressed turbulence intensities in those axes. The flow asymmetry died out in down stream direction where core of the jet vanished.

ACKNOWLEDGEMENT

With deep sincerity, the author express his profound indebtedness to Professor M. A. Taher Ali for his guidance and invaluable suggestion in achieving every minute detail of this thesis.

The author is highly grateful to Professor Dipak Kanti Das, Head , Department of Mechanical Engineering for constant encouragement and providing all necessary assistance in various way at different stages of the work.

The author is also grateful to Dr. M. Quamrul Islam, Assoc. Professor, Dr. Sadrul Islam, Mr. M. A. Azim , Mr. A. K. Mesbah Uddin, Assistant Professor, Department of Mechanical Engineering and Mr. Imtiaz Kamal, Engr., Atomic Energy Commission for their suggestions and help.

Sincere thanks are offered to all Foreman, Instructors and technicians of Machine shop, Carpentry shop and Welding and Sheet-Metal shop for their cooperation and care in constraction of the experimental setup.

Thanks are also due to Lab. Assistants of Fluid Mechanics Laboratory for their cooperation in fabricating and assembling different components of the experimental setup.

The author thanks Mr. A. Jalil for typing the thesis and Mr. M. A. Salam for drawing the figures with care.

Finally "a thank you" to all of his colleagues in Mechanical Engineering Department and members of his family for their cooperation and inspiration during work.

TO MY MOTHER

CONTENTS

NOMENCLATURE

Symbol	Meaning
Latin Letters :-	
A	constant
B	shear layer width
A_1, B_1	constants of hot-wire calibration equation.
C, D, E	constants
G	constant
H	shape factor of velocity profile
I	heating current
J	momentum
K	constant
L	length of the hot-wire
L_b	length of the beam
P	pressure
Pr	Prandtl number
Q	heat transfer rate from hot-wire.
Re	Reynolds number
Rg	resistance of hot-wir at temperature t_g.
Ro	resistance of hot-wire at reference temp.
Rw	resistance of hot-wire at temperature t_w.
U	mean axial velocity
V	mean transverse velocity
X	co-ordinate axis direction
Y	co-ordinate axis direction
b	width of the jet

Symbol	Meaning
e	voltage drop in hot wire
f	function
k_f	thermal conductivity of gas
l	Prandtl mixing length
r	polar co-ordinate
s	substitution parameter
t	time and temperature
t_g	temperature of gas
t_w	temperature of hot-wire
u'	longitudinal component of rms of turbulence intensity
$\bar{u}$	average velocity
v	velocity in Y direction
w	velocity in Z direction
x	distance in x co-ordinate
x_o	virtual origin
y	distance in Y co-ordinate
z	polar co-ordinate

Greek letters :-

α	temperature coefficient of electric resistance of hot-wire and angle of divergence (App-B)
β	constant
δ	boundary layer thickness
δw	vorticity thickness
η	substitution parameter

Symbol	Meaning
θ	momentum thickness
ξ , λ	substitution parameter
ϵ	velocity factor
ν	kinematic viscosity
μ	absolute viscosity
ρ	density

Subscripts :-

e	exit
c	centre line
f	film
g	gas
m	maximum
max	maximum
o	origin
w	wall or hot-wire
b	beam

CHAPTER - I

INTRODUCTION

1.0 General :

A jet is created by the flow of fluid through an orifice or a nozzle into a stagnant reservoir or co-current stream of fluid. There are different types of jet viz. bounded jet, wall jet, free jet etc. In the case of bounded jet, the fluid discharges from a nozzle or an orifice in to a confined region bounded by solid surfaces; while in the case of wall jet fluid from an opening flows over the solid surfaces. Free jet is formed when the jet flows in an infinite fluid reservoir having no influence of solid surfaces. If a wedge shaped segment is cut off from a circular nozzle a wedge shaped jet is found and the flow fluid created by the flow issuing from a wedge shapped jet is a case of asymmetric three dimentional flow.

1.1 Free Turbulent Jet :

Free jets have many practical applications and researchers are working on it for many years. Jets may be laminar and turbulent. Turbulent jets out strip the laminar jets in respect of its occurrence in practice and have achieved much engineering importance in relation to noise, propulsion etc.

When an incompressible turbulent jet discharges into still air, the shear layer grows continuously. With the entrainment of ambient air surrounding the turbulence originates as instabilities in laminar flow when Reynolds number exeeds some critical value. Using flow visualization (Hussain [55]), it has been shown that these instabilites due to interaction of viscous terms and non-linear inertia terms in the equation of motion, generate waves. These waves starting from the nozzle out-let grow with unstable amplitude within two to three wave

lengths from the exit. These waves intern forms ring of vortex core which rolls down-stream. After one or two revolutions the vortices interact strongly with the waves behind and break down into turbulent eddies. The eddy structures in the shear layer is complicated. The characteristics behaviour of these eddies enables the researchers to divide the turbulent jets into three principal regions, viz. initial region, transition region and developed region. The initial region extends until the center line mean axial velocity changes and the transition region starts after the initial region. Further down-stream, these exists a developed region where the eddy structure become uniform.

1.1.1 Coherent-Structure :

The interactions (like vortex pairing) of turbulent eddies cause large scale vortical motions. Small scale vortical motions also evolve through break-down of large eddies. Many recent researchers concentrate their efforts and interests in finding the existence and role of large scale coherent structures (previously termed as large scale vortical motion) in turbulent shear flows. Although the occurence of large scale coherent structured in all turbulent shear flows has neither been confirmed nor universally accepted (Chandrasuda et al [12]). Inspite of extensive use of the term, there is no agreement among the researchers to what precisely meant by a 'coherent structure' (Hussain(20)). The term has different meaning to different researchers; no two of them even agree with each other. It is not likely that a defination could be agreed upon without loud protests. According to Hussain [20] a coherent structure is a turbulent fluid mass connected by a phase correlated vorticity. That is, underlying three dimentional, random vorticity fluctuation & characterising the turbulence,

there must be a coherent vorticity which is instantaneously correlated over the entire fluid mass. This fluid is singly-connected and the coherent vorticity must be instantaneously of the same sign in any plane ; thus a collection of vortices within with phase connected vorticity is not a " coherent structure ". These structures, characterized by coherent vortical (mass of) fluid have length scales of the order of the free shear layer width. The boundary layer is quit likely to have more than one kinds of coherent structures ('hair pins', typical edies , 'pocket' folds' stakes etc.) and as such of is not suprising that the understanding is not clear. These structure believed to play a dominant role in the entrainment ; mixing, noise generation and other transport phenomena.

1.1.2 Initial Condition and Stability :

When the Reynolds number is sufficiently high, the turbulent free shear layer can only be a function of the boundary and initial conditions which can affect the formation of the coherent structures (through the shear layer instability, saturation, and roll up) as well as their evolution and even successive interaction. The boundary conditions can also affect the coherent structure by feed back mechanisms (Dimotakis & Brwn [14], Hossain & Zaman [21]. The stability characteristics of free boundary layer are rather different from those flows with a solid wall. The main reason for the difference seems to lie in the existance of a point of inflexion of free boundary layers.

In the case of mixing layer the velocity profile in fully developed region take the self preserving from $U/U_m = f(y/(x-x_o))$ where origin of the co-ordinates is at the seperation point (the nozzle tip) and $x = x_o$ is the virtual origin of the flow, which depends on the initial conditions and therefore on the

Reynolds number. At the first sight one would expect that the virtual origin would be up-stream from the nozzle (by a few times thickness of the boundary layer $x = 0$, and this prediction of the mixing length theories of the development of mixing layer from a turbulent boundary layer, reviwed by Nash( ). When the initial boundary layer is laminar, shear stress in the transition where the velocity fluctuations can rise to double the value in the fully developed turbulent flow, the actual peak value depending strongly on the Reynolds number.

1.2 Motivation behind Problem Selection :

The isothermal incompressible, single phase free shear layer of a Newtonian fluid is probably the simplest practical turbulent shear flow and as such, has been the fertile ground for a number of investigations to understand the flow structure. The concept of asymptotic and local invariances suggests that the flow structure sufficiently down-stream from the origin should be universal. Accumulated data in the in compressible free shear layer, however, reveal wide spread discrepancy even in its characteristic integral measures, Champagne, Pao & Wygnoski [10], Hussain & Zaman [21], thus indicating the lack of understanding of even this simplest flow. The inherent complexity of the shear flow turbulence, and the need for additional careful measurements in this flow is thus needed most successive investigations continue to raise many more questions and subsequently their answers. The coherent structures are typically stonger (owing to larger gradient of velocity) in the near fields of free flows in the flow field. The near field being also relevent to the majority of technological applications including mixing and noise production. So the present study gives special attraction on the near fluid of jet.

From accumulated knowledge, there is a strong possibility that all the turbulent shear flows are characterised by large-scale coherent structure (Roshko [40], Townsend [47]. Recent researchers advances continue to suggest that the large scale structures and their interaction play a significant role in the transport of momentum, heat and mass and presumably, in noise production.

The special attention which the present study devote to turbulent boundary layer has two justifications, first most boundary layers occuring in the engineering practice and in nature are turbulent ; and secondly there is much more to say about relevant transport properties of turbulent flows there about those of Laminar ones.

Here three dimentional boundary layer is taken for study, three dimentional boundary layers are more common, in practice than two dimentional ones. Theories of the three dimentional boundary layer are still only embyonic and experemental works on free three dimentional boundary layer also few in numbers.

1.3 Scope of Application :

The findings about the mean flow characteristics within the jet is relevent to many problems of diffusion, discharge of pumps, mixing of burners air craft design, flame pattern fluid amplifier and driers. The diffusion phenomena in free jets is associated with flows in the exhaust of rocket engine, fluid injector of internal combustion engine and gas turbine combustion chamber, waste disposal plumes. Free jets in the exhausts of the rocket and jet engines create aerodynamic noise which in many cases objectionable and should be controlled.

As the transport of heat, mass and momentum and also presumably aerodynamic noise production in a shear layer depends on large such structure, so detial knowledge of these structure will show the path of way out from the problems of aerodynamic noise suppression.

Increased turbulence (characterized by Hill & Grene as " Super turbulence") and mixing can be obtained through excitation could be effectively utilized in application like V/STOL air crafts, ejectors, superession of air craft wave detectability, mixer, combustor, chemical lesers, fluidic devices etc. The results of the present study is appkicable to the incompressible flow case and also can be applied to the compressible flow cases as a first approximation.

1.4 Objective :

The above discussion suggests the need to gain clear knowledge about the flow characteristics in the free boundary layer fromed in free jet and the coherent structure in initial region of free jet. The objectives of the research program are set accordingly. The objectives of present study are as follows :

1. To measure the mean flow characteristics and longitudianl turbulence intensities the initials and transition region of the (circular and wedge shaped) unexited jet with untripped boundary layer.

   This part of investigation include determining the velocity (mean fluctuating intensity) profiles in the free shear layer at different down-stream axial position from the nozzle lip ($x/D = 0^+$, .25, .5, 1, 1.5, 2, 2.5, 3, 3.5, 4, 5, 6, 7), calculation of displacement and momentum thickness, investigation of jet spread by determining location of fixed U/U_m values, determing the location of virtual origin, and investigate centre line

velocity variation with variation of axial distance. The self preservation of the flow also checked. All these were done to predict the basic flow characteristic.

2. To measure the mean and specially the turbulence characteristics of the flow field with circular wedge shaped jet.

   This include the measurements mentioned in the previous objective . This also include measurement of centre line longitudinal amplitudes , investigate oscilloscope traces of center line u' - signal. This is directed at providing insight into coherent structures. Specially the vortex-pairing process in circular wedge shaped jet.

3. To compare the results of present study with related investigation results found by other reasearchers.

1.5 Research High Light :

The free jet was created by a circular jet facility, which was designed and manufactured by the author for this experiment. The circular air jet facility have a over all length of 8.1 cm with two settling chamber. The facility also provide the provision for controlled exitation. The flow was tested to be axisymmetric for the all circular jets by measurements of longitudianl mean and fluctuation intensity profiles at different axial locations, for four radial traverses 90° apart. So the characteristics for a particular radial direction were investigated for circular nozzles. For wedge shaped jet characteristics for the half domain were taken because of the three dimentional free boundary layer formation with plane of symmetry.

In the present study two circular nozzle and a wedge shaped nozzle were investigated. The profile of the nozzle follow the so called cubical one. The flow characteristic were investigated for all the nozzles for different Reynolds number with a view to corelates results with Reynolds number and also observe the influence of initial condition on flow characteristics of downstream (initial and transition region).

The experimental results also compared with the other researchers studies related to the problem under present study , and possible interpretations of experimental results were made to extend explanations of different characteristics of present flow field.

CHAPTER - II

LITERATURE REVIEW

The most studies so far have focused to know detail of flow structure on flow visualization, but little on quantative measurements. Flow visualization, which was extensively used in the early stages of the turbulence research decades ago and pused aside because of increasing emphasis on quantitative data. In the early stage of turbulence research there were no high friquency sensitives equipment to read correctly the turbulent quantity so early investigators devote themself fo use flow visualization technique. With the increasing availability of hot-wire anemometers recent researchers give emphasis on quantitative data. The earliest investigator of free jet include Anderson [1,2], Sato [42,43], Michalke [32], Hinze [17], Lamb [24].

Sato [44] studied experimentally the instability of two dimensional air jet (issuing from laminar channel flow). The response characteristics of laminar to the sinusoidal external disturbances are found to be in good agreement with theoretcal prediction of Lassen & Fox [26]. Sato also investigate the effect of excitation, effect of excitation becomes maximum, where the frequency of external excitation coincides with that of naturally excited sinusoidal velocity fluctuation in the laminar layer. No remarkable abrupt turbulent brusts are found in the transition region. The wave form of the velocity fluctuation changes gradually from sinusiodal to irregular patterns.

Hinze [17] measured the mean velocity and temperature variation in radial and axial direction in a turbulent jet issuing from round orifice into quieseent ambient air. The result showed that the rate of spreading of the heat and mass are mutually equal but grater than that of velocity. A constant

ratio between coefficient of transfer of heat or mass and the coefficient of shearing stress does not seem to exist. The results have been subjected to a theoretical analysis and found radial velocity distribution in central zone agrees with the theory based on a constant coefficient of shearing stress of the jet.

Michalke [32] developed a theory on the growth of small amplitude disturbance in a inviscid, laminar parallel flow with a hyperbolic tangent mean velocity profile agreed well with Freymuth's [15] data. Both Michalke and Freymuth has observed coaliseence of vortices, formed through instability and roll-up of initial shear layer. A velocity signal from region of vortex interaction is periodic and sub hermonic (of fundamental or initial roll-up) frequency. Experimental investigations of free boundary layers of plane and axisymmetric jets carried out by Sato [44], Schade & Michalke [45] and Michalke and Wille [33] had shown that for large Reynolds numbers the instability properties of free boundary layer are not noticeably affected by viscosity. Sato found that the measured growth rates were of the same order of magnitude as transformed theoretical ones, where the line dependent growth rate of disturbance were transformed linearly into a special growth rates by means of disturbance phase velocity.

Bradshw [6] did some experimental job on axisymmetry jet with a view to study the effect of initial condition on the development of flow field. From this investigation, it has been concluded that the distance between the seperation point and final approach to a fully developed turbulent mixing layer is found to be of the order of a thousand times the momentum thickness of the initial boundary layer, wheather the latter be laminar or turbulent. It was also reported that virtual origin shifts significantly with the change in Reynolds

number. The effect of Reynolds number on transition process also investigated by Wille [51] and Sato [42]. Chapman, Kuehn & Lerson [1958] give examples of the large effect of transition in free shear layer and the related subject of Reynolds number effect on bubble seperation was discussed by Tani [1964]. The shifting of virtual origin with Reynolds number reviewed by Nash [1962].

Kelly [22] analytically showed that a sub harmonic disturbance in a free shear layer with a periodic structure (linke a vortex train) can be reinforced by the structure itself as a result of its own (secondary) instability. Surprisingly, this result also follows directly from Lamb's [24] earlier analysis which showed that the most unstable mode for a raw of vortices was the one with a wave length twice the vortex spacing.

Wygnaski and Fiedler [52] studied the axismmetric turbulent incompressible and isothermal jet by linearized constant temperatur hot-wire anemometers. They reported that jet became truely self preserving some 70 diameter down stream of the nozzle. From this study it apears that Taylor's hypothesis is not applicable to this flow, but the corrected velocity of the appropriate scale for transformation from temporal to spetial quantitives appears appropriate. The energy balance was calculated from various measured quantities and the result was found quit different from the measurements of Sami [41] which were obtained twenty diameter down stream from the nozzle.

Townsend [47] did theoretical investigation on the nature and origin of the ' Universal ' structure of fully sheared turbulence as it appears in different flows, and entrainment mechanism that conforms to the wide range of entrainment rates prescribed by the structural similarity and energy blance. From this investigation, it was concluded that the relatively rapid entrainment

in a plane wave depends on active instability of the interface, not present in a constant pressure boundary layer whose flow rate of entrainment is form ' Passive' distortion of the boundary surface by eddies of the main turbulent motion. Observations made by Grant [16], Rose [39], Marechal [30] and by Tucker and Reynolds [49], to support Townsend's conclusion.

Crow and Champagne [13] investigate axisymmetric jet with tripped boundary layer inside the nozzle to isolate the large scale pattern at Reynolds number around 10^5. For the purpose of this investigation periodic surging controllable frequency and amplitude was imposed and flow visualization technique was also applied. From this study it was concluded that the preferred mode having a strouhal number of 0.3 is in some sense the most dispersive wave on a jet column, the wave least capable of generating a harmonic, and therefore the wave most capable of reaching a large amplitude before saturation.

Champagne et al [10] studied experimentally the two dimentional incompressible mixing layer. The measurements provided new information on the development of the mean and turbulent fields towards a self preserving state and on the higher order statistical characteristics of the turbulent field . Measurements of spectra, probability densities and moments to eights order of all three velocity-components fluctuations were also determined. The profile appears to be similar from x = 39.5 cm (x/H = 2.2) and about 8 cm (x/H = 5). The turbulence level of the nozzle exit was .1% . All measurements were made at a nozzle exit speed of 8 m/s. The growth rate was nearly the same as found by Patel [36], Liepmann & Laufer [27] and some what less than that in the corresponding flow reported by Wygneski & Fiedler [52]. The virtual origin was found.28 width down-stream from the exit which was nearly equal to the value found by Batt et al [4] and Batt [5]. The longitudinal fluctuating

intensity profile of Champagne's investigation was similar as found by Patel [36] and considerably higher in magnitude than that of Liepmann & Laufer [27].

Hussain & Zaman [19] experimentally studied the effects of initial condition on the characteristics measures of an axisymmetric free shear layer. The initial, boundary layer state (i.e. laminar or turbulent), momentum thickness, Reynolds number $R_{\theta e}$, and longitudinal turbulence intensity u'_{pe}/U had been taken as three characteristic identifiers of initial condition. It was found that the spread rate, similarity parameter, peak turbulent intensity in the self-preserving region are essentially independent of $R_{\theta e}$, but depend on wheather the initial boundary layer is laminar or tripped (turbulent). Initially tripped shear layers manifest two stages of linear growth. The virtual origin was as well as the distance required for attainment of self-preservation depend noticeably and systematically on $R_{\theta e}$. The mean velocity and turbulent intensity profiles appear to reach self similarity together, when the initial boundary layer is laminar, but not when the initial boundary layer is turbulent.

Zaman and Hussain [55] evaluated applicability of Taylor hypothesis to large scale coherent structures in turbulent shear flows, by comparing actual spatial distributions of the structure profiles with those deduced through the use of hypothesis. Hypothesis works quite well for isolated coherent structure if a constant convection velocity equal to the structure centre velocity, is used in the hypothesis every where across the shear flow. When structure interaction like vortex pairing are involved no convection velocity can be found with which the hypothesis works. Champagene [11] obtained an analytical solution for the true spectrum, but found that the measured spectrum near

Kolmogrove's frequency can exceed the true spectrum by 238% . Taylor's hypothesis has also been found to produce large distortions in the spectra of lateral velocity and scaler functions (Wyngaard & Clifford [53], and probability density functions of velocity and temperature derivations (Antonia, Chambers & Phan-Thien [3]).

Zaman and Hussain made [57] an attempt to explain the mechanism of turbulence suppression previously observed in jets under controlled excitation, near field of jet with laminar flux boundary layers, had been explored through hot-wire measurements. Turbulent intensities reduction by as much as 80% was observed, the maximum decrease occuring at about 400 θe down-stream from the exit ; θe is the initial momentum thickness. Maximum supression effect was found at strouhal number Stθ (= f θe/Ue) of about 0.017, the turbulence suppression was observed over the range $0.75 < x/D < 8$. Some other investigator also reports suppression of turbulence intensities and noise . Vlasoy & Ginevskiy [50] observed suppression of the turbulence intensities in a circular air jet when excited at StD of 2.75 (StD = f^D /Ue). Peter et al [37] observed turbulence suppression at x/D = 4 for StD 3.0 and ReD = 5.2×10^4. Moore [34] has observed a small reduction fore-field broad-band noise level in circular jets with laminar and turbulent exit boundary layers, for excitation at StD = 1.5 and for Mach number upto 0.70.

Hussain and Zaman [21] experimentally investigate to the "preferred mode" of an incompressible axisymmetric free jet through controlled perturbation, and spatial distributions of time average as well as phase average flow properties in the near field of jet. The changes in the time and phase average quantity were found less dramatic than those for the excitation produce stable vortex pairing from the experiment. The shape and size of structures found by Hossain

and Zaman agree closely with those inferred from the average streamline pattern of the natural structure educed by Yule [54]. Hossain & Zaman data as well as u' spectra show that even excitation at the prefered mode can not sustain the initially organized large scale coherent structure beyond eight diameter downstream from the jet exit. Mumford [35] investigate the fully developed region of a plane turbulent jet. The results indicate that the large eddies in the fully turbulent region of the flow are roller-like structure, with axis alined approximately either with the mean-velocity gradient or with the direction of homogenity. It was found that these basic structure, tended to occur in various preferred combination.

Zaman and Hossain [58] tried experimentally to optimize the conditional sampling technique for education of naturally occuring large-scale structures in an axisymmetric mixing layer, comparison of natural structure with that induced via controlled excitation, and the sensitivity of the educed structure to the exci tation amplitude and of the natural coherent structure to Reynolds number and initial condition. It was observed that the simple criterion of triggering on the positive peaks of the longitudinal velocity signal derived from the high speed edge of the mixing layer results in the optimum eduction. The characteristics of the natural structures, educed by the optimum detection criterion, are found to be optimum detection criterion,are found to be independent of ReD over the measurement range $5.5 \times 10^4 - 8 \times 10^5$. A mild dependence on the initial condition (viz. laminar vs. turbulent) is observed.

CHAPTER - III

THEORY

3.1 General :

The basic equations of free layer parameters and principle of measurements of mean and fluctuating quantities are presented in this chapter. Location of virtual origin of free jet is also discussed.

3.2 Free Shear Layer Parameters :

Turbulent flows will be turmed free if they are not confined by solid walls.

A jet boundary occurs between two streams which move at different speeds in the same direction. Such a surface of discontinutity in the velocity of flow is unstable and gives rise to a zone of turbulent mixing downstream of the point, where the two stream first meet. The width of the mixing region increases in a down stream direction, Fig. 3.2.1.

A free jet is formed when a fluid is discharged from a nozzle or orifices Fig. 3.2.2. It is found that the jet becomes completely turbulent at a short distance down-stream from the point of discharge even when the exit velocity is very small. Owing to turbulence, the emarging jet becomes partly mixed with the surrounding fluid at rest. Particles of fluid from the surroundings are carried away by the jet so that the mass flow increases in the down-stream direction. Concurrently the jet spreads out and its velocity decreases, but the total momentum remain constant.

It is usually assumed that the mixing length is proportional to the width of the jet, b, because this way useful results can be obtained.

Hence,

$$\frac{1}{b} = \beta \text{ (constant)} \qquad (3.2.1)$$

In addition the following rule has withstood the test of time : The rate of increase of the width, 'b' of the mixing zone with time is proportional to the transverse velocity 'u' .

$$\frac{D_b}{D_t} \sim v'$$

where, $$\frac{D}{D_t} = u \frac{\partial}{\partial x} + v \frac{\partial}{\partial y} \qquad (3.2.2)$$

From Prandtl's mixing length hypothesis

$$v' \sim l \frac{\partial u}{\partial y}$$

Therefore, $$\frac{D_b}{D_t} \sim l \frac{\partial u}{\partial y} \qquad (3.2.3)$$

Further, the mean value of $\partial u / \partial y$ taken over the half the width of jet may be assumed to be approximately proportional to u_{max}/b.

Consequently,

$$\frac{D_b}{D_t} = \text{const} * \frac{1}{b} * u_{max} = \text{const.} * u_{max} \qquad (3.2.4)$$

The rate at which the free mixing zone increases is proportional to down-stream distance, x.

Therefore,

$$\frac{D_b}{D_t} \sim u_{max} \frac{db}{dx} \qquad (3.2.5)$$

Comparing eqn. - (3.2.3) & (3.2.4) it can be obtained that

$$\frac{db}{dx} = \text{const.} * \frac{1}{b} = \text{const} \qquad (3.2.6)$$

$$b = \text{const.} * x$$

Which means that the width of the mixing zone associated with a free jet boundary is proportional to the distance from the point where the two jets meet. The constant of integration which must strictly speaking in the above equations can be made vanish by a suitable origin of coordinate system. This is the so called virtual origin which can also be found from stream-wise evolution of momentum thickness.

For circular jet, u_{max} denoting the centre line velocity. Thus for this case also

$$b = \text{cont} * x \qquad (*)$$

The relation between u_{max} and x can be obtained from momentum equation. Since pressure remain constant for free shear layer, so the integral of x component of momentum taken over the whole cross-sectional area remain constant and independent of x, i.e.

$$J = \rho \int U^2 \, dA = \text{const.} \qquad (3.2.7)$$

In case of circular jet the momentum is $J = \text{const} * \rho \, u_{max}^2 \, b^2$ (3.2.8)

and hence $u_{max} = \text{const.} \times \frac{1}{b} \sqrt{\frac{J}{\rho}}$ In view of eqn. 3.2.6,

$$u_{max} = \text{const} * \frac{1}{x} \sqrt{\frac{J}{\rho}} \qquad (3.2.9)$$

In the self preserving region of the free jet the shear layer width(B), momentum thickness (θ) and vorticity thickness (δ_w) increases linearly with x so that each can be represented as

$$f = C_1 (x - x_o) \qquad (3.2.10)$$

where x_o is the location of virtual origin. since the flow dynamics at any x in the self-preserving region should depend only on x, it is clear that B, θ, δ_w all should have the same virtual origin.

The shear layer width $B = (Y_{0.95} - Y_{0.10})$ (3.2.11)

where, $Y_{.95}$ and $Y_{.10}$ is the transverse locations

where, U/U_e is 0.95 and 0.10 respectively.

The displacement thickness δ of the boundary layer is the distance the actual boundary layer would have to be displaced in order that the actual flow rate would be the same as that of the core flow passed the displaced boundary.

Accordingly,

$$U_m \delta = \int_0^\infty (U_m - U) \, dy$$

$$\delta = \int_0^\infty (1 - U/U_m) \, dy \qquad (3.2.12)$$

where, U_m is the maximum velocity (i.e. the core value of U)

The momentum thickness of the free boundary layer is the distance from the actual boundary such that the momentum flux through the actual boundary layer,

$$(\rho \theta U_m) U_m = \int_0^\infty \rho (U_m - U) U \, dy$$

The momentum thickness,

$$\theta = \int_0^\infty (U/U_m)(1 - U/U_m) \, dy \qquad (3.2.13)$$

The distance $Y' = \frac{1}{2} D - Y$. Local momentum thickness of the shear layer,

$$\theta_{.1} = \int_0^{y_1} (U/U_m)(1 - U/U_m) \, dy \qquad (3.2.14)$$

$Y_{.5}$ is called the half thickness which is the transverse location where $U/U_m = 0.5$,

The ratio of the displacement thickness and momentum thickness gives the shape factor of the boundary layer.

$$H = \frac{\delta}{\theta} \qquad (3.2.16)$$

3.3 Method of Measureing Turbulence :

During the experimental investigations of fluid flow a great number of methods are used by the investigators. Most of these method and instruments have been developed and are used for measuring the mean velocities in fluid flows.

The main difficulty in measuring turbulence is caused by the fact that turbulence is a random three dimensional fluctuating flow. Moreover high frequencies of fluctuations occuring in turbulent flows make it very difficult for a measuring instrument to record all the quantities free of distortion.

In measuring turbulent flows distinction is to be made between measurement of mean flow and measurement of turbulence. The problem connected with these two typed of measurement are to certain extent related, the requirements to measure them are different. For instance a measurement of mean velocity is more or less affected by the turbulence present in the flow, and it is necessary to know that correction must be made in the reading of measuring instrument, but in measuring the turbulence itself any influence of the mean velocity that produces an error in the turbulence can not be tolerated.

Various methods and techniques which are used in turbulence measurement can be divided into two groups.

In the first group, use is made of a tracer or other indicator which is introduced in the flow field to make the flow pattern visible or observable by a suitable detecting apparatus outside the field of flow. Due to very rapid

change with respect to time an place, this method is not suitable for the measurement of turbulence.

In second group a detecting element is introduced into the flowing fluid and the turbulence is measured by the change in mechanical physical or chemical nature that occur in this element.

Accordingly, the normal pitot tube which is employed so successfully in measurement mean flow, is completely ruled out for measuring turbulence, mainly because of excessive inertia. The hot-wire anemometer does not have these draw backs. Its application in the measurement of turbulent flow has been universal.

3.4 Basic principles of hor-wire Anemometer:

The hot-wire anemometer is a instrument used for measuring instantaneous velocities in a fluid stream by instantaneous cooling effect on a very thin, electrically heated wire filament.

A hot-wire probe has at its working end a thin wire (typically about 1-1.5 mm long and 1-5 μ m diameter). Through which an electric heating current is passed. The voltage across the hot-wire may be amplifited and presented on a monitor. This voltage depends on the electrical resistance of the hot-wire, which depends on its temperature, in turn, its temperature depends on the cooling effect of the air stream. Because of small wire diameter, the instrument is able to response very rapidly to fluctuations in air velocity. For steady thermal equilibrium conditions, the rate of heat loss by the hot-wire in the fluid stream must be equal to the heat generation rate by the electrical current passing through the wire, whcih is given by

$$Q = I^2 R_w \qquad (3.4.1)$$

I, being the heating current and R_w the total electric resistance of the wire. Thus with the air of Kramer's correlation,

$$I^2 R_w = e\pi K_f L(t_w - t_g) \left[0.42(Pr_r)_f^{0.20} + 0.57 (Pr)_f^{0.33} (Re)_f^{0.50}\right] \quad (3.4.2)$$

where e is a suitable conversion factor.

The temperature dependence of hot-wire resistance may be expressed as

$$R_w = R_o \left[1 + \alpha (t_w - t_g)\right] \quad (3.4.3)$$

where R_o is the wire resistance at a reference temperature to and α is the temperature coefficient of the electric resistivity of the wire.

Substituting the value of $(t_w - t_g)$ from equation (3.4.3) into equation (3.4.2)

$$I^2 R_w = \frac{e \pi K_f L_{fL}}{\alpha} \cdot \frac{R_w - R_g}{R_o} \left[0.42 (Pr)_f^{0.20} + 0.57 (Pr)_f^{0.33} (Re)_f^{0.50}\right] \quad (3.4.4)$$

which can be reduced to the form

$$I^2 = \left(\frac{R_w - R_g}{R_w}\right) \left[A_1 + B_1 \sqrt{U}\right] \quad (3.4.5)$$

where $A_1 = 0.42 \cdot \frac{\pi K_f L_{fL}}{\alpha R_o} (Pr)_f^{0.20}$ (3.4.6)

and $B_1 = 0.57 \frac{\pi K_f L_{fL}}{\alpha R_o} (Pr)_f^{0.33} \left(\frac{\rho_f d}{U_f}\right)^{0.5}$ (3.4.7)

and A_1 and B_1 are essentially constant. Equation (3.4.5) is the fundamental and most useful equation in hot-wire anemometry.

Two types of electric circuitry " constant current" (Fig. 3.4.2) and " constant temperature" (Fig. 3.4.1) have been used with hot-wire instruments. In constant current system, the hating current is kept constant (usually by placing a very large fixed resistor in series with the hot-wire) and voltage across the hot-wire is examined. In these system the response of the hot-wire to a velocity fluctuation is modified by its own internal heat capacity, which becomes important for fluctuation frequencies above about fifty cycles per second. It is therefore necessary in the constant current type of instrument, where examining velocity fluctuations, to include a compensating circuit in the amplifier which automatically corrects for this internal heat capacity. The appropriate setting of the compensation circuit depend on the operating conditions of the hot-wire and is usually found by what is called a " square wave " calibration circuit. The method depends on the well-establish fact that when a small square-wave current is superposed on the steady heating current of the hot-wire, the amplifier output as seen on a oscilloscope will reproduce this sqwuare-wave pattern only when the compensation control is correctly suit. A useful frequency range of 100,000 cps or more can be achieved in the constant current system. In the constant temperature type of instrument, a feedback circuit maintains constant the resistance and so the temperature of the hot-wire. The energy input to the hot-wire must then go entirely into the air stream, the internal capacity of the hot-wire is no longer of important, because its temperature is constant, and consequently this energy input (proportional to the square of the current) is measure of the instanteneous air velocity. In past the design of feed back system faces serious problem to attain high frequency to match the performance of the best constant current system at excessively high frequency operation. But modern technique of electronics solve the problems of feed back system of constant temperature system.

3.5 Principles of plug in Units of DISA constant current hot-wire Anemometer (CTA 56C00 system) :

3.5.1 Linearizer 56 N21 :

The voltage signal from bridge come to linearizer 56 N21. It linearizes the non-linear output signal, from the 56 C01 CTA hot-wire bridge before these are transmitted to other units. As shown in fig. 3.5.1 the incoming signal in subjected to amplification and as subtraction by the OFSET voltage. Here by the input signal 'V' is transformed to normalized signal x. When the velocity varies from 0 to U_{max}, the input signal V changes from V_o to V_{max}, and its corresponds value of x from 0 to 10 v. The rest of the block diagram show the very linearizing circuit implements the methematical expression

$$Y = 10^{A + Bx + Ey + Cx - D}$$

where A, B, C, D and E are constant and Y is the linearizer output. Normally the constant are selected to give Y = 10 v for x = 10 v and give optimum linarity over the chosen range of velocites.

3.5.2 Signal Conditioner (Model 56 N20) :

The linearized output of linearizer was then feed into the next plug in module 56 N20 signal conditioner, which can seperate the AC : part of the signal and amplify and filter AC signals within presented frequecny band. The simplified block diagram (Fig. 3.5.1) shows the construction of 56 N20 signal conditioner.

3.5.3 Digitizer (Model 56 N01) :

Conditioned analog signals from the SIGNAL CONDITIONER the through digitizer before finally reach the RMS UNIT. The 56 N01 DIGITIZER converts analog signal into digital signals. The very fast analog to digital conversion

ratio is obtained (1 Mega sample per second) by using the digitizing technique designated Random signal processing. Where the input voltage level is compared with the signal designated pesendo Random Noise (VPRN) at a sampling rate of 10^6 sample per second. The VPRN signal is a 1 M HZ sample an hold analog signal with a rectangular frequency distribution between minor full scale and plan full scale.

Unipolar representation

$$O\,v < V_{PRN} < +\ 10.24\ v \qquad P('1') = \frac{V_{input}}{10.24}$$

Functional action of RMS unit is shown in the simplified diagram Fig.(3.5.4).

3.5.4 Mean value unit (Model 56 N22) :

The signal is rated to the lp filter with a selectable cut-off freq. of either 6 Hz to 6 Hz. The low cut-off frequency (0.6 Hz) is applied for extra attenuation of any super imposed AC signal to avoid fluctuation in the DC measurement.

The input voltage is digitized into 20 Hz. impulse signal with control amplitude and a pulse width to the input signals. Dynamically the A/PW converter operates as a 20 Hz sampling-rate device. The sampling signal to the mean value of the filtered input signal over 50 m sec.

In the subsequency Gate circuit the pluses with a frequency of 5.12 M Hz. are turned on and off. The resulting frequency is driectly proportional to be instantaneous valve of the filtered input voltage.

The input signal can therefore be integrated by counting at this frequency (5.12 M Hz) through out the integration period and divide the result by the duty cycle of the integration (Fig. 3.5.5).

CHAPTER - IV

EXPERIMENTAL SET UP AND MEASUREMENT PROCEDURE

4.1 The Flow System : The Circular air Jet facility :

The experiment was carried out in a air jet facility (Fig. 4.1) plate 4.1.1)which was designed and fabricated for this experiment and other experiments on jets. The experimental set up consists of two settling chambers, fan unit, flow controller diffusers and flow nozzle. The overall length of the set up is 8.1 meters. Two 19 inch diameter woods aerofoil Fans, Model 19J6, were used for the supply of air in the jet. The fans are capable of supplying 1600 CFM against 1.7 inch of water gauge height.

Air enters to the fan unit through the butterfly valve (plate 4.1.2) which controls the air flow. The damp out the transmission of any possible vibrations from the fan unit to the down stream side of the test set up, the fan unit is seperated from the rest of the set up by a below (fig. 4.1.2) made of canvas and steel rings. A silencer (plate 4.1.3) was fitted at the discharge of the fan. The silencer was used to reduce noise generated at the fan discharge. Flow from the silencer enters to the first settling chamber through a diffuser. In this chamber there is a flow straightner and a wire screen net of 30 mesh to straighten the flow as well as to break down large eddies generated at the fan discharge. In this chamber a 100 watt speaker was fitted. This speaker may be used to exite the flow at desired frequency with the help of a suitable frequency generator and a maching amplifier. Air from this settling chamber flows to the second settling chamber through a 15.25 cm (6 inch) nozzle and the second diffuser. The second settling chamber with the diffuser is 2.9 meter long. In this settling chamber a flow straightner made of 1 inch PVC pipe and five wire screens of meshes 30 and 50 were used before entering

the flow to the discharge nozzle. These were used for ensuring axial flow free of large eddies which may be generated in the upstream side of the flow. In this set up two settling chambers were used to get the organ pipe effect to carryout the experiments on exite flow. In the case of flow exitation first one would act as the source and the second one as the wave carrier. The whole set up was mounted on rigid frames made of M.S. pipes and sheets, and these frames were securely fixed with the ground so that any possible unwanted vibrations of the system were reduced to a minimum.

In the experiment three nozzle of thesame profile and the same exit diameter (7.62 cm(3"))but with different exit conditions were used. Nozzles may be named as normal neck nozzle (NN Nozzle) Long neck nozzle (LN Nozzle) and wedge shaped nozzle (WS Nozzle)(Fig. 4.1.3). Main purposes were both verification of the present measurement technique as well as study of the flow characteristics for different nozzle exit conditions.

The design and fabrication details of silencer, diffusers and nozzles are given in appendices A, B and C.

4.2 Coordinate and dimension of the flow system :

In the present investigation nozzle exit centre was chosen as the origin. The centre line of the nozzle in the direction of the flow was taken as the positive X-axis and radial distance pointingupwards as positive Y-axis and the remaining axis 90° clockwise from positive Y-axis as the positive Z-axis. The above system is shown in figures 4.2.1 and 4.2.2.

In presenting measurements points all distances are nondimensionalized by the nozzle exit diameter. D, displacement thickness δ_e and momentum thickness θ. While the mean and turbulence intensities are nondiamensionalized by nozzles

exit velocity U_e and local centreline velocity U_c . These have been done to suit the requirements of flow characteristics and for camparison with the similar experimental results performed by previous researchers.

4.3 Calibration Rig :

The calibration rig was a low turbulence round jet issuing from a 31 mm nozzle. The flow was produced by a centrifugal blower run by an one hp d.c. motor whose speed could be varied from 0 - 1450 rpm by varying its supply voltage. The blower discharged air into a 10.16 cm (6 inch) diameter P.V.C. pipe of 2.44 meter (8') length through a butterfly valve. So the flow through the nozzle could be varied both by controlling the speed of the motor as well as by controlling the butterfly valve. To ensure the flow direction and to break up any possible big eddies a flow straigtner and a pair of screen of 60 mesh were placed before the exit nozzle. A cylindrical filter was fitted at the suction side of the blower to get dust free air at the nozzle delivery. This would remove any possible wire drift during calibration process of the hot-wire. The core of the jet offered the desired flow field for calibration of both the hot-wire and the transducer. The veloicity of the calibration jet could be varied from 0.5 m/sec to 60 m/sec. which covered well the requred range of the experiment. The calibration rig was placed just below the jet flow facility (fig. 4.1.1) to facilitate the calibration as when requred.

4.4 Experimental Program :

The experimental program compraised of measurements of mean velocity and longitudinal turbulence intensity of free turbulent jet. For the purpose of compriison and prior test of the jet flow facility, mean axial velocity at different axial positions, down stream from the exit were taken for two circular nozzles, one with

conventional cubical converging profile . (Fig. 1a) and other with extention of constant exit area of the previous nozzle (Fig. 1b) were taken with special attention to the presence of the free shear layer.)

After proper comparison of data yielded from the preliminary test the circular nozzle with long neck was converted to circular wedge shapped jet by cutting off a 45° wedge shapped segment from it. The mean axial velocities and longitudinal turbulent quantities were measured for the circular wedge shapped jet at various downstream positions. for wedge shapped jet measurement covers the half domain in the y-z plane for each station. The extent of measurement was with in the initial and developing zone of the jet. The whole set of experiments was performed for three different Reynolds numbers.

Mean velocities were sensed by a pitot static tube and also with the help of single wire normal hot-wire probes placed normal to the direction of flow . Measurements of fluctuating components were obtained with the help of normal single hot-wire probes. All the measurements, were recorded by appropriate recording instruments. The raw datas obtained were processed by computer (main frame). The results obtained were compared with finding of other investigators related to present investigations.

4.5 Traversing Mechanism and Probe Setting :

The pitot static tubes and the hot-wire probe traversed in the air stream with the help of a Mitutoyo (Japan) coordinate measuring machine (Type CX 652) with ranges X coordinate 24 inch, Y coordinate 20 inch and Z coordinate 10 inch (plate 4.5.1). The probe traverses were made through the action of wheel through rack and pinion arrangement in each axis. A position can be fixed with resolutions of .0005 inch with the help of the whell. The traversing

mechanism was placed over a rigid table with its X-axis parallel to axis of the nozzle . The alignment of both the axes was secured with the help of plumbob and cathetometer.

In order to prevent undue vibration of the sensing probe, the pitot-static tube was supported by a stepped almunium rod of diameter 3/8 in.as shown in Fig. 4.5.1. The pitot tube was placed inside a groove cut through out the length of the aluminium rod and fastening the tube with the rod. The rod was rigidly fixed to the holder, which was again fixed with travesingmechanism. The sensing probe was kept 3 inches beyond the end of the smaller diameter of the rod to avoid any major disturbance initiated from the probe support. The hot-wire probe was fitted with a DISA probe holder tube, which gave of enough rigidity against any vibration.

Great care was taken to set the probes as correctly as possible with respect to flow direction and centre line of nozzle. The base of coordinate measuring machine was kept parallel to the centre line of the circular jet facility and horizontal with the help of high precision level , plumbob and cathetometer. The alignment of coordinate measuring machine was necessary to ensure correct axial and cross movement of probes.

4.6 Test of Symmetry of Circular Air Jet Facility :

In order to check the axisymmetry of the nozzle flow facility, the axial mean velocity measurements were taken at three axial locations, namely $x/D = 0^+$, 1 and 2. For each location four sets of data were taken for four radial traverses 90° apart. Longitudinal fluctuating intensity measurements were also taken in the same way. Ploting the data of axial mean velocity and longitudinal fluctuating intensities it was found that longitudinal mean and fluctuating intensities profiles from four radial traverses 90° apart, were found to be congruent

with in experimental errors, for each three axial locations. The same procedure was followed for both the NN & LN nozzle fitted with the flow facility. The turbulent fluctuating intensity level at centre line was found to be .07% which is quite satisfactory comparing with data of (Ref. 48).

4.7 Measurement of Mean and Turbulent Quantities :

The mean velocities were measured by united sensor (USA) pitot-static tube of 1.6 mm O.D. with a Furnace Controls Ltd. (UK) pressure transducer (Model MDC FC001) and Keithly (USA) digital microvoltmeter with data logging system (Model 2426) to get the ultimate signal. Mean velocities also measured by hot-wire anemometer DISA 56C00 CTA system.

Turbulent quantities were measured by employing constant temperature hot-wire technique. The DISA 56C00 CTA system was used with the plug in modules viz. CTA Bridge 56C16, LINEARIZER 56N21, SIGNAL COND. 56N20 , DIGITIZER Type 56N01 and RMS Unit Type 56N10 shown in fig. 4.7.1 and plate 4.7.1.

4.7.1 Measurement of Mean Quantities :

The mean quantities i.e. the mean velocities at different locations of the flow field were measured by pitot static tube and the readings found by pitot static tube also checked by Mean Value Unit reading (linearized) of DISA 56C00 CTA system (fig. 4.7.2 a & b). A comparison of two measurement methods for jet centre line velocity is shown in fig. 4.7.3. Readings of both the methods are found to be within 5% which is acceptable within experimental uncertainity. The head of the pitot static tube was hemispherical to avoid seperation on the static hole. According to Huston [22] it can give accurate signal within ± 10° deviation with the direction of flow. Due to small tip height of the pitot static

tube used in the measurements, Mc Millan correction factor for the effective displacement of the pitot static tube centre towards the region of higher velocity was negligible and so it was not considered. The signals of the pitot static tube were transmitted to pressure transducer through a 1.4 mm bore flexible PVC tube. The signal of the digital micro voltmeter corresponds to the velocity head of the pitot static tube.

The expression of the velocity for pitot static tube

$$U = \frac{2}{\rho}(P_o - P)$$

where P, P_o are the static and stangnation pressure respectively. The output voltages of the transducer for different ranges of scale were calibrated in the calibration rig with micromanometer before starting of the experiment. The output voltage was found to vary linearly with the pressure. For the measurement of all signals with microvoltmeter, an intregration time of 3 secs was used.

4.7.2 Measurement of Turbulent Quantity :

In the present investigation longitudinal turbulence quantites were measured by constant temperature anemometer DISA model 56C01 along with the general purpose Bridge DISA 56C16 using 5 diameter platinum wire as the flow sensing element. DISA normal probe Model 55P11 was used in the measurement. A signal conditioner DISA 56N20 and a Linearizer 56N21 were also used to filter and modify the output signals of the hot-wire bridge while DISA Mean value Unit Model 56N22 and DISA RMS Unit Model 56N10 were also used for the measurement of mean and turbulent quantities respectively. During the hot-wire measurement the signals were constantly observed on the oscilloscope's screen and changes of flow turbulence character was attempted to identify by analysing the photographs of the screen.

Before taking the measurement with the hot-wire it was calibrated in the calibration rig. During the calibration the bridge was set at desired resistance ratio to get maximum sencitivity for the experimental velocity range. The mean value output was recorded for different velocities and different transfer constant of the LINEARIZER was set to get the best possiblelinear output for the said velocity range.

4.8 Recording of Oscillograms of Turbulence Signals :

As illustrated above in article 4.7.2 a oscilloscope was connected at the output of the signal conditioner (Fig. 4.7.1) for continuous observation of the turbulence signals. The very nature of the oscilloscope traces such as frequencies wave forms and amplitudes continuously gave the qualitative indications of the hot-wire probe signal. To record the turbulence behaviour, oscilloscope traces were photographs directly from the oscilloscope screen. The photographic arrangement is shown in figure 4.8.1. A sheet metal cone was made for the purpse to avoid external light. The inside surface of the cone was painted black to avoid any reflection. One end of the cone was fitted with the oscilloscope screen and the other end with the camera lense. In this system Patrica LB (E. Geramn) detachable single lense reflex camera was used. To facilitate the close distance photography a extension tube of proper length was fitted with the camera. In the photography high speed film (ASA 400) with 1/30 sec. shutter speed was used. This type of photographic record would have been much better with a storage oscilloscope. In the present system sometimes overlapping of two traces or a part of the traces recorded in the film. So for clear representation of turbulence behaviours the photographs of signals marked by the brighter lines were traced in tracing paper and were presented in this thesis (figures 5.4, 33 - 35).

4.8 Error Analysis :

In this section a brief account of error and uncertainties associated with different stages of measurements are given the errors that creptinto the analysis are also discussed. The uncertainity were introduced in the system of measurements during calibration of sensing elements and were later cumulated to those during the final measurements.

The error in the fixation of centreline distance was critical when the spread rate and virtual origin were calculated. As indicate in section 4.5, the sensing probes could be placed in the flow field with an uncertainty of ± .00063 cm (± . 00025 inch). This could result error of upto 0.50% inmean velocity measurements within the free shear layer. The probe was placed in the centreline of the nozzle (i.e. X axis) and alinged its axial traversing with X axis with great accuracy by using cathetometer plambob and high accuracy level. However ,the initial error in alining the probe with centre line had relative and cumulative effects on the subsequent distance measurements.

During experimental measurements, exit velocity of the nozzle varied for a particular valve setting due to the variation of fan speed for transient motor core resistance characteristics and changes in atmospheric conditions. To minimize the first effect, the fan was kept running for half hour before taking actual measurements.The exit velocity of the jet was monitored intermitently by recording the velocity head at the reference station in the flow field. The velocity head found to vary within. 1mm of water in one experimental run and flow reproducibility between different runs was also maintain within the same range. In all measurements, the maximum transducer error was .75% of the measured value. This is smaller than experimental scatter which can be seen in the plots of mean velocity profiles.

In measurements of turbulent quantities, the possible sources of error were related to probe setting, level of turbulence, environmental condition etc. The misalignment of the probe wire with respect to the flow direction was with in± 3°. Also for the same alignment of the wire, the response to the turbulence property would vary due to the variation in the flow field. For example, flow direction other than the true axial one would cause to record a longitudianl turbulence quantity different from the desgnated one. The secondary flow due to entrainment caused such deviation of the measurement of longitudinal turbulence intensity. However this effect would be only secondary compared to those of the external error sources mentioned in the measurement of turbulence. To minimize error inmeasurements of turbulence due to change in environmental change the air conditioner unit was kept running at least one hour before starting actual measurement, so that within that time the temperature and humidity came to a steady state condition.

CHAPTER - V

RESULTS AND DISCUSSIONS

5.1 General :

In this investigation turbulent jet flow of three nozzles were studied. Experimental results of these nozzles are presented, compared and discussed in this chapter. By analysing the physical behaviour of different curves, the influence of different flow parameters on the flow field was attemted to ascertain.

In the present experimental programme the jet behaviour was studied only changing the single boundary condition at the exit. All the three nozzles had the same inlet conditions and the same profile and surface finish. Firstly exit boundary condition was changed from the normal nozzle (NN nozzle) by increasing the length of exit neck (LN nozzle) thereby increasing the exit boundary layer thickness. Secondly that was changed by removing a wedge shaped portion from the LN nozzle thereby creating a case of asymmetric jet (circular wedge shaped jet). In all the above three case i.e. NN nozzle. LN nozzle and WS nozzle flow field was studied for three different Reynolds number viz. 4.5×10^4, 5.4×10^4 and 6.1×10^4. Reynolds number was based on nozzle exit diameter 'D' and nozzle exit centre line velocity Ue.

In this chapter results are presented in three sub-sections one for NN nozzle, one for LN nozzle and one for WS nozzle flow. Along with presentation results are compared with each other and with similar works of other authors to establish the physical controlling parameters influencing the flow.

Centre line variation of mean velocity profile is presented in fig. 5.2.3. The centre line mean velocity remain constant upto x/D = 3.0, 3.5 and 3.8 for Reynolds number 2.78×10^4 , 4.5×10^4 and 5.4×10^4 respectively. From this behaviour it can be said that the potential core extends in the down stream direction with the increase of Reynolds number. In the figure profile of mean velocity shows to decrease in the same rate of Zaman and Hussain [55]. The decrease rate of centre line velocity of Crow and Champagne [15] with tripped boundary layer is found to be lower than present finding. The higher decay rate of U_c/U_e at lower Re was observed in the figure. This v ariable variation in decay rate was also observed by Hill et al [16a] and Hussain and Clark [20].

The corresponding centre line longitudinal turbulence intensity, u' profiles (Re = 2.78×10^4, 4.5×10^4 and 5.4×10^4) are shown in fig. 5.2.4. The variation of Reynolds number shows small change in u'/U_e for different Re. in the range x/D = 1.5 to 6.0 it is found that the increase of Reynolds number decreases the value of turbulence intensity. This may be due to more organised flow at lower Reynolds number. This type of behaviour was also found by Zaman & Hussain [55]. The data of Crow and Champagne [13] are fairly lower but the trends of behaviours are similar. The difference may be due to tripped exit boundary of Crow & Champagne's experiment. The u'_c/U_e varies from 0.006 to 0.225 for all the Re with in the range x/D = 0 to 7.

The mean velocity profile at different down stream distance, x/D = 0.5, 1.0, 1.5, 2.0, 3.0 are shown in fig. 5.2.5. From the U profiles of this figure it is clear that the boundary layer zone is increased with the increase in axial distance. Mean velocity gradient (dU/dy) decreases as the distance increaes but when the flow is developed the gradient remain unchanged which is beyond the present measuremental extent.

The corresponding longitudinal fluctuating intensities are shown in fig. 5.2.6. Here the peak value of u'/U_e reaches to 0.26 at x/D = 2.0 from u'/U_e= 0.17 at x/D = 0.25 but location of peak did not changed with change in x/D distance which was also reported by many other researchers.

Self-preservation profiles of U for Re = 5.4×10^4 are shown in fig.5.2.7 it is customary to infer self-preservation from the congruence of mean velocity profile (U/U_e vs. self-preserving variable). In present study sefl-preserving variable was considered as $(y - y_{.5})/\theta_{.1}$ which is also considered by Zaman & Hussain [55] and Hussain & Clark [20]. It is noted that the profile of integration is terminated on the low-speed side at y-location where U/U_e = 0.1 in order to avoid the effect of entrainment induced transverse mean velocity and flow reversal (Hussain & Zaman [21). The jet is found to self-preserving from x/D= 1.5 to 3.5 after that the jet looses its self-preservation. This may be due to the absence of potential core after x/D = 3.5. The extent of potential core upto x/D = 3.5 is also evident from the centre line U_c profiles in fig. 5.2.3 . The congruence of U/U_e profiles however, is not a sensitive indicator of self-preservation. To judge actual self-preservation the fluctuating intensities come into consideration.

Self-preservation profile of u'/U_e are presented in fig. 5.2.8. From this figure it is clear that the congruence of u'/U_e profiles is comparatively worse then that of U/U_e. Thus similarity is achieved earlier for U/U_e profiles than for u'/U_e.

The constant mean velocity lines are shown in fig. 5.2.9. These lines show that the spread of the shear layer. The spread rate is linear from x/D - 1.0 to 4.0, i.e. upto the extent of the initial region. After the end of potential core transition starts and accordingly the constant mean velocity lines no longer

varies linearly with x. Which was also observed by Hussain & Zaman [55].

The stream wise evolutions of the shear-layer momentum thickness $\theta_{.1}$ is shown in fig. 5.2..10 . By linear extrapolation it shows that the virtual origin is located at x/D = -0.023 upstream for Re = 2.78 x 10^4 and x/D = 0.071 down stream for Re = 5.4 x 10^4. However many investigator reported the location of virtual origin in upstream only. But Bradshaw [6] found that for jets with laminar exit boundary layer, virtual origin varies between $-200 < x/\theta_e < 350$. The studies of Hussain & Zedan [20], Wygnanski & Fiedler [52] and Batt [5] shows that the virtual origin is located upstream of the seperation point for initially tripped (turbulent) boundary layer.

5.3 Long Neck Nozzle :

Long neck nozzle was manufactured with the same converging profile of the NN nozzle but with the extension of the prallel exit portion from 5.08 cm (2 inch) to 15.24 cm (6 inch). This extention of the parallel exit portion thickens the boundary layer at the exit thereby changing the exit condition of the nozzle. Flow field of this nozzle will be studied in light of the NN nozzle so that the effect of initial boundary layer thickness on the down stream flow-field can ascertained.

The exit boundary layer mean velocity profile for the two Reynolds number (Re = 4.5 x 10^4, 5.4 x 10^4) was plotted in fig. 5.3.1. the solid line in the figure shows the Blasius profile. As in the NN nozzle the experimental points lie on the Blasius profile within the experimental uncertainties. So it can be concluded that thickening of bounary layer virtually has little effect on the exit mean velocity profile. However this has tremendous influence on displacement thickness and shape factor. In fig. 5.3.2 these are plotted against different

Reynolds number. It is found that δe for both the nozzles decreases with increase of reynolds number. The same trend of behaviour was also found by Zaman and Hussain [55]. However in present study δe values are higher than Zaman's finding. This is because of initial thicker boundary layer in both the nozzles than Zaman's value..

Longitudinal turbulence intensity in the exit boundary layer is shown in fig. 5.3.3. Comparing this figure with that of the NN nozzle (fig. 5.2.2.) it found that in the centre line the turbulence intensity remain the same while the pick value in present case is much lower, i.e. about 20% of the previous case. However the location of the peak and the distribution behaviour remains the same in both the cases.

The centre line variation of mean velocity is shown in fig. 5.3.4. For comparison curves Crow & Champagne [13] and Zaman & Hussain [55] are also shown. The nature of variation here is same but the decrease rate is in between Zaman's and Crow's values.

The centre line variation of longitudinal turbulence intensity, u'/U_e is shown in fig. 5.3.5. Here also the nature of behaviour is nearly the same as before but the Reynolds number response in the present case is found to be much pronounced than the N N nozzle's case. Distribution of turbulence intencity at the Re = 4.5×10^4 seems to follow the behaviour of excited flow of Zaman and Hussain [55].

Stream wise variation of mean velocity profiles for different x/D is shown in figure 5.3.6. The profiles here show the same trend as the NN nozzle but with higher boundary layer width than the previous one at the same x/D location.

The stream wise variation of longitudinal turbulence intensity, u'/U_e is shown in fig. 5.3.7 for different x/D. Turbulence intensity in the shear layer

increase from 0.05 at x/D = 0.25 to 0.35 at x/D = 1.5. While the corresponding values for NN nozzle (fig. 5.2.6) were 0.17 and 0.26 respectively. So it is found that turbulence intensity in the LN nozzle was much less near the exit, but it increased sharply in the down stream side. This sharp increase was not found in the NN nozzle.

Self-preservation profiles of mean velocity is plotted in fig. 5.3.8. The curve shows the self preservation in the same extent as observed in case of NN nozzle.

Self-preservation profile of u'/U_e are shown in fig. 5.3.9. The self-preservation character is clearly exhibited in the figure. The figure shows the existance of self-preservation only between distances x/D = 2.0 to 2.5.

The axial variation of $\theta_{.1}/D$ is shown in figure 5.3.10. The figure shows the virtual origin of the LN nozzle at Re = 4.5×10^4 is situated at x/D = + .083. Different researchers of course found virtual origin both before the exit as well as after the exit. Since this value is very small and there is controversy about its positive and negative locations. So its value was neglected in the calculation of x distances.

The constant velocity lines are shwn in fig. 5.3.11. In this nozzle the spread rate is higher than the NN nozzle and losses its linearity earlier than the previous case.

5.4 Wdge Shaped Nozzle :

To study the asymmetric effect the LN nozzle exit face was cut at 45° at one side from the centre line of the exit section. Thus making the nozzle wedge shape the flow coming out from it became three dimensional. The WS nozzle flow was of course sysmmetric about xy-plane in the coordinate system

described in section 4.2. For analysing the flow, measurements were taken in all the three coordinates and they are then compared with the previous measurements and influence of exit asymmetric condition was studied.

Mean velocity profiles in x, y and z axes at different x/D (= 0, .25, .5, 1, 1.5, 2, 3, 4 and 5) locations are shown from figures 5.4.1 to 5.4.9. In those figures similar profiles for NN and LN nozzle are also shown for comparison. At x/D = 0 profile of LN nozzle and those of wedge shaped nozzle for - Y and Z axes are found to coinside indicating the little effect on these profiles due to the presence of wedge shape on the other side of the nozzle. The profile in the + Y axis spreads much more than normal exit condition of the nozzle. Profile of LN nozzle shifts left ward from that of the NN nozzle due to the presence of more thicken boundary layer. Observing the figures from 5.4.2 to 5.4.6 it can be seen that transition occurs in these region. Velocity profiles in this region spread at different rates in different axes and in different locations. Strong acceleration and deceleration, hence intermixing is taking place in these zone. Profiles in the Z-axis spread faster than those in the -ve Y- axis upto x/D = 1.0. Then the spreading rate in the -ve Y-axis increases and at x/D = 1.5 it is seen that spreading of the profiles in the axes - ve Y and Z- are the same. from x/D = 3 profiles in all the three axes of WS nozzle and those of NN nozzle and LN nozzle are found to coincide each other. So the effect of asymmetry and boundary layer thickness at the exit condition do not seem to influence the flow in the down-stream side from x/D = 3.0.

Profiles of longitudinal turbulence intensities for the three axes at different x/D (= 0. 0, .25, .5; 1.0, 1.5, 2.0, 2.5, 3.0 and 4.0) locations are shown in figures 5.4.10 to 5.4.18. The figures 5.4.10 to 5.4.18 shows the

variation of the turbulence intensities at different locations of the flow field. For comparison those of the NN nozzle were also shown in the figures. At the exit plane in the +ve Y axis while the turbulence intensities increase about four times the NN nozzle values, those in the -ve Y and Z axes are seemed to be supressed. Afterwards these suppressed values increase quickly and obtain the peak value $u'/U_e = 0.24$ at $x/D = 0.5$. After $x/D = 0.5$ while peak value of u'/U_e in -ve Y and Z axes still go on increasing and spreading over the axes length, the peak value of u'/U_e in the +ve Y axis starts decreasing. At $x/D = 2.0$ the distribution of u'/U_e in all the three direction (axes) are found nearly the same. After $x/D = 2.0$ the turbulence intensity of the WS nozzle starts further spreading while the peak value decreasing. At $x/D = 4.0$ and 5.0 it is seen that turbulence intensity of the WS nozzle is 60% of the NN nozzle.

The centre line variation of mean velocity at different Reynolds number ($Re = 4.5 \times 10^4$, 5.4×10^4, 6.1×10^4) is shown in figure 5.4.19. The decrease of centre line veloicty with the axial distance shows the same pattern of the other nozzle i.e. the decrease rate increase with the decrease of Reynolds number. The centre line variation of mean velocity of the three nozzles under study shows that in the WS nozzle the decrease rate is less than the other two nozzles.

The centre line longitudinal turbulence intensity for different Reynolds number ($Re = 4.5 \times 10^4$, 5.4×10^4, and 6.1×10^4) are shwon in fig. 5.4.21. The turbulence intensity in the centre of the WS nozzle seems to insensitive to the experiment range of Reynolds number variation.

Centre line variation of longitudinal turbulence intensity, u'/U_e for the three nozzles are shown in figure 5.4.22. In the centre line the NN and LN nozzle

exhibit higher u'/U_e values than that in the WS nozzle.

The stream-wise evolutions of the shear layer local momentum thickness $\theta_{0.1}$ for Re = 5.4 x 10^4 of different axes (+ve Y, -ve Y and Z axis) are shown in fig. 5.4.23. By linear extrapolation it was found that the virtual origin for three axes are located at different x/D location. For +ve Y virtual origin was found at x/D = -0.46 (i.e. x/D = 0.04 upstream from the point of separation), and those of Z and -ve Y axis are x/D = 0 and 0.06 respectively. All these values of virtual origin are very close to the point of seperation as observed in cases of LN and NN nozzle. These values of x_0 were not considered in analysing different quantities as done in NN and LN nozzle for the same reason state before.

The self-preservation profiles of mean velocity in three axes (+ve Y, -ve Y and Z axis) for Re = 5.4 x 10^4 are presented in figures 5.4.24, 5.4.25 and 5.4.26. It is clear from these figures that for all the three axes mean velocity shows, jet flow was self-preserved in all the axes from x/D = 1.5 to 3.0 which was within the extent of potential core, as observed in centre line mean velocity distribution profile (fig. 5.4.19). The self-preservation of U/U_e profiles in all the three axes behaves insensitive to the initial three dimentionality involved due to wedge shaped exit condition, because NN and LN nozzle flows also shows self-preservation in the same extent of axial distence.

Self-preservation profiles of longitudinal turbulence intensity in +ve, -ve Y and Z axis of WS nozzle are shown in figures 5.4.27, 5.4.28 and 5.4.29 respectively. Congruence of self-preservation profiles is worst in -ve Y axis. In positive Y axis self-preservation is attained from x/D = 2.0 but perfect congrunce is not observed it may be because of flow instability. Self-preservation in both -ve Y and Z axis was found from x/D = 2.5. From this observation it

seemed that the distance of attainment of self-preservation from point of seperation is unique. Here the congruence of self-preservation profiles are worse compared to those of NN and LN nozzle. This may because of less organised flow pattern of WS nozzle than of NN and LN nozzle which is also focused in comparison of centre line longitudinal turbulence intensity profiles shown in fig. 5.4.22.

The spread rates of the shear layer for +ve Y, -ve Y and Z axes of WS nozzle are shown in figures 5.4.30-32. Due to the presence of the wedge in +ve Y axis high interaction of the shear layer is observed in this zone. Most probably large vortices created in the shear layer at about x/D = 1.0 try to roll inside the core of the jet shifting the core inward at x/D = 1.5 where interaction of two more vortices break up into smaller sizes expanding the core of the jet at x/D = 2.5. Similar interaction can be observed in -ve Y axis, (Fig. 5.4.31), LN nozzle (Fig. 5.3.11), NN nozzle (Fig. 5.2.9) but of much less strength.

Oscillograms for centre line turbulence intensities are shown in figure 5.4.33. Figure shows that flow with turbulence intensities of lower amplitude and higher frequencies (on the order of 1KHz) emerges from the nozzle. These high frequency fluctuations in the centre line takes energy from the shear layer producing high amplitude and low frequency fluctuations (on the order of 72 Hz) at x/D = 1.5 probably caused by interaction of vortices. Formation of pairing of vortices and their mixing are observed conjequtively at x/D = 2 - 2.5 and x/D = 3 - 3.5. After 3.5 i.e. after the end of the potential core all the vortices break into small eddies of high frequencies and amplitude carrying high energies. Which indicate start of transition zone of the jet.

The oscillograms at x/D = 0 & 1.0 for different +ve Y - locations are shown in figures 5.4.34 and 5.4.35. The increase of turbulence intensities in the shear layer are clearly exhibited in the figures. Quantitiative measurement of maximum vlaue of turbulence intensity in the middle of the boundary can be compared with figures 5.4.10 & 5.4.13.

CHAPTER - VI

CONCLUSIONS

6.1 Introduction :

The present research objective was to study some fundamental aspects of nozzle flow behaviour. In the present work the research objective have been fulfilled. The results of the present work which have been discussed in the previous chapter are summarised in this cahapter and the possible extension of present work is recommended.

6.2 Findings of the Present Work :

Measurements in the turbulent flow field created by the round shaped nozzle of different exit conditions revealed both well known and as well as not-so-well known features. To the best of author's knowledge study on wedge shape nozzle flow is the first of its kind in the field of turbulent research. The study of asymmetric turbulent flow in the wedge shaped jet showed that in the down stream side longitudinal turbulence intensity was suppressed instead of increasing.

6.3 Conclusions :

The following conclusions are drawn as consequence of the present research work :

1. Increase boundary layer thickness at the exit has little effect on exit mean velocity profile.
2. Increases exit boundary layer increases the shape factor of exit velocity profile.
3. With the increase of Reynolds number the exit boundary layer thickness decreases for different exit conditions.

4. Thickening of the exit boundary layer suppressed the exit peak turbulence intensity.

5. Thickening of the exit boundary layer decreases the decrese rate of centre line mean velocity in the down stream direction.

6. Effect of change of Reynolds number is more pronounced in thick exit boundary layer condition.

7. Thicknening of exit boundary layer increases the spread rate of the jet.

8. Asymmetry in one axis of the nozzle has little effect on mean velocities in other axes at the exit but has great effect on turbulence intensities on those axes of the jet.

9. In the asymmetric axis while the turbulence intensity at the exit increased those in the other axes are suppressed.

10. In the down stream side flow asymmetry began to decrease both turbulent and mean quantities became nearly symmetric at x/D = 3.

11. In the asymmetric flow condition (wedge shaped jet) at x/D = 3, the turbulence intensity became lower than symmetric flow conditions.

6.4 Extension of the Present Work :

The present study of circular nozzle flow is a preliminary work in the field of turbulent flow. The research in this field can be extended in different directions. As a direct extension of the present work, the following suggestions may be made for continuation of the research in this field.

1. The same measurements can be extended in the axial direction to have total focus in transition and developed zone of the just performed nozzle flow studies.

2. The measurement details can be extended to determine transverse mean velocity, transverse turbulence intensity, turbulent shear stress, correlation coefficient and turbulence spectra.

3. To study the flow structure detail flow visualization technique can be applied.

4. circular wedge shaped jet can be studied with different wedge angle of wedge shaped nozzle.

5. All the above measurements can be taken under controllable excitation at different frequencies.

APPENDIX - A

CONSTRUCTION AND DESIGN OF SILENCER

A.1 General :

The fan unit along with flow controller and vibration isolator was fitted with the tunnel via silencer. The silencer's role is to remove or strain the noise (sound) generated by the moving blade and pressurized air.

A.2 Construction and Design :

The silencer was made about 0.762 meter (2.5 feet) long and an inside diameter of 0.48 meter (19 inch). The outer cover was made of G. I. sheet (24 US standard gauge). The internal drum was made of perforated mild steel sheet (22 US standard gauge having 3.2 mm (1/8 inch) diameter holes 16 per sq. inch). These two drums held 6.35 cm apart by 6.33 mm (¼ inch) mild steel flange. The perforated inner drum was screwed up with tie angle (31 mm x 4 mm x 4 mm) welded between two end of the flanges. Provision was made to remove the outer cover by simple nut-bolt system. Glass-wool sheets were placed between the gap of two drums layer by layer to fillup the 6.25 cm (2.5 inch) gap arround the perforated drum as shown in Fig.A.1 & Plate 4.1.3.

APPENDIX - B

DESIGN OF DIFFUSERS

In order to obtain the optimum value of 'θ' for the diffuser, the flow through the diffuser was analysed as follows :

As the flow field is two-dimentional, the Navier Stock's equation in polar co-ordinates are,

$$\frac{\partial u}{\partial t} + u\frac{\partial u}{\partial r} + \frac{v}{r}\frac{\partial u}{\partial \theta} - \frac{v^2}{r} = \frac{1}{\rho}\frac{\partial P}{\partial r} + \nu\left(\nabla^2 u - \frac{2}{r^2}\frac{\partial v}{\partial \theta} - \frac{u}{r^2}\right)$$

$$\frac{\partial u}{\partial t} + u\frac{\partial u}{\partial r} + \frac{v}{r}\frac{\partial v}{\partial \theta} + \frac{uv}{r} = -\frac{1}{\rho}\frac{\partial P}{r\partial \theta} + \left(\nabla^2 v + \frac{2}{r2}\frac{\partial u}{\partial \theta} - \frac{v}{r2}\right)$$

and the continuty equation is,

$$\frac{\partial u}{\partial t} + \frac{1}{r}\frac{\partial v}{\partial \theta} + \frac{u}{r} = 0$$

Assuming radial flow and steady state of motion,

i.e. $u = f(r,\theta)$ and $v = 0$.

With the above value of u and v the governing equations beocmes

$$u\frac{\partial u}{\partial r} = -\frac{1\partial P}{\rho\partial r} + \left(\frac{\partial^2 u}{\partial r^2} + \frac{1}{r}\frac{\partial u}{\partial r} - \frac{u}{r^2} + \frac{1\partial^2 u}{r^2\partial \theta^2}\right) \qquad (B.1)$$

$$0 = -\frac{1}{\rho}\frac{\partial P}{\partial \theta} + \left(\frac{1}{r^2}\frac{\partial u}{\partial \theta}\right) \qquad (B.2)$$

and $$u\frac{\partial u}{\partial r} + \frac{u}{r} = 0 \qquad (B.3)$$

From equation .3, $\frac{d(u.r)}{d(r)} = 0$

After integration, it becomes,

$$u = \frac{f_2(\theta)}{r}$$

To make the function dimension less the above equation can be written as -

$$u = \frac{\nu f(\theta)}{r} \qquad \text{(B.4)}$$

where ' f ' is a function of ' θ ' only.

Using the substitution (eqn. B.4) eqn. B.1 and eqn. B.2 becomes,

$$-f^2 = -\frac{r^3}{\nu^2}\frac{1}{\rho}\frac{\partial P}{\partial r} + f'' \qquad \text{(B.5)}$$

and $$0 = -\frac{1}{\rho r}\frac{\partial P}{\partial \theta} + 2\nu^2\frac{f''}{r^3} \qquad \text{(B.6)}$$

From equation B.6

$$\frac{\partial}{\partial \theta}\left(\frac{P}{\rho}\right) = \frac{2\nu^2}{r^2} f$$

Integrating

$$\frac{P}{\rho} = \frac{2\nu^2}{r^2} f + F(r)$$

Differentiating with respect to ' r ' results

$$\frac{\partial}{\partial r}\left(\frac{P}{\rho}\right) = \frac{4\nu^2}{r^3} f + F' \qquad \text{(B.7)}$$

Now substituting equation B.7 in eqn. B.5, gives,

$$f'' + 4f + f^2 + \left(-F'\frac{r^3}{\nu^2}\right) = 0 \qquad \text{(B.7a)}$$

Replacing $\frac{r^3}{2}(-F')$ by K,

The optimum value of ' α ' determined from the fact that there should not be any seperation in the full length of the diffuser.

At the point of seperation,

$$f'(\theta) = 0 \text{ at } \theta = \pm\alpha$$

Putting the above boundary condition in equation B.8a, tives

$$G = 0$$

So the integral equation becomes,

$$-\int_0^{\alpha} d\theta = \sqrt{\frac{3}{2}} \int_0^{f_1} \frac{df}{(f_1 - f)^{\frac{1}{2}} (f^2 + 6f + ff_1)^{\frac{1}{2}}}$$

substituting $f = f_1 \cos^2 \eta$,

$$\alpha (f_1 + 3)^{\frac{1}{2}} = \sqrt{3} \int_0^{\pi/2} \frac{d\eta}{1 - \frac{1}{2}(1 + 3/f_1)^{-1} \sin^2}$$

If Reynold's number is defined over the characteristic length ' r ' as follows,

$$R_e = \frac{U_{max.}\, r = f_1}{\nu}$$

Therefore,

$$\alpha (R_e + 3)^{\frac{1}{2}} = \sqrt{3} \int_0^{\pi/2} \frac{d\eta}{1 - \frac{1}{2}(1 + 3/R_e)^{-1} \sin^2 \eta}$$

for large values of 'R_e',

$$\alpha \sqrt{R_e} = \sqrt{3} \int_0^{\pi/2} \frac{d\eta}{(1 + \frac{1}{2} \sin^2 \eta)^{\frac{1}{2}}}$$

Which is a elliptical integral of first kind. Its vlue may be taken from the table of integration.

$$f'' + 4f + f^2 + K = 0 \qquad (B.8)$$

Multiplying the equation B.8 by f',

$$f'' f' + 4ff' + f^2 f' ; Kf' = 0$$

which may be expressed as

$$\frac{d}{d\theta} \left(\frac{f'^2}{2} + 2f^2 + \frac{f^3}{3} + Kf \right) = 0$$

After integration it becomes,

$$\frac{f'^2}{2} + 2f^2 + \frac{f^3}{3} + Kf = \text{const.}$$

$$\text{or,} \quad f'^2 = \frac{2}{3} \left(G - 3Kf - f^3 - 6f^2 \right) \qquad (B.8a)$$

where 'G' is a constant.

At $\theta = 0$, due to symmetry, $\frac{\partial u}{\partial \theta} = f'(\theta) = 0$. If the maximum radial velocity, which occur at $\theta = 0$ is denoted by f_1, then $f_1 = (U_{max} \cdot r)/\nu$

Substituting these conditions in the above relation, gives,

$$3K = \frac{G}{f_1} - f_1^2 - 6f_1$$

Replacing 'K' from eqn. B.8a it becomes,

$$f' = \sqrt{\frac{2}{3}} \left(f_1 - f \right)^{\frac{1}{2}} \left(f^2 + 6f + ff_1 + \frac{G}{f_1} \right)^{\frac{1}{2}}$$

$$\text{or,} \quad d\theta = \sqrt{\frac{3}{2}} \frac{df}{\left(f_1 - f \right)^{\frac{1}{2}} \left(f^2 + 6f + ff_1 + G/f_1 \right)^{\frac{1}{2}}}$$

Now, at $\theta = 0$, $f = f_1$

and at $\theta = \alpha$, $f = 0$.

Therefore,

$$- \int_0^{\alpha} d\theta = \sqrt{\frac{3}{2}} \int_0^{f_1} \frac{df}{\left(f_1 - f \right)^{\frac{1}{2}} \left(f^2 + 6f + ff_1 + G/f_1 \right)^{\frac{1}{2}}}$$

$$\int_0^{\pi/2} \frac{d\eta}{\left(1 - \frac{1}{2}\sin^2\eta\right)^2} = F\left(\frac{1}{2}, \frac{\pi}{2}\right) = 1.8540$$

Therefore, $\alpha\sqrt{R_e} = \sqrt{3}\ (1.85410)$

or, $\alpha = \dfrac{3.2154}{\sqrt{R_e}}$

For different values of Reynolds numbers the angle of divergence 'α' was plotted in fig. B.2. It is seen that at a very high Reynold's number 'α' is less than 5 degree.

In the designed diffuser 'α' was keeped close to 3 degree.

Now, question of length arises, what should be the length limit of the diffuser to avoid seperation i.e. energy loss. The seperation point may be defined by $\frac{\partial u}{\partial \theta} = 0$ at $\theta = 0$. So from velocity distribution the length limit could be found out.

The equation B.8 may be solved for the velocity function $f(\theta)$ by the linearization technique. The eqn. B.8 is a nonlinear second order ordinary equation. The equation was made linear by introducing a new term 'ε', called velocity factor, to weigh the mean velocity function $\bar{f}$.

Then equation B.8 becomes,

$$f'' + 4f + \varepsilon \bar{f} f = -K \qquad \text{(B.8b)}$$

where $\bar{f} = \frac{1}{\alpha} \int f d\theta$

Let, $\bar{u} = \frac{\nu \bar{f}}{r}$

Then, $\bar{f} = \frac{\bar{u}.r}{\nu} R_e$

This shows that $\bar{f}$ is equivalent to Reynolds number based on the characteristic length ' r '.

Therefore,

$$f'' + (4 + \varepsilon R_e) f = - K$$

It is clear from the flow conditions that $(4 + \varepsilon R_e) > 0$. So, the solution of the above equation is,

$$f = A \cos\sqrt{(4 + \varepsilon R_e)}\,\theta + B \sin\sqrt{(4 + \varepsilon R_e)}\,\theta - \frac{K}{4 + \varepsilon R_e} \qquad (B.9)$$

The constants 'A' and 'B' are determined from the boundary conditions,

$$f (\pm \alpha) = 0$$

The constants are,

$$B = 0, \text{ and } A = \frac{K}{(4 + \varepsilon R_e) \cos\sqrt{(4 + \varepsilon R_e)}\alpha}$$

Substituting these values in equation B.9 gives,

$$f = \frac{-K}{4 + \varepsilon R_e} \left[1 - \frac{\cos\sqrt{(r + R_e)\theta}}{\cos\sqrt{(4 + R_e)\alpha}} \right] \qquad (B,10)$$

Substituting equation B.10 in expression of $\bar{f}$ and integrating,

$$\bar{f} = \frac{-K}{4 + \varepsilon R_e} \left[1 - \frac{\sin\sqrt{(4 + \varepsilon R_e)\alpha}}{\alpha (4 + \varepsilon R_e) \cos\sqrt{(4 + \varepsilon R_e)\alpha}} \right] \qquad (B.11)$$

From equation B.4 it is possible to write,

$$\frac{u}{\bar{u}} = \frac{f}{\bar{f}}$$

Dividing equation B.10 by equation B.11

$$\frac{u}{\bar{u}} = \frac{1 - \dfrac{\cos\sqrt{(4 + \epsilon R_e)}\,\theta}{\cos\sqrt{(4 + \epsilon R_e)}}}{1 - \dfrac{\sin\sqrt{(4 + \epsilon R_e)}}{\alpha\,(4 + \epsilon R_e)\cos\sqrt{(4 + \quad)}}}$$

Putting $\alpha\,(4 + \epsilon R_e) = \lambda$, and $\xi = \dfrac{\theta}{\alpha}$

$$\frac{u}{\bar{u}} = \frac{\cos\lambda - \cos\lambda\xi}{\cos\lambda - (1/\lambda)\sin\lambda} \qquad \text{(B.12)}$$

Velocity 'u' is still undetermined becouse the velocity factor ' ϵ ' is unknown. To determine the factor ' ϵ', it is assumed that the local pressure gradient $\frac{\partial P}{\partial r}$ calculated from momentum principle should be equal to that calculated from mechanical energy consideration. for a given velocity function ' f ', the equality of pressure gradient may be obtained by equating the gradient dF/dr.

Equation B.7a can be written as,

$$\frac{r^3}{\nu^2}\,\frac{dF}{dr} = \frac{d^2f}{d\theta^2} + 4f + f^2 \qquad \text{(B.13)}$$

Integrating with respect to $\xi = \theta/\alpha$,

$$\frac{r^3}{\nu^2}\,\frac{dF}{dr}\int_0^{'} d\xi = \frac{1}{\alpha^2}\int_0^{'}\frac{d^2f}{d\xi^2}\,d\xi + 4\int_0^{'} f d\xi + \int_0^{'} f^2 d\xi$$

or, $$\frac{r}{\nu^2}\,\frac{dF}{dr} = \frac{1}{\alpha^2}\,\frac{dF}{d\xi} + 4f' + \int_0^{'} f^2 d\xi \qquad \text{(B.14)}$$

Mechanical energy equation is formed be multiplying equation B.13 by f(θ) , and another by integrating the obtained equation with respect to $\xi = \theta/\alpha$ in term of dF/dr.

$$\frac{r^3}{\nu^2}\ \frac{dF}{dr} = f\ \frac{d^2f}{d\theta^2} + 4f^2 + f^3$$

or, $$\frac{r^3}{\nu^2}\ \frac{dF}{dr}\int_o^1 f\,d\xi = \frac{1}{\alpha^2}\int_o^1 f\ \frac{d^2f}{d\xi^2}\,d\xi + 4\int_o^1 f^2 d\xi + \int_o^1 f^3 d\xi$$

or, $$\frac{r^3}{\nu^2}\ \frac{dF}{dr} = \frac{1}{\bar{f}}\ \left[\ \frac{1}{\alpha^2}\int_o^1 f\ \frac{d^2f}{d\xi^2}\,d\xi + 4\int_o^1 f^2 d\xi + \int_o^1 f^3 d\xi\ \right] \qquad \text{(B.15)}$$

from equation no. B.12.

$$f = \bar{f}\ \frac{t - \cos\lambda\xi}{t - s}$$

When , $t = \cos\lambda$, $s = \frac{1}{\lambda}\sin\lambda$

Now, $$\left.\frac{df}{d\xi}\right]_{\xi=1} = \frac{\bar{f}^2 s}{t-s}$$

$$\int_o^1 f^2\,d\xi = f^{-2}\ \frac{t^2 - \frac{3}{2}ts + \frac{1}{2}}{(t-s)^2}$$

$$\frac{d^2f}{d^2} = f^{-2}\ \frac{\lambda^2\cos\lambda\xi}{t-s}$$

or, $$\int_o^1 f\ \frac{d^2f}{d^2} = \bar{f}^2\lambda^2\ \frac{\frac{1}{2}st - \frac{1}{2}}{(t-s)^2}$$

then, $$\int_o^1 f^3 d\xi = \bar{f}^3\ \frac{t^3 - \frac{11}{6}st^2 + \frac{3}{2} + \frac{3}{2}s}{(t-s)^3}$$

Equalising the equations B.14 and B.15, gives,

$$\left(\frac{\lambda}{\alpha}\right)^2\ \frac{s}{} + 4 + \bar{f}\ \frac{t^2 - \frac{3}{2} + s + \frac{1}{2}}{(t-s)^2} = \frac{1}{2}\left(\frac{\lambda}{\alpha}\right)^2\frac{st - 1}{(t-s)^2}$$

$$+\ \frac{4t^2 - 6ts + 2}{(t-s)^2} + \bar{f}\ \frac{t^3 - \frac{11}{6}st^2 + \frac{3}{2}t - \frac{2}{3}s}{(t-s)^3}$$

$$\text{or,} \quad \left(\frac{\lambda}{\alpha}\right)^2 \frac{st - 1 - 2st + 2s^2}{2(t-s)^2} + \frac{4t^2 - 6ts + 2 - 4t^2 + 8st - 4s^2}{(t-s)^2}$$

$$= \bar{f} \frac{t^3 - \frac{3}{2}t^2 s + \frac{1}{2}t - st^2 + \frac{3}{2}s^2 t - \frac{1}{2}s - t^3 + \frac{11}{6}st^2 - \frac{2}{3}t + \frac{2}{3}s}{(t-s)^3}$$

As, $\lambda = \sqrt{(4 + Re)\alpha}$

Therefore,

$$(4 + Re) \frac{2s^2 - st - 1}{2(t-s)^2} - \frac{4s^2 - 2st - 2}{(t-s)^2}$$

$$= \bar{f} \frac{9s^2 t - 4t^2 s - 6t + s}{6(t-s)^2}$$

$$\text{or,} \quad \varepsilon \, Re \frac{2s^2 - st - 1}{2(t-s)^2} = \bar{f} \frac{9s^2 f - 4t^2 s - 6t + s}{6(t-s)^2}$$

Further more, $\bar{f} = \frac{\bar{u} r}{\nu} = Re$

So, $$\varepsilon = \frac{9st - 4ts - 6t + s}{3(t-s)(2s^2 - st - 1)}$$

For different values of 'λ', the velocity function 'ε', tabulated as bellow,

λ	1.0	1.25	1.5	1.75	2.0	2.25	2.5	2.75	3.0	3.14
ξ	1.715	1.73	1.749	1.762	1.79	1.83	1.86	1.9	1.95	2.0

The figure shows the points of ε against λ, the curve shows that seperation may be avoided if 'λ' is less than 'π'. The point of seperation may be obtain from the expression,

$$\frac{du}{d\xi} = 0$$

Writting the equation B.12,

$$u = \bar{u} \quad \frac{\cos\lambda - \cos\lambda\xi}{\cos\lambda - \frac{1}{\lambda}\sin\lambda}$$

Therefore, $\frac{\partial u}{\partial \xi} = \bar{u} \quad \frac{\sin\lambda\xi}{\cos\lambda - \frac{1}{\lambda}\sin\lambda}$

As, $\frac{\partial u}{\partial \xi}\Big]_{=1} = 0$ (condition of seperation)

So, $\sin\lambda = 0$

$= n\pi$, for $n = 01$, $\alpha = \pi$

Therefore, $\alpha\sqrt{(4 + Re)} = \pi$

Squaring, $(4 + 2Re)\alpha^2 = \pi^2$ (since at $\lambda = \pi$, $\epsilon = 2$)

Again, $Re = \bar{f}$

Therefore, $(4 + 2f)\ \alpha^2 = \pi^2$ (B.17)

Taking $\bar{f} = \bar{u}r$, and substituting in equation B.17,

$$(4 + 2\bar{u}r)\alpha^2 = \pi 2 \qquad \text{(B.18)}$$

The angle of divergence for the diffuser is 3 degree only. Seperation may be taken place only when the equation B.18 is satisfied. In this case the length of the diffuser is selected to be 5 ft. for 1st diffuser and 8.5 ft. for second diffuser. With these length Eqn. B.18 is not satisfied because of small degree of divergence (3°). Hence there would be no seperation within the entire length of the diffusers.

APPENDIX - C

NOZZLE DESIGN & FEBRICATION

C.1 General :

In the flow system there were kinds of nozzle one kind was jute glass fibre composite nozzles, which were part of the jet flow facility and the other kind was the wooden test nozzle. The jute glass fibre composite nozzles were provided for sharp construction of flow area after each settling chambers to ensure settling of air in the settling chambers and to suppress the turbulence intensity of down stream. The wood made test nozzles were used for the study of the basic flow characteristics and structure of flow in the near field of jet formed when air issuing out of the nozzle in the free air.

C.2 Cubic Profile :

The profile all the nozzles (jute glass-fibre composite nozzle and wooden test nozzles) had same cubic profile. The cubic profile was chosen to minimize the flow loss and smoothen the flow.

The profile was nothing but the deflection curve yeild by a fixed beam when it under goes deflection at one end with out any load. (Fig. - c.1). for unloaded fixed beam, general equation of deflection is,

$$\frac{d^4y}{dx4} = 0 \qquad \text{(C.1)}$$

The boundary condition are,

(i) $\frac{dy}{dx} = 0$ at, $x = 0$ -

(ii) $\frac{dy}{dx} = 0$ and $x = L_b$ - (L_b = length of the beam)

(iii) $y = 0$, at $x = 0$

(iv) $y = \delta_b$, at $x = L$ (δ_b deflution of the beam)

So there are four boundary condition to solve the fourth order differential eqn. Integrating the general equation three –

$$\frac{dy}{dx} = Ax^2 + Bx + C \qquad (C.2)$$

Integrating eqn. (C.2) again

$$y = \frac{Ax^3}{3} + \frac{Bx^2}{2} + Cx + D$$

Now applying the boundary condition (i) & (ii)

$$C = 0 \qquad D = 0$$

$$\text{i.e,} \quad = \frac{Ax^3}{3} + \frac{Bx^2}{2} \qquad (C.3)$$

$$\text{and} \quad \frac{dy}{dx} = Ax^2 + Bx \qquad (c.4)$$

Using the other two boundary condition

$$y = 3 \left(\frac{x}{L_b}\right)^2 - 2 \left(\frac{x}{L_b}\right)^3 \qquad (C.5)$$

which is the general equation of the cubic profile.

For first jute glass fibre compsite nozzle and a upstream diameter 24" , contraction ratio 16 : 1 (area base) and 1.5 feet length. Therefore the equation of the profile was —

$$y = .0833\ x^2 \text{ ——— } .003086\ x^3 \qquad (C.6)$$

The second nozzle made of jute glass-fibre composite material had a upstream diameter of 18 inch, contraction ratio 4:1 and over alllength of 18 inch. so from equation C.5 the profile equation for the second jute glass-fibre composite nozzle was,

$$y = .04167\ x^2 - .00154\ x^3 \qquad (C.7)$$

For the test nozzles with upstream dimeter 9 inch and contraction ratio of 9 :1 with the length of 12 inch. The cubic profile for the test nozzles was —

$$y = .0615\ x^2 - .0034\ x^3 \qquad (C.8)$$

C.3 Nozzle Fabrication :

The fabrication of jute glass-fibre composite nozzle require cores for inside shape. The cores were made of low grade wood, but with a high surface finish. The polishing of cores surface was very essential to ensure smooth inner surface of the finished nozzle. The layers of resin glass fibre and jute was given arround the finished wooden core to obtain the jute glass fibre nozzle. Where three glass fibre and are jute layer were given for each nozzle. The test nozzles were made of Teak wood. The nozzles were obtained by turbing off woods from a teak wood block according to given profile. After turning the surface (mainly inside surface) were polished and varnished to get a smooth finished surface.

REFERENCES

1. Anderson, A.B.C., 1955, J. Acous Soc. Amer. Vol. 27, pp. 13.

2. Anderson, A.B.C., 1956, J. Acous Soc. Amer. Vol. 28, pp. 914.

3. Antonia, R., Chambers, A. J. & Phan-thien, N., 1980, J. Fluid Mech. Vol. 100, pp. 193.

4. Batt, R. G., Kubota, T. & Laufer, J., 1970, AIAA Reacting Turbulent flows conf. San Diego.

5. Batt, R. G., 1974 TRW TR Rep. No. 18117-6023 (See also SAMSO TR No. 74 - 62).

6. Bradshow, P., " The effect of initial conditions on the development of a free shear layer ", 1966, J. Fluid Mech., Vol.26, part.2, pp. 226 - 266.

7. Bradshow, P., 1978, J. Fluid Mech., Vol. 85, pp. 693.

8. Champagne, F. H., Sleicher, C. A. & Wehrmann, O., 1967, J. Fluid Mech., Vol. 28, pp. 153.

9. Champagne, F. H., Harris, V. G. & Corrsin, S., 1970, J. Fluid Mech. Vol. 28, pp.

10. Champagne, F. H., Pao, Y. H. & Wygnaski, I. J., " On the two dimensional mixing region ", 1976, J. Fluid Mech. Vol. 74, part.2, pp. 209 - 250.

11. Champagne, F. H., 1978, J. Fluid Mech., Vol. 86, pp. 67.

12. Chandrasuda, C., Mecha, R. D., Weir, A. D. & Bradshaw, P., 1978, J. Fluid Mech., Vol. 74, pp. 209.

13. Crow, S. C. & Champagne, F. H. " Orderly structure in jet turbulence" 1971, J. Fluid Mech. Vol. 48, part - 3, pp. 547 - 591.

14. Dimotakis, P. I. & Brown, G. L., 1976, J. Fluid Mech., Vol. 78, pp. 535.

15. Fremuth, P., " On transition in a seperated laminar boundary layer", 1966, J. Fluid Mech., Vol. 25, pp. 683 - 704.

16. Grant, H. L., 1958, J. Fluid Mech., Vol. 4, pp. 149.

16.a. Hill, R. G., Jenkins, R. C. and Gilbert, B. L., 1975, Grumman Research Dept., Report RE - 508.

17. Hinze, J. O. and Zijnen, VanDer, H., " Transfer of heat matter in the turbulent mixing zone of an axially symmetrical jet", 1949, Appl. Sci. Res. Vol. 14, pp. 435.

18. Hinze, J. O.,. Turbulence, 1975, McGraw Hill Book Company, NY.

19. Hussain, A.K.M.F. and Zedan, M. F., " Effect of initial condition on the axisymmetric free shear layer : Effect of initial momentum thickness", 1978, Phys., Fluids, Vol. 21, No. 7, pp. 1100-1112.

20. Hussain, A.K.M.F, and Clark, A. R., " On the coherent structure of the asisymmetric mixing layer : A flow-visualization study", 1981, J. Fluid Mech., Vol. 104, pp. 263 - 294.

21. Hussain A.K.M.F. and Zaman K.B.M.Q., " The preferred mode of axisymmetric jet", 1981, J. Fluid Mech., Vol. 110, pp.39-71.

22. Huston, W.B., " Accuracy of air speed measurements and flight calibration procedures", NACA Technical report No. 919, 1948.

23. Kelly, 1967, J. Fluid Mech., Vol. 27, pp. 657.

24. Lamb, H., 1945, Hydrodynamics, Dover.

25. Lessen, M., 1950, Nat. Adv. Comm. Aero, Wash, Tech. Rep. No.979.

26. Lessen, M. and fox, J. A. 1955, 50 Jahre Grenzschichtforschung,pp.112.

27. Liepman, H. W. and Laufer, J., 1947, NACA : Tech. Note, No. 1257.

28. Lin, C. C., 1955, The theory of Hydrodynamic stability, Cambridge University Press.

29. Lumley, J. L., 1965, Atmospheric turbulence and radio wave propagation, In Proc. Int. Colloq, Moscow, pp. 166.

30. Maiechal, J., 1967, C. R. Hebd, Seanc. Acad. Sci., Paris, Vol. 265A, pp. 478.

31. Mc Millan, F. A., " Experiments on pitot tubes in shear flow", Report Memor, Aeronotical Research Council, London, No. 3028,1956.

32. Michalke, A., " On spetially growing disturbances in a inviscid shear layer", 1965, J. Fluid Mech. Vol. 23, part - 3, pp. 521 -594.

33. Michalke, A. and Wille, R., 1965, Proc. 11th Intern. Congr. Appt., Mech., Munich, 1964.

34. Moore, C. J., 1977, J. Fluid Mech., Vol. 80, pp. 321.

35. Mumford, J. C., " The structure of the large eddies in fully developed turbulent shear flows", 1982, J. Fluid Mech., Vol. 118, pp. 241 - 268.

36. Patel, R. P., 1973, AIAA J., Vol. 11, pp. 67.

37. Petersen, R. A., Kaplan, R. E. and Laufer, J., 1974, N.A.S.A. contractor Rep. No. 134733.

38. Rayleigh, L., 1980, Sci. Papers, Vol. 1, pp. 474-484, Cambridge University Press.

39. Rose, W. G. 1966, J. Fluid Mech., Vol. 25, pp. 97.

40. Rosko, A., 1966, AIAA J., Vol. 10, pp. 1349.

41. Sami, S. 1967, J. Fluid Mech., Vol. 29, pp. 81.

42. Sato, H. 1956, J. Phys. Soc. Japan, Vol. 11, pp. 702.

43. Sato, H. " Further investigation on the transition of two dimensional seperated layer at subsonic speeds", 1959, J. Phy. Soc. Japan, Vol. 14, No. 12, pp. 1797 - 1810.

44. Sato, H. " The stability and transition of two-dimensional jet", 1959, J. Fluid Mech., Vol. 7, pp. 53.

45. Schade, H. and Michalke, A., 1962, Z. Flugwises, Vol. 10, pp. 147-154, (also A FOSR Tech. Note No. 3191).

46. Schlichting, H., 1979, Boundary layer theory, Seventh edition, McGraw Hill Book Co., New York.

47. Townsend, A. A., " Entrainment and the structure of turbulent flow", J. Fluid Mech., 1970,Vol. 41, part-1, pp. 13-46.

48. Townsend, A. A. " The structure of turbulent shear flow", 1976, Cambridge University Press.

49. Tucker, H. J. and Reynolds, A. J., 1968, J. Fluid Mech. Vol. 32,pp.1.

50. Valasov, Y. V. and Ginevaskiy, A.S., 1974, N.A.S.A.,TT F-15,pp.721.

51. Wille, R. 1963, Z. Flugwisss, Vol. 11, pp. 222.

52. Wygnaski, I, and Fiedler, H. " Some measurements in the self preserving jet", 1969, J. Fluid Mech., Vol.38,part-3,pp. 577-612.

53. Wyngaard, J. C. and Clifford, S. F., 1977, J. Atoms. Sci., Vol.34,pp.922.

54. Yule, A. J., 1978, J. Fluid Mech., Vol. 89, pp. 413.

55. Zaman, K.B.M.Q. and Hussain, A.K.M.F., " Vortex pairing in a circular jet under controlled exitation part-1 : General jet response", 1980, J. Fluid Mech., Vol. 101, pp. 449.

56. Zaman, K.B.M.Q. and Hussain, A.K.M.F., " Taylors hypothesis and large scale coherent structure", 1980., J. Fluid Mech. Vol.112., pp. 379 - 396.

57. Zaman, K.B.M.Q. and Hussain, A.K.M.F., " Turbulence suppression in free shear flow by controlled excitation", J. Fluid Mech.,1981, Vol. 103, pp. 133-159.

58. Zaman, K.B.M.Q. and Hussain, A.K.M.F., " Natural large-scale structure in the axisymmetric mixing layer", 1983, J. Fluid Mech.,Vol. pp.

FIGURES

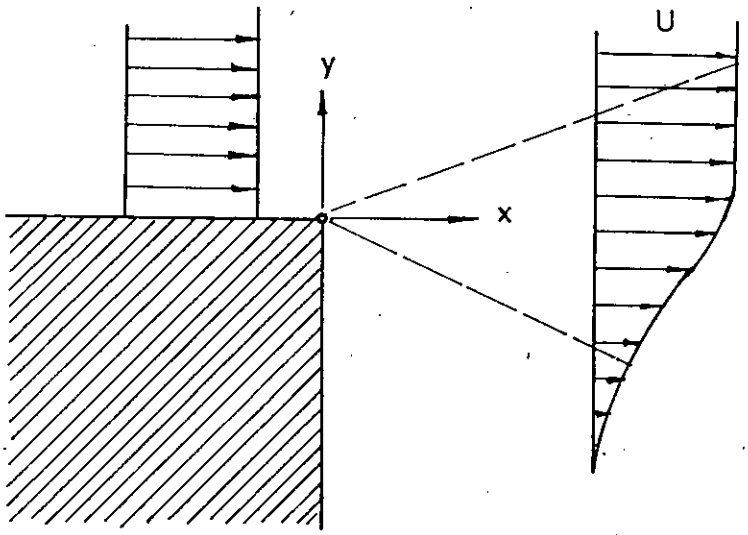

Fig. 3.2.1 Jet boundary.

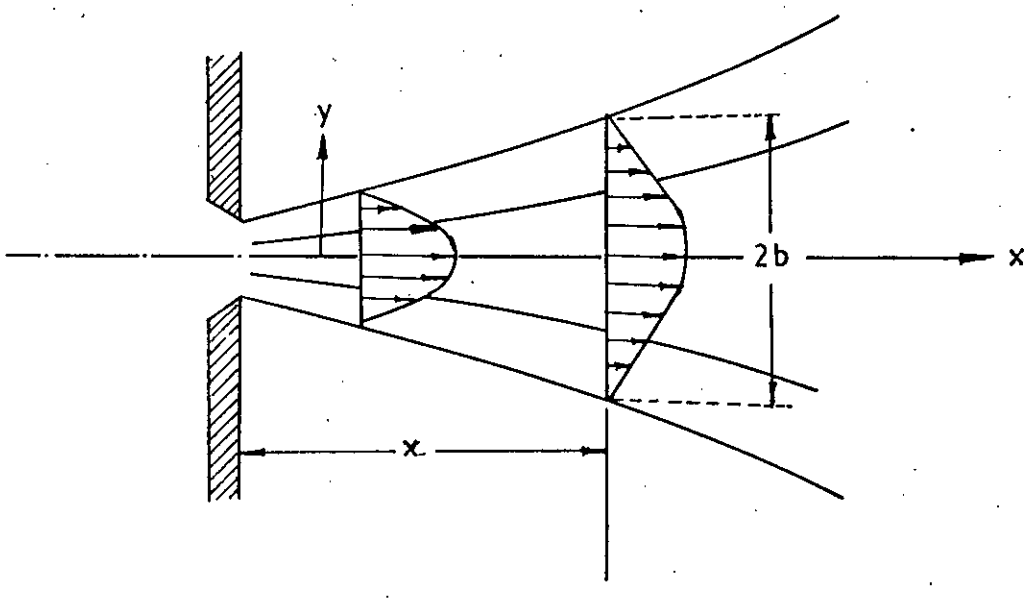

Fig. 3.2.2 Free Jet.

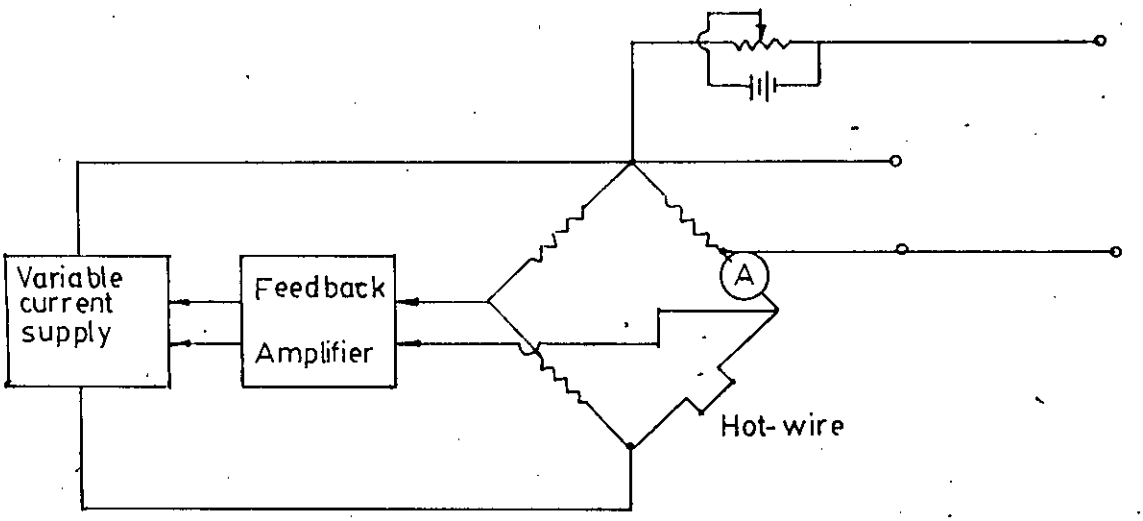

Fig. 3.4.1 : Basic constant temp. hot-wire circuit.

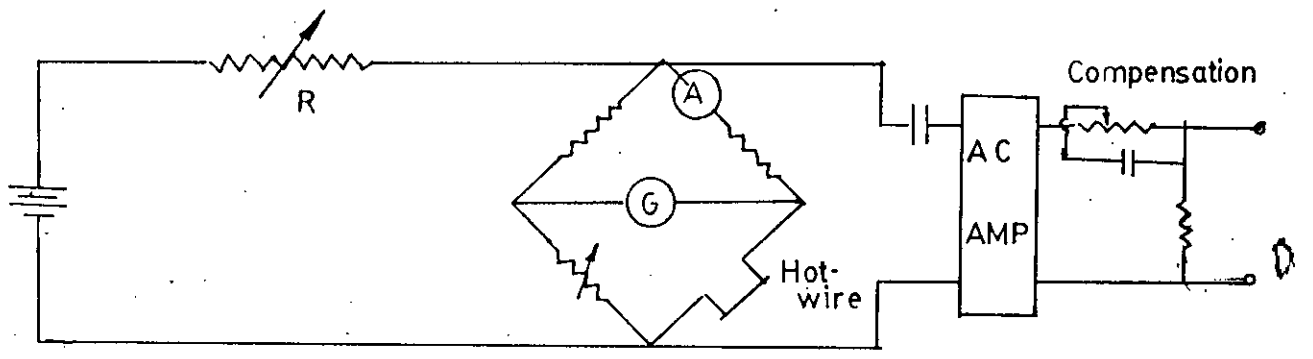

Fig. 3.4.2 : Basic constant current hot-wire circuit.

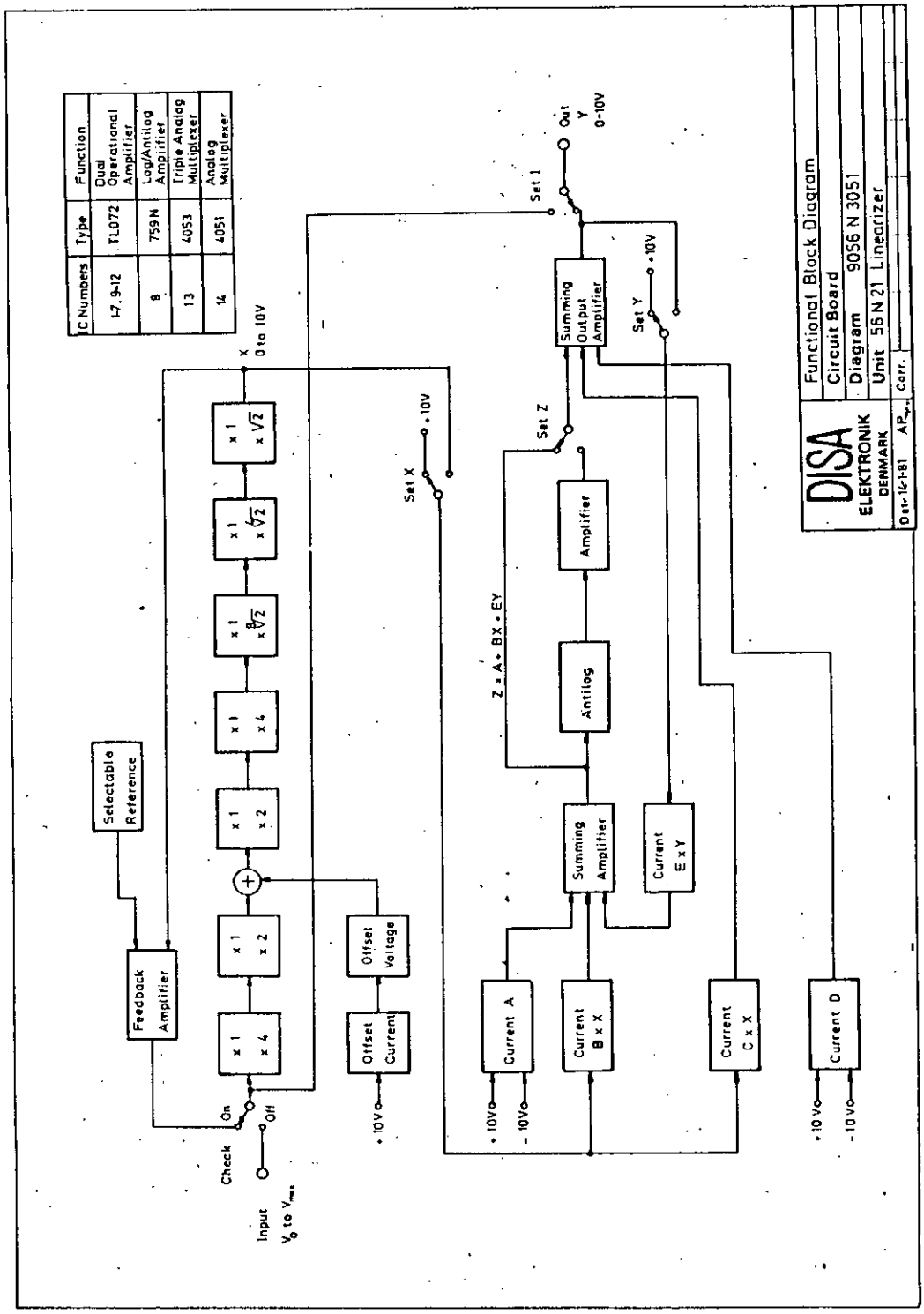

Fig. 3.5.1 Functional Block Diagram of LINEARIZER.

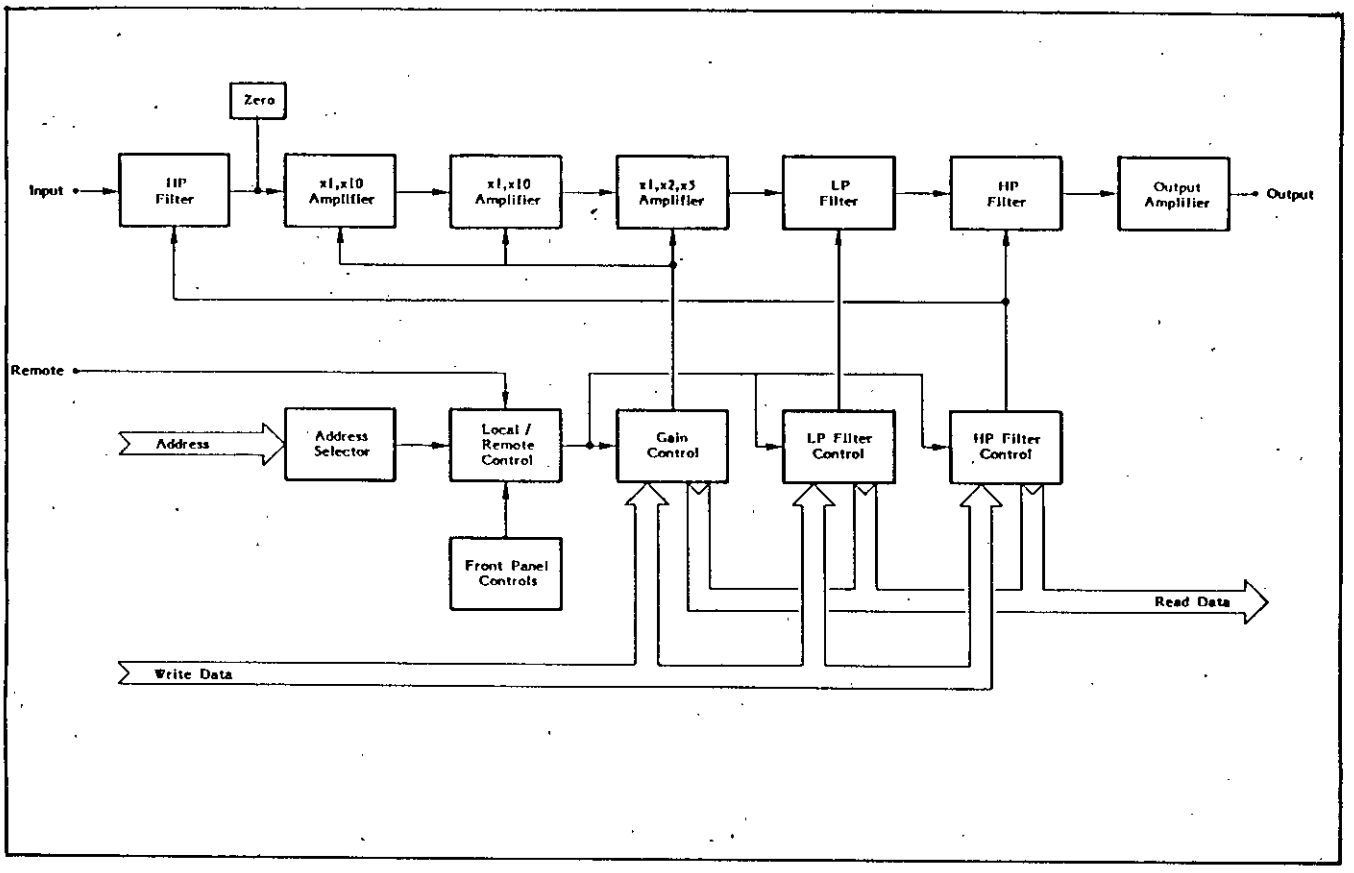

Fig. 3.5.2 *Block diagram of the 56N20 Signal Conditioner.*

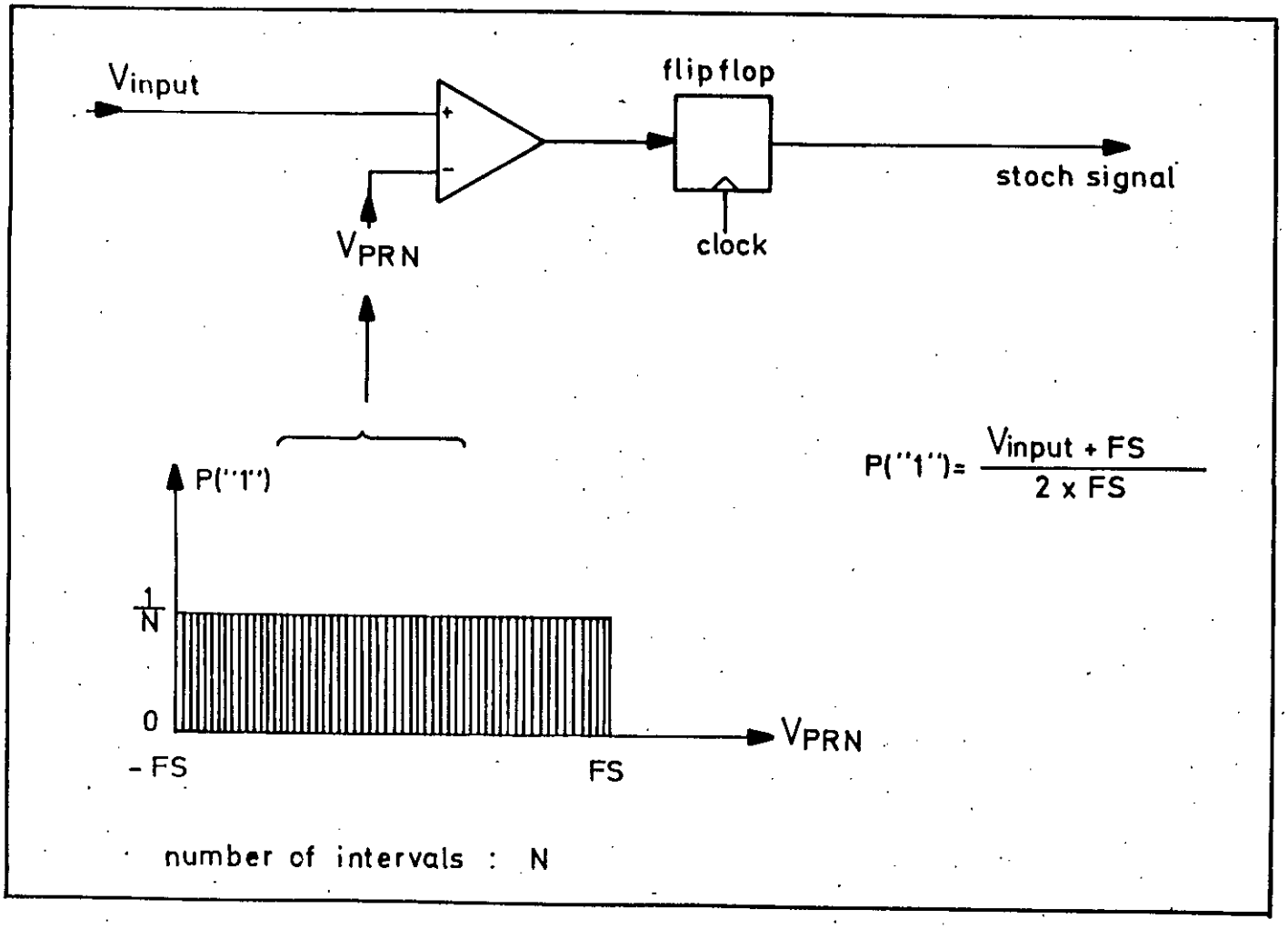

Fig. 3.5.3 : Functional diagram of DIGITIZER 56NO1.

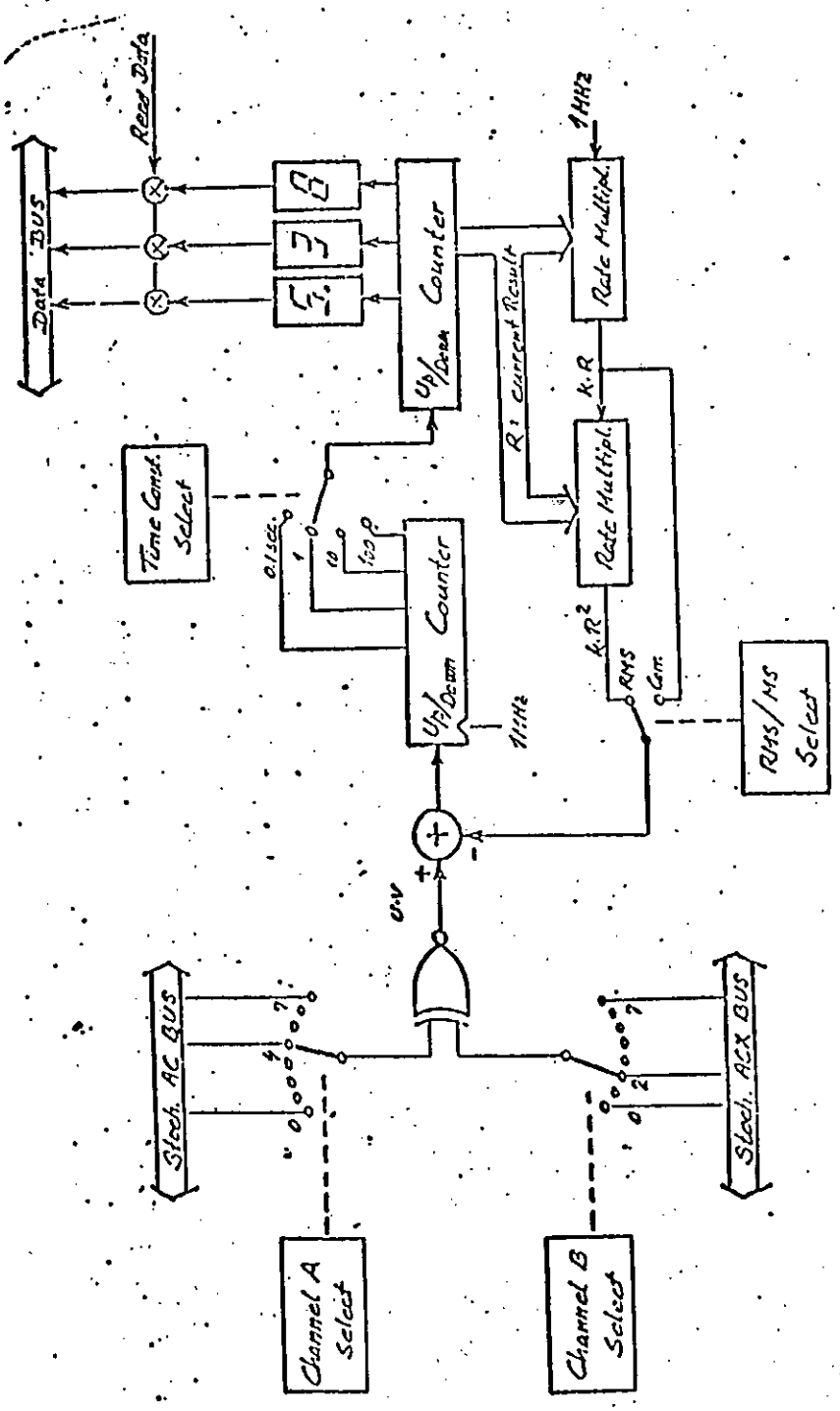

Fig. 3.5.4 : Functional block diagram of the DISA Type 56N10 RMS Value Unit.

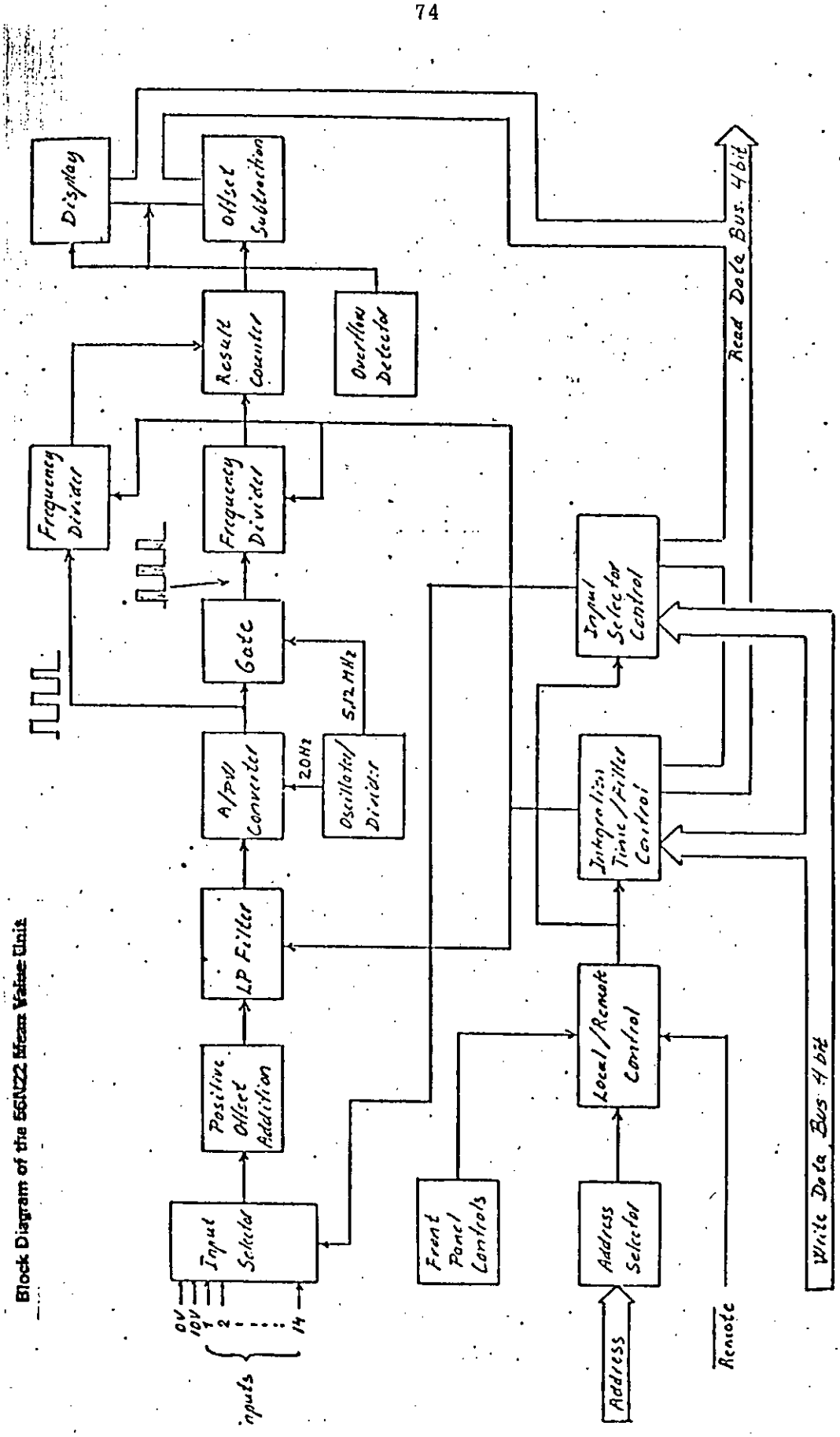

Fig. 3.5.5 : Block diagram of the 56N22 Mean Value Unit.

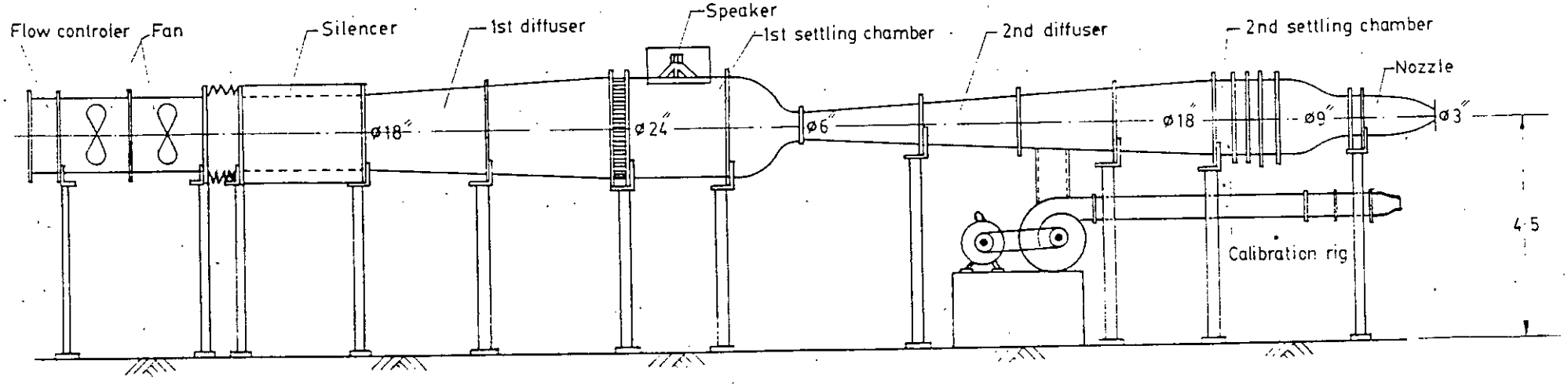

FIG. 4.1.1 CIRCULAR JET FLOW FACILITY & CALIBRATION RIG.

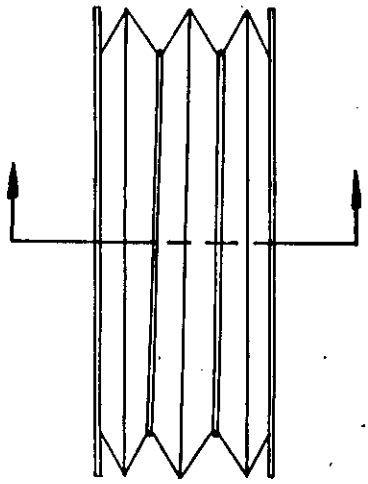

TOP VIEW

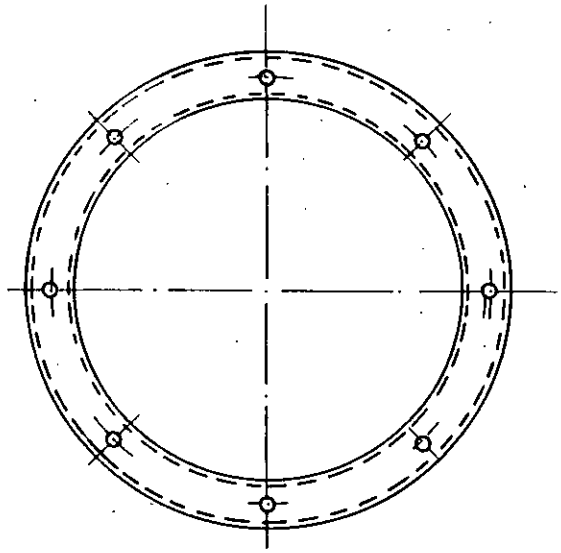

SIDE VIEW

Scale :- 1 : 10

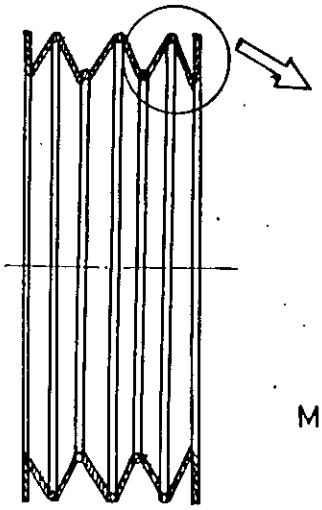

SECTIONAL FRONT VIEW

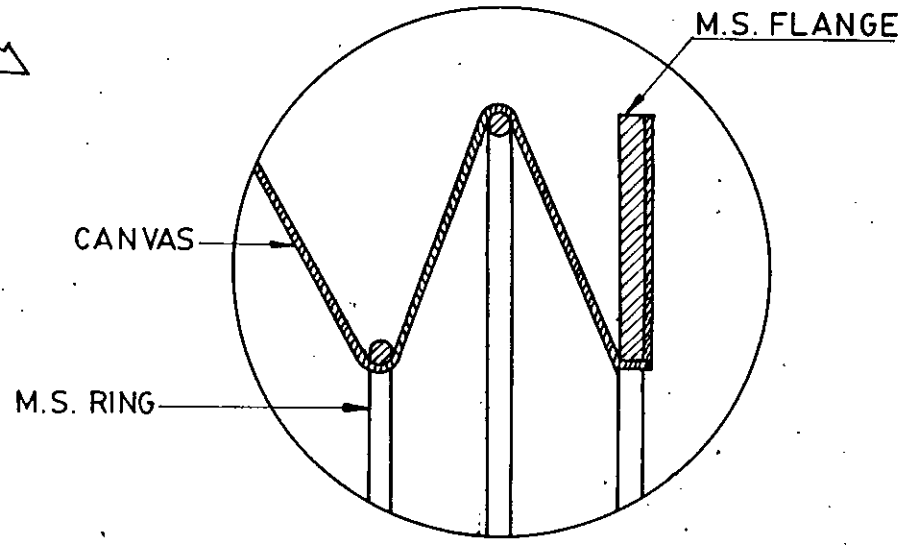

FIG. 4.1.2 VIBRATION ISOLATOR

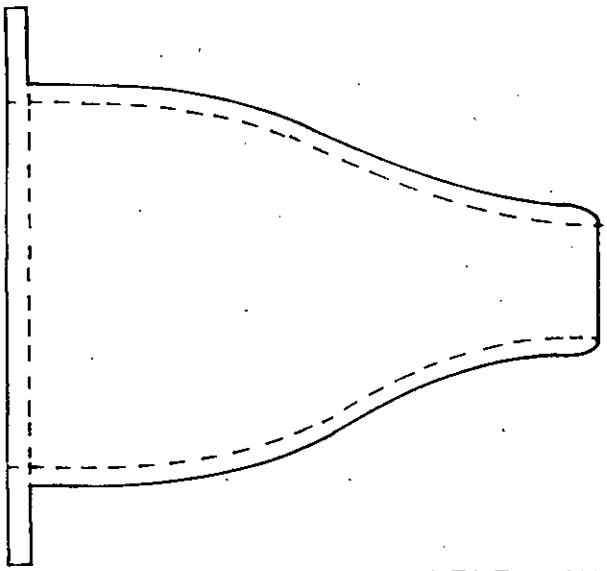

(a) NORMAL NECK NOZZLE (NN NOZZLE)

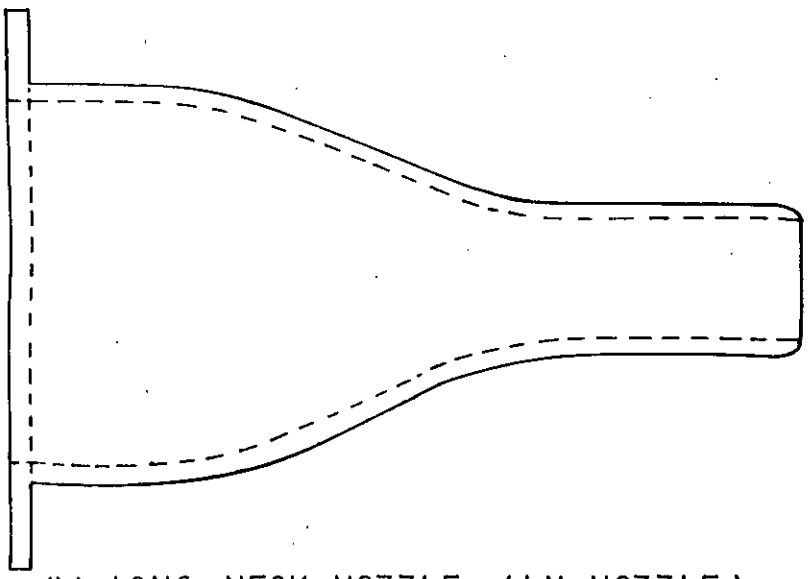

(b) LONG NECK NOZZLE (LN NOZZLE)

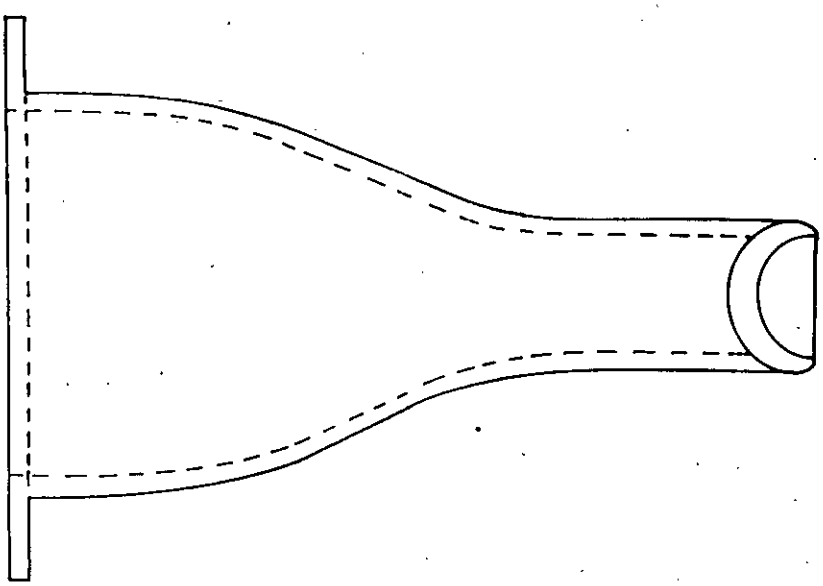

(c) WEDGE SHAPED NOZZLE (WS NOZZLE)

FIG. 4.1.3 NOZZLES

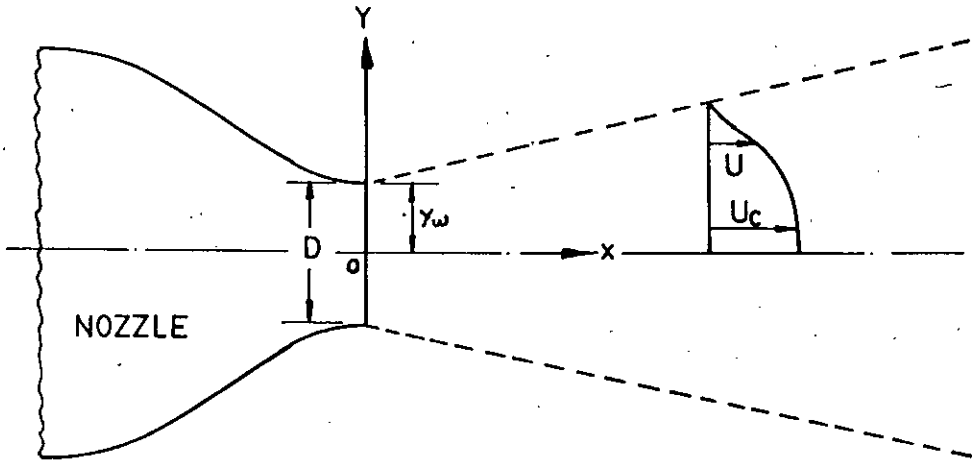

FIG. 4.2.1 COORDINATE SYSTEM OF THE FLOW

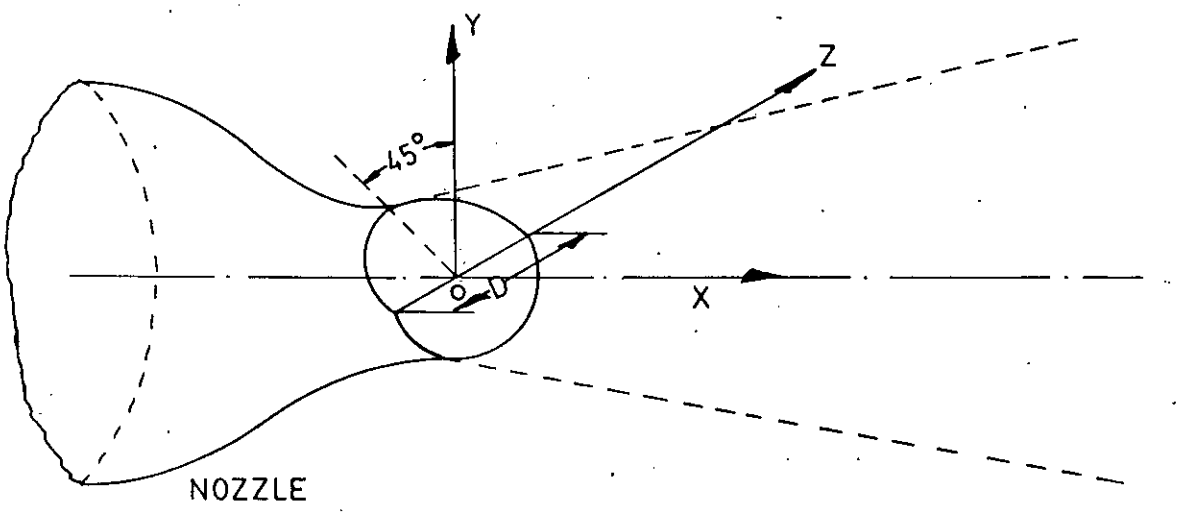

FIG. 4.2.2 CO-ORDINATE SYSTEM OF WEDGE SHAPED JET

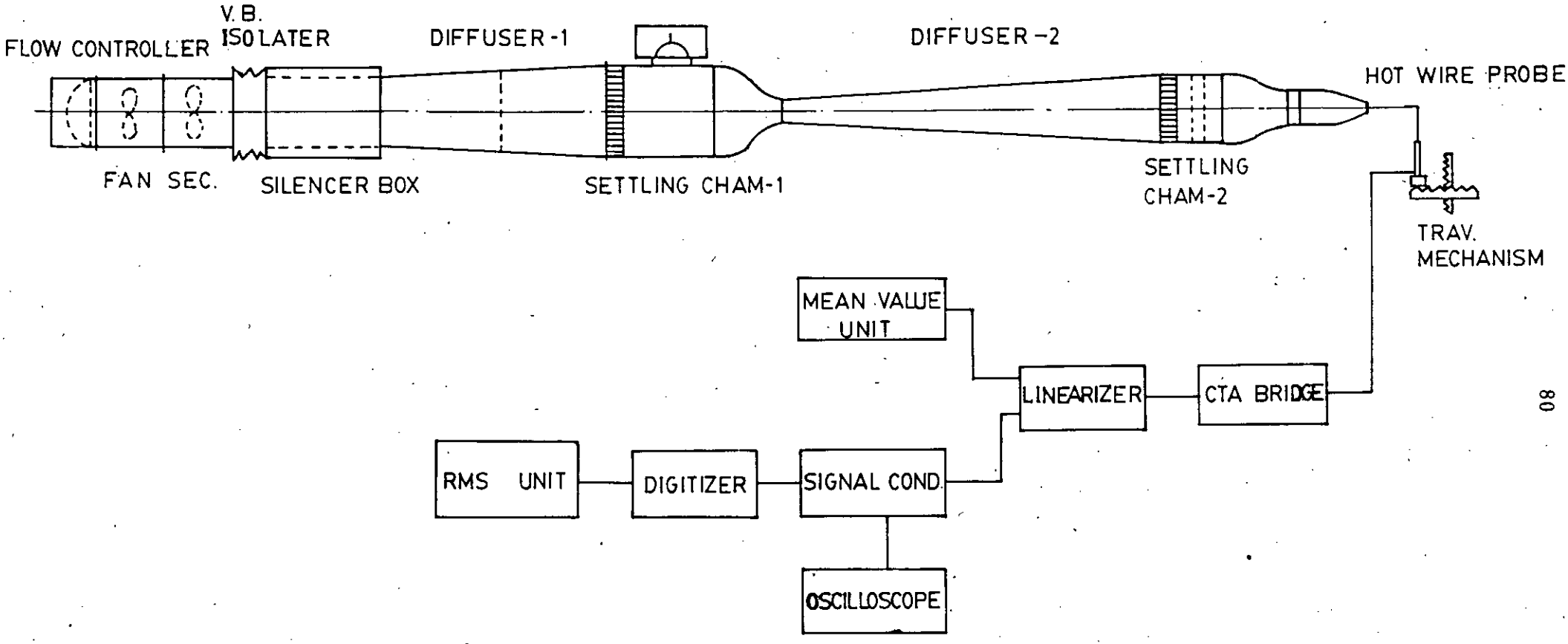

FIG. 4.7.1 SCHEMATIC DIAGRAM OF FLOW FACILITY WITH CTA001 MEASURING SYSTEM

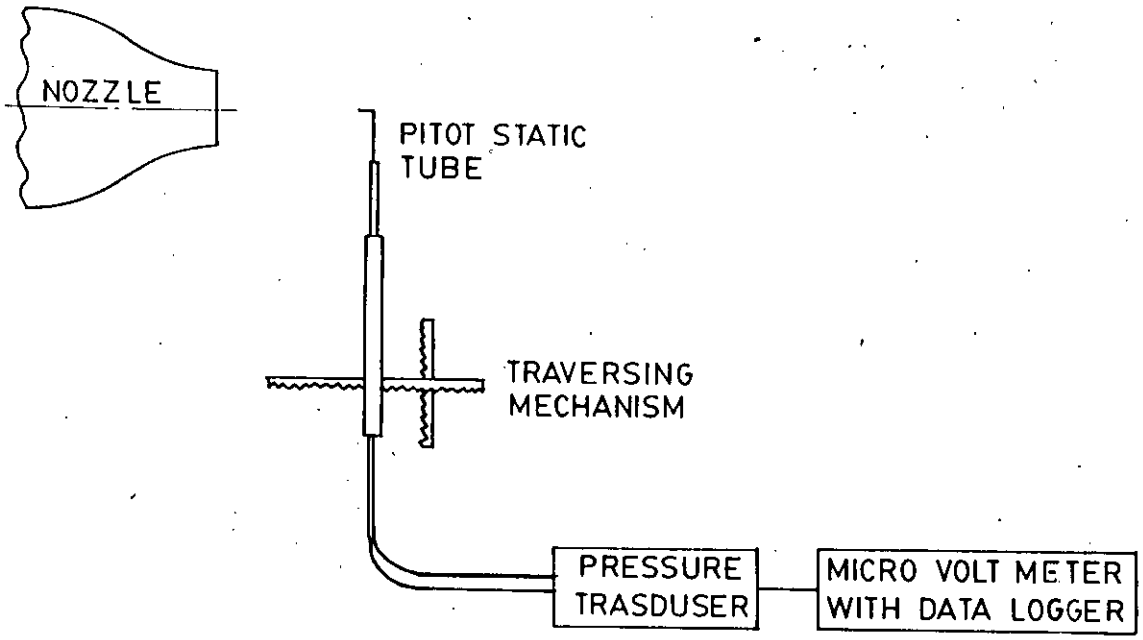

(a)

FIG. 4.7.2.SCHEMATIC DIAGRAM OF APPARATUS SET-UP FOR MEAN MEASUREMENT WITH PITOT STATIC TUBE

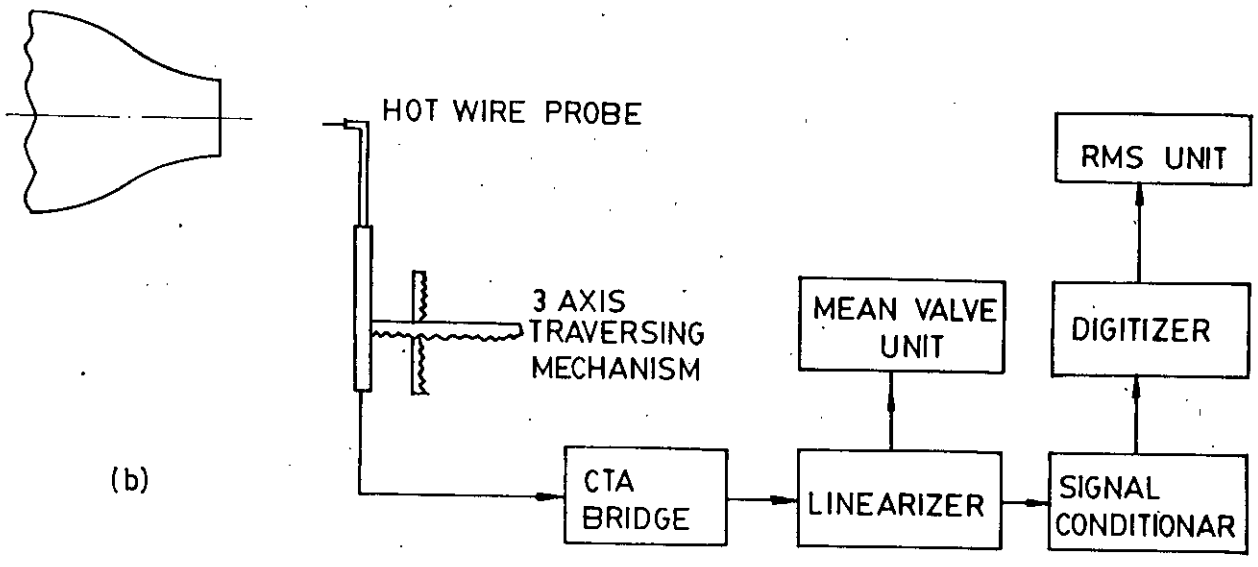

(b)

FIG 4.7.2b SCHEMATIC DIAGRAM OE SET-UP FOR MEASUREMENT OF MEAN AND TURBULENT QUALITY BY HOT-WIRE TECHNIQUE

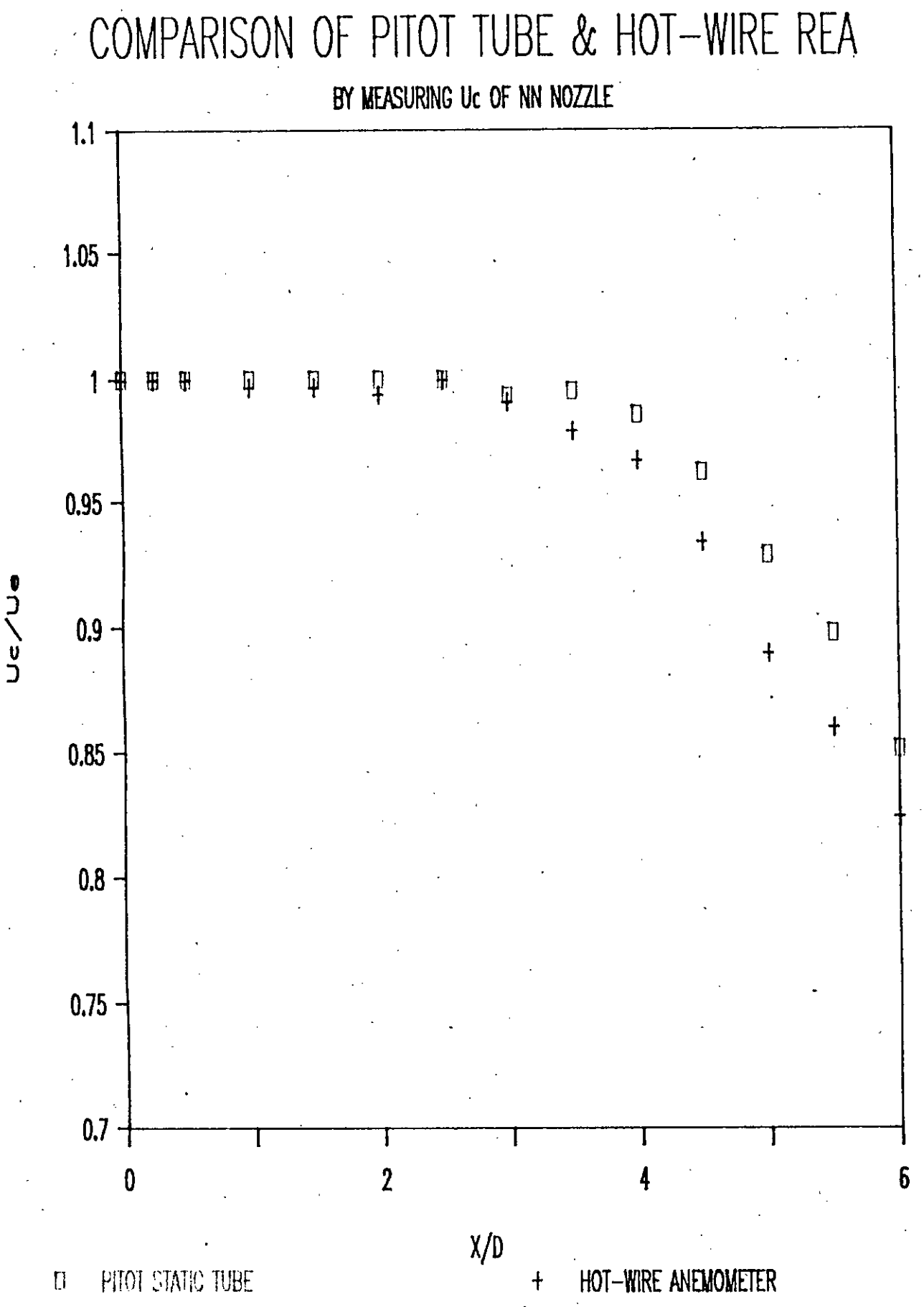

Fig. 4.7.3 : Comparison of hot-wire reading with that obtained by pitot-static tube and transducer.

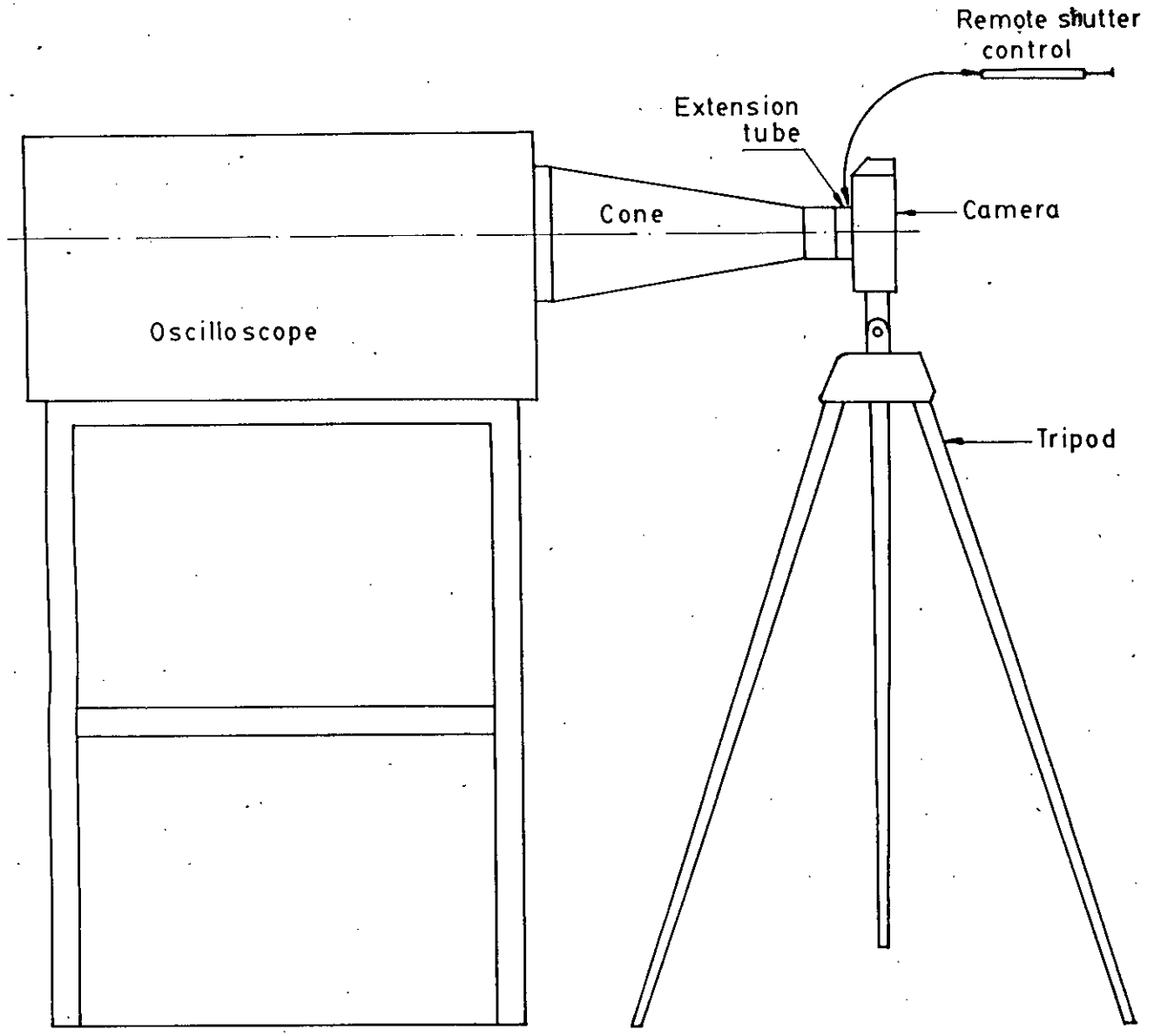

Fig. 4.8.1 Schemetic diagram of the arrengement for recording the oscilloscope traces

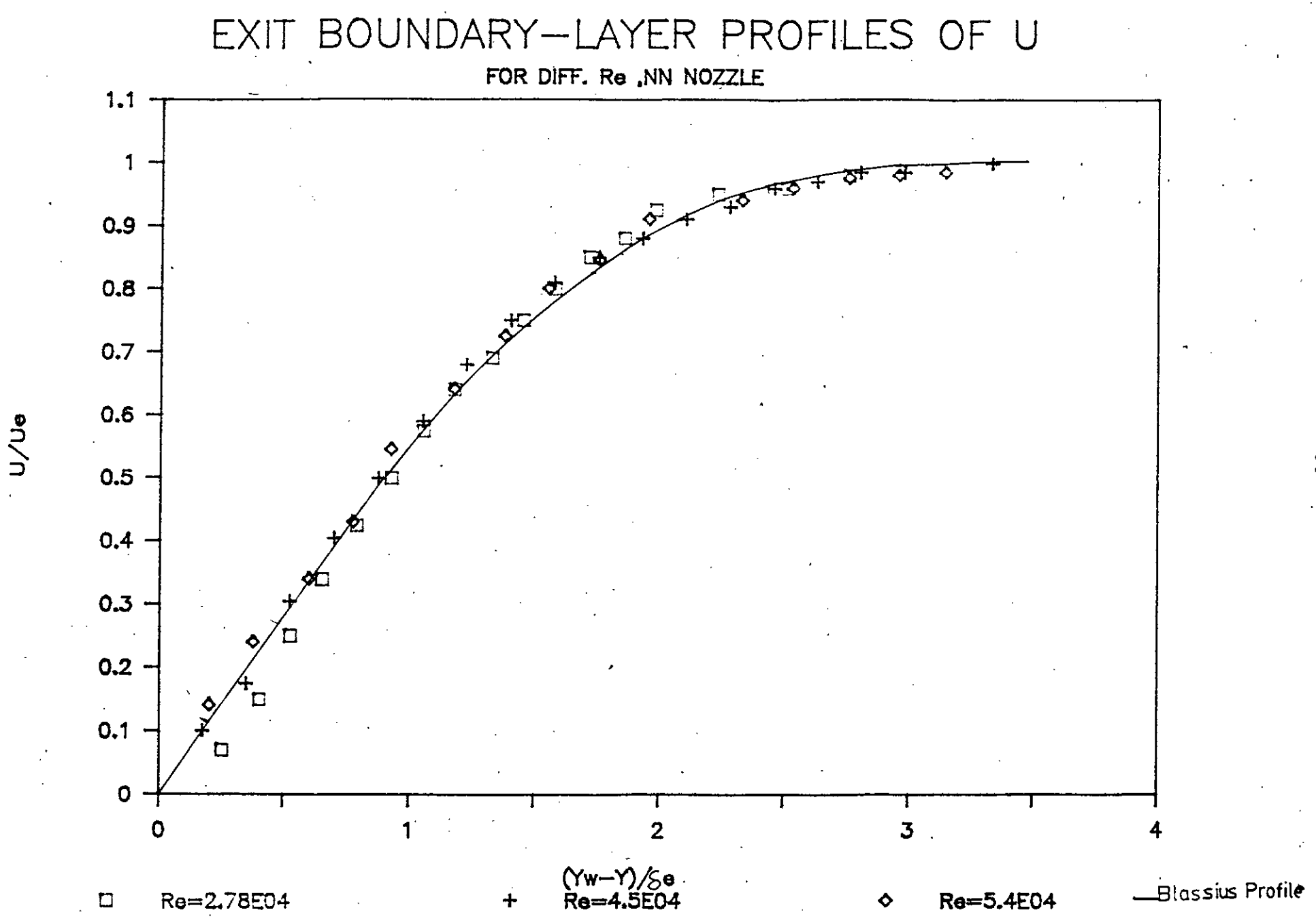

Fig. 5.2.1 : Exit boundary layer profiles of mean velocity (U) for different Reynolds numbers, of NN nozzle.

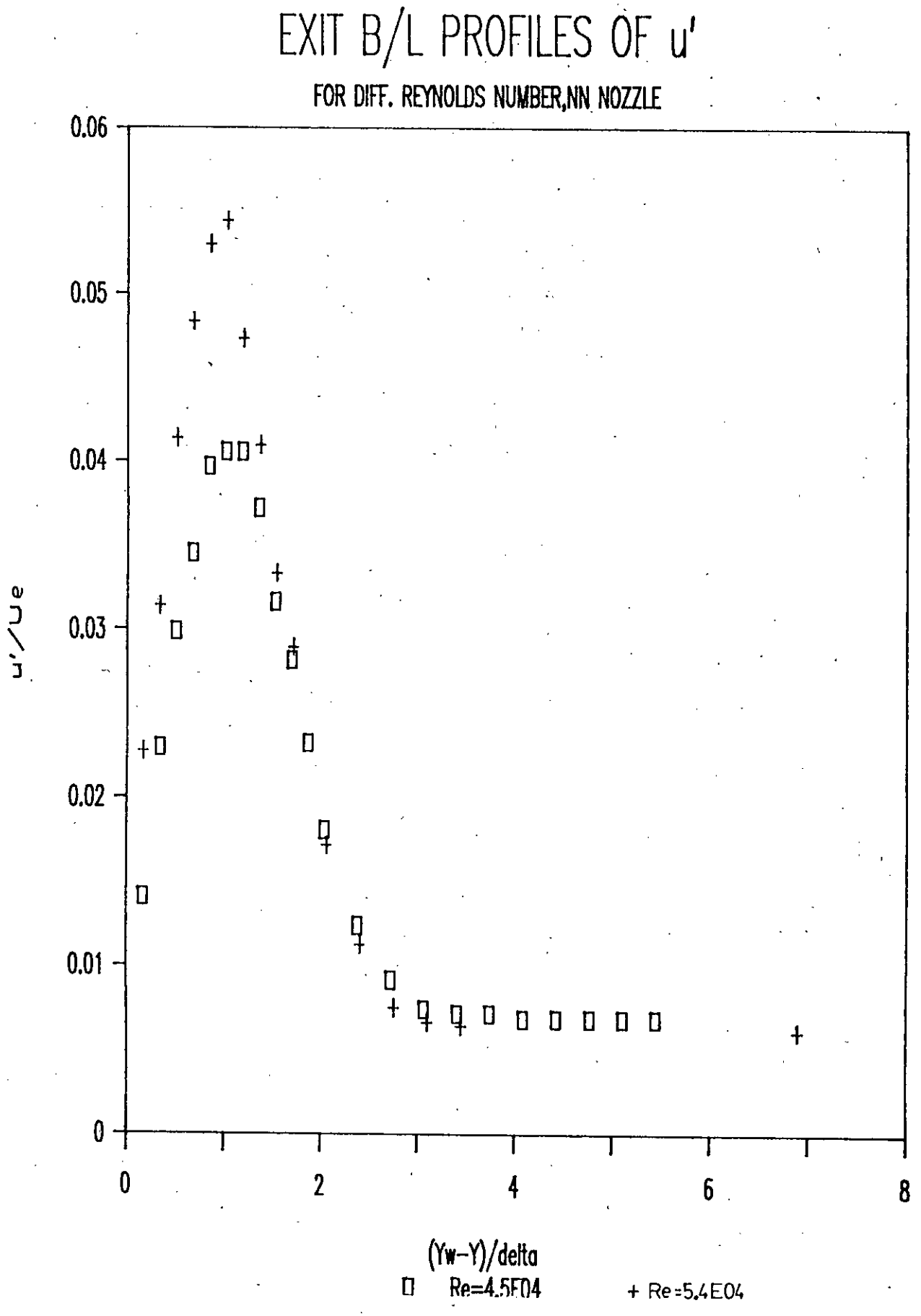

Fig.5.2.2 : Exit boundary layer profiles of longitudinal turbulence intensity for different Reynolds numbers of NN nozzle.

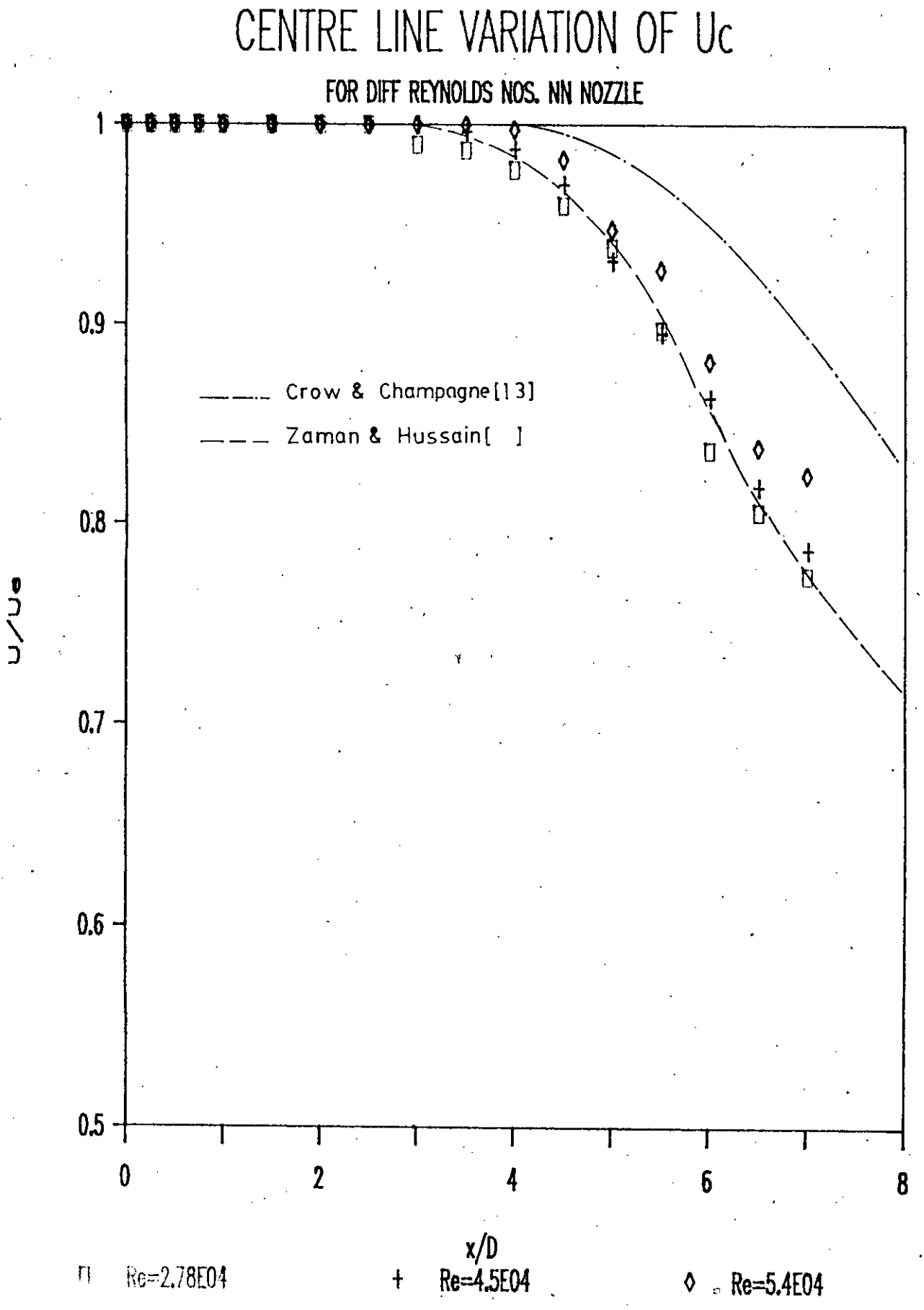

Fig. 5.2.3 : Centre line variation of mean velocity profiles for different Re of NN nozzle.

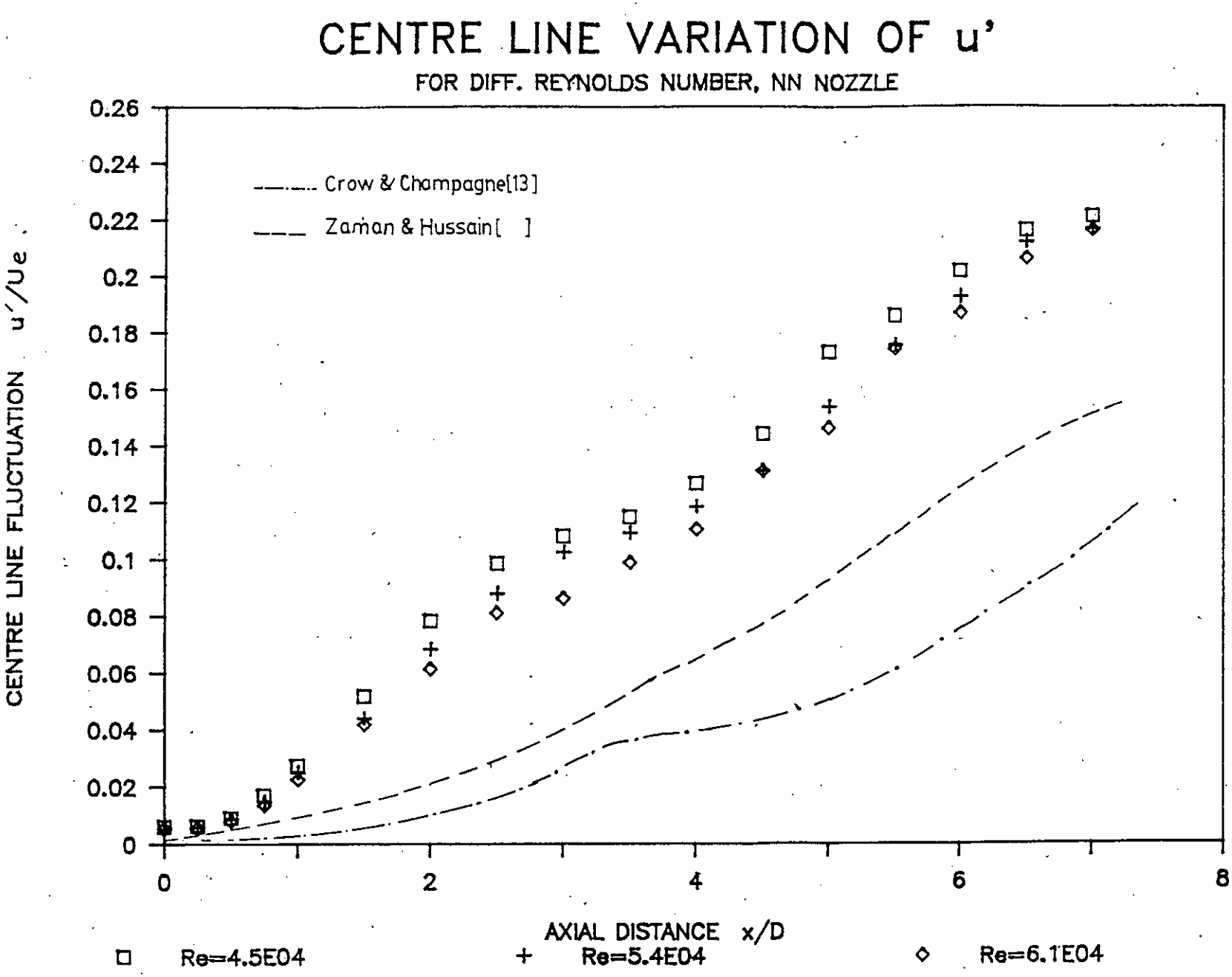

Fig. 5.2.4 : Centre line variation of lingitudinal turbulence intensity (U') profile for different Reynolds number of Nn nozzle.

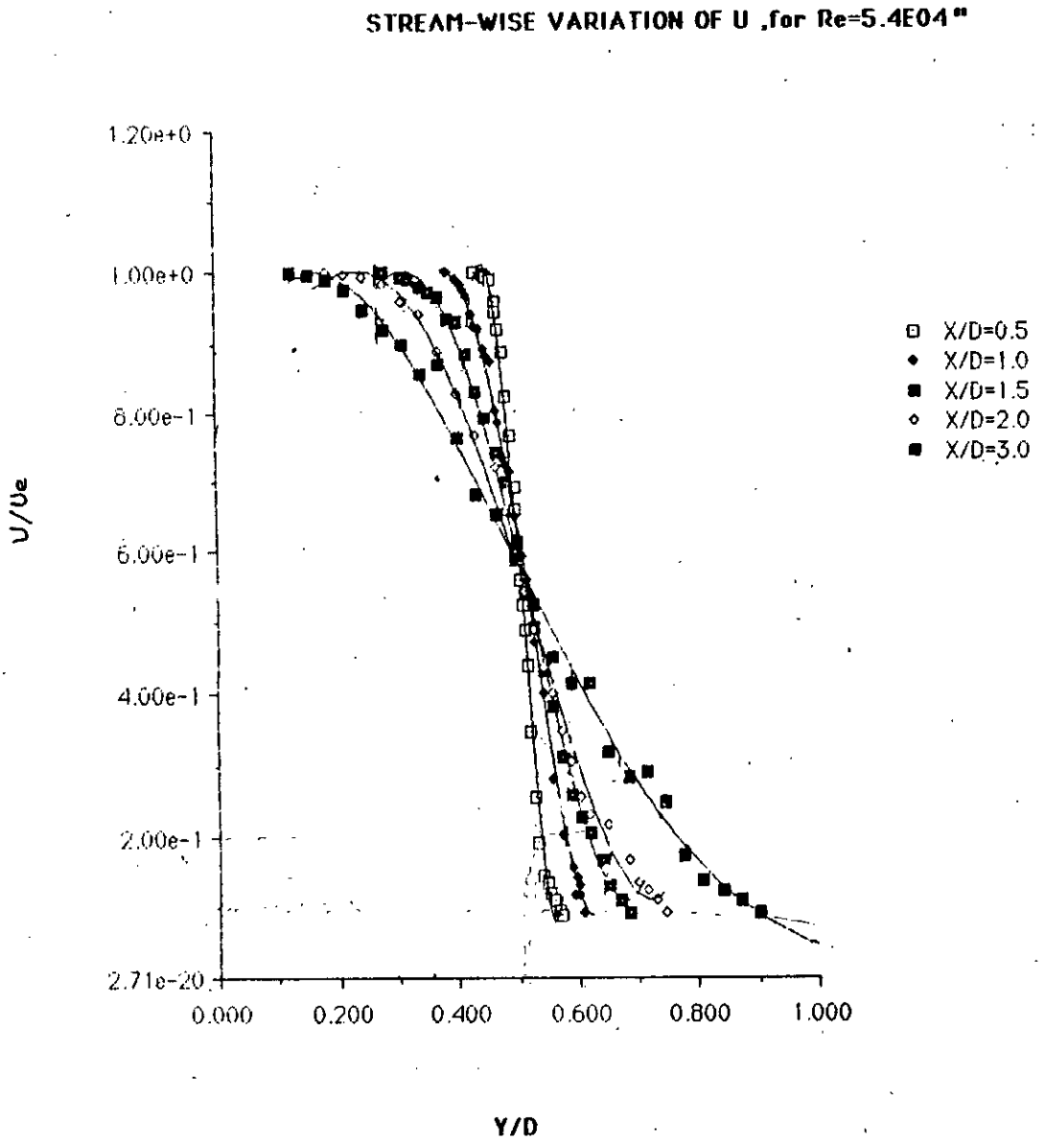

Fig. 5.2.5 : Stream-wise evolution of mean velocity (U) profiles for different x/D location of NN nozzle.

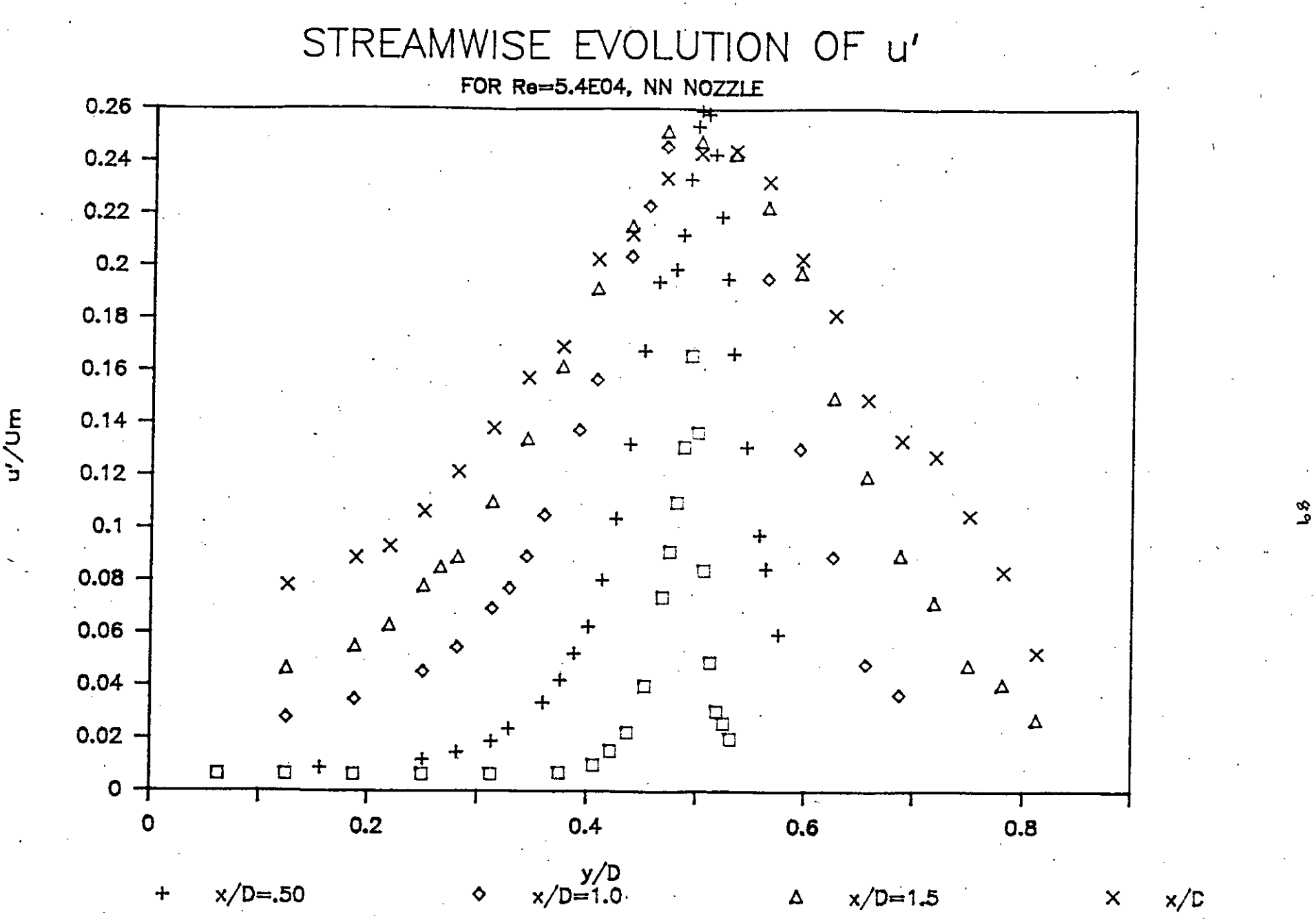

Fig. 5.2.6 : Stream-wise evolution of longitudinal turbulence intensity (u') profiles of NN nozzle.

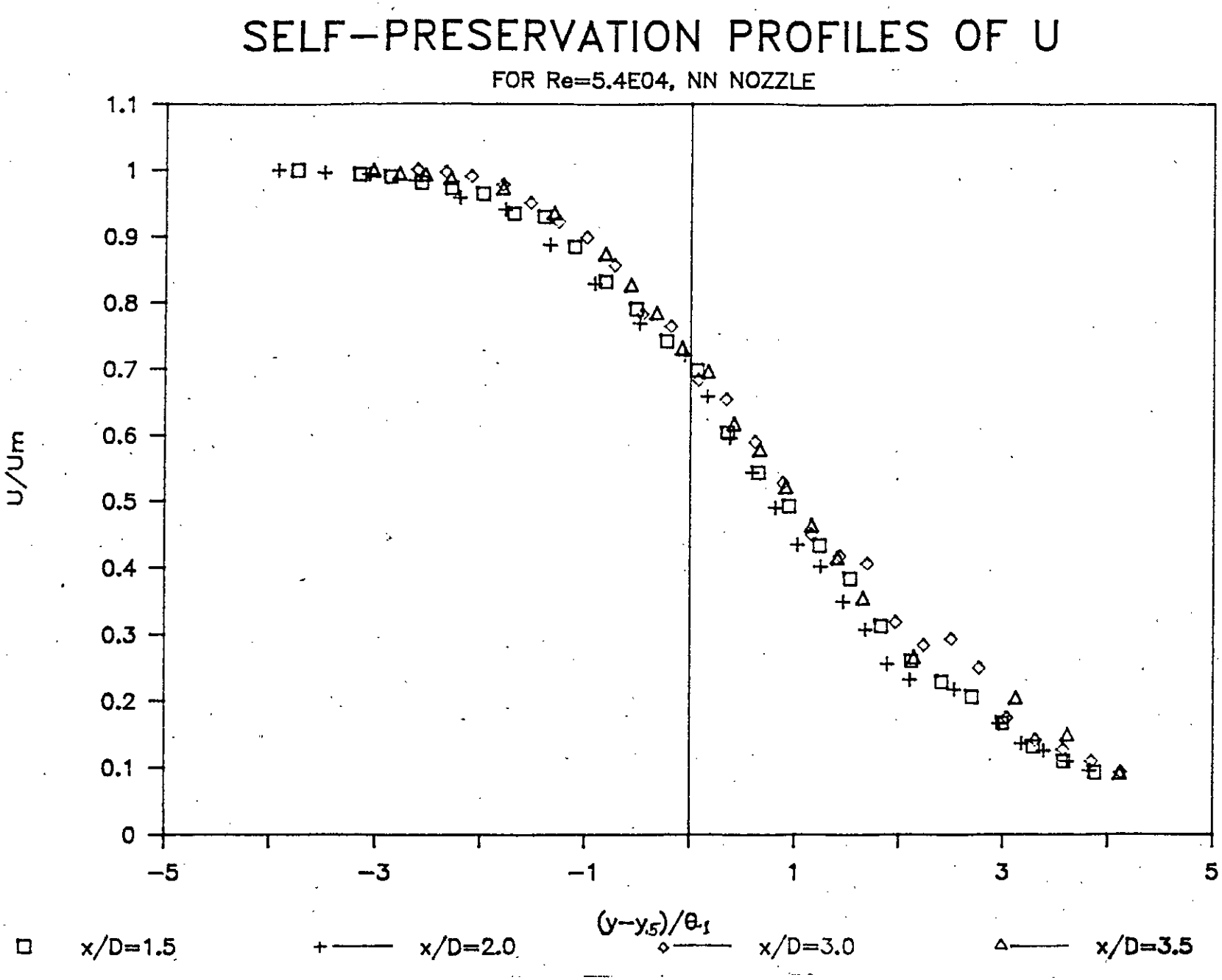

Fig. 5.2.7 : Self-preservation profiles of mean velocity (U) for Re = 5.4 x 10^4, of NN nozzle.

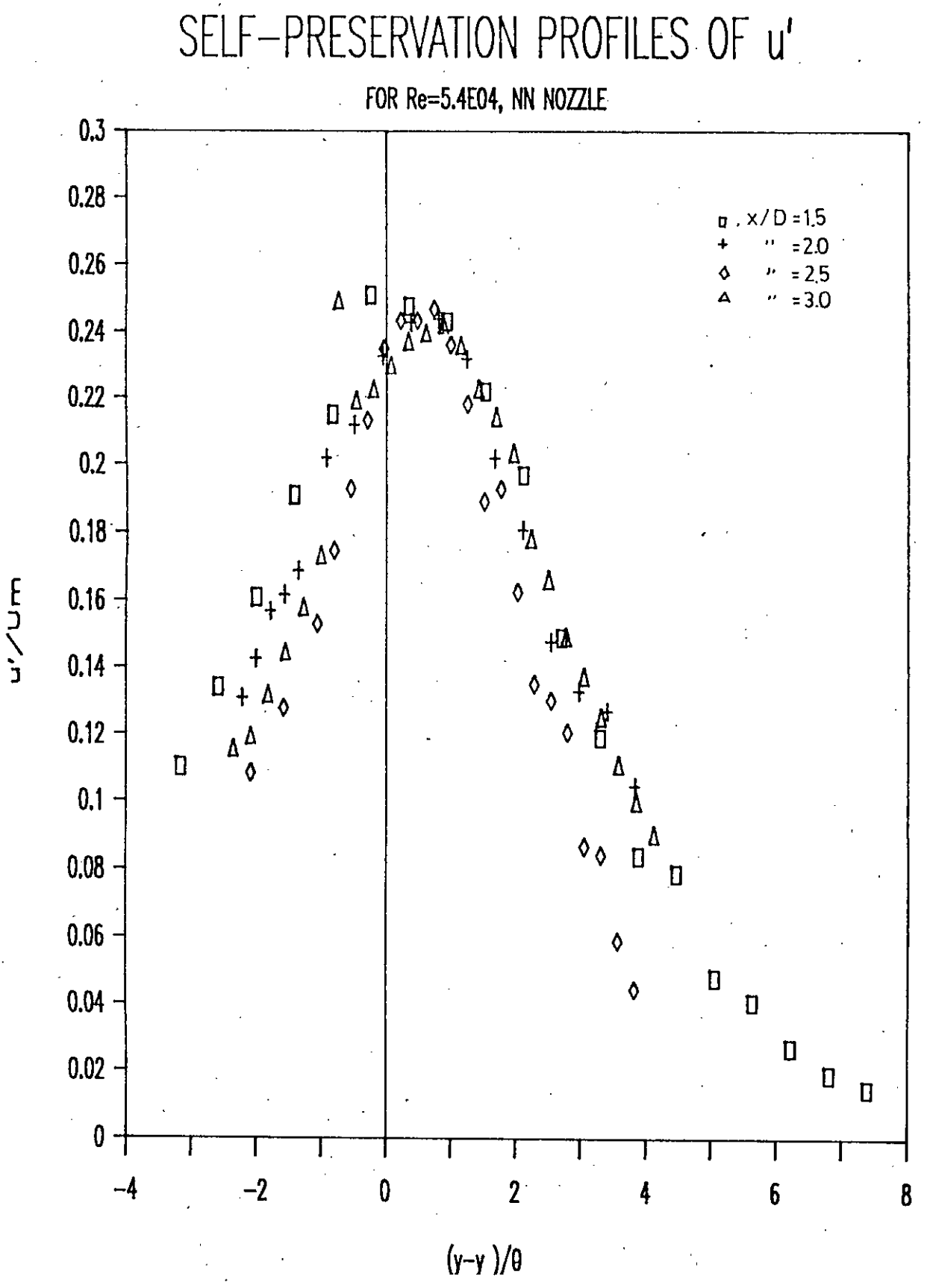

Fig. 5.2.8 : Self-preservation profiles of longitudinal turbulence intencity (u') for Re = 5.4 x 10^4 of NN nozzle.

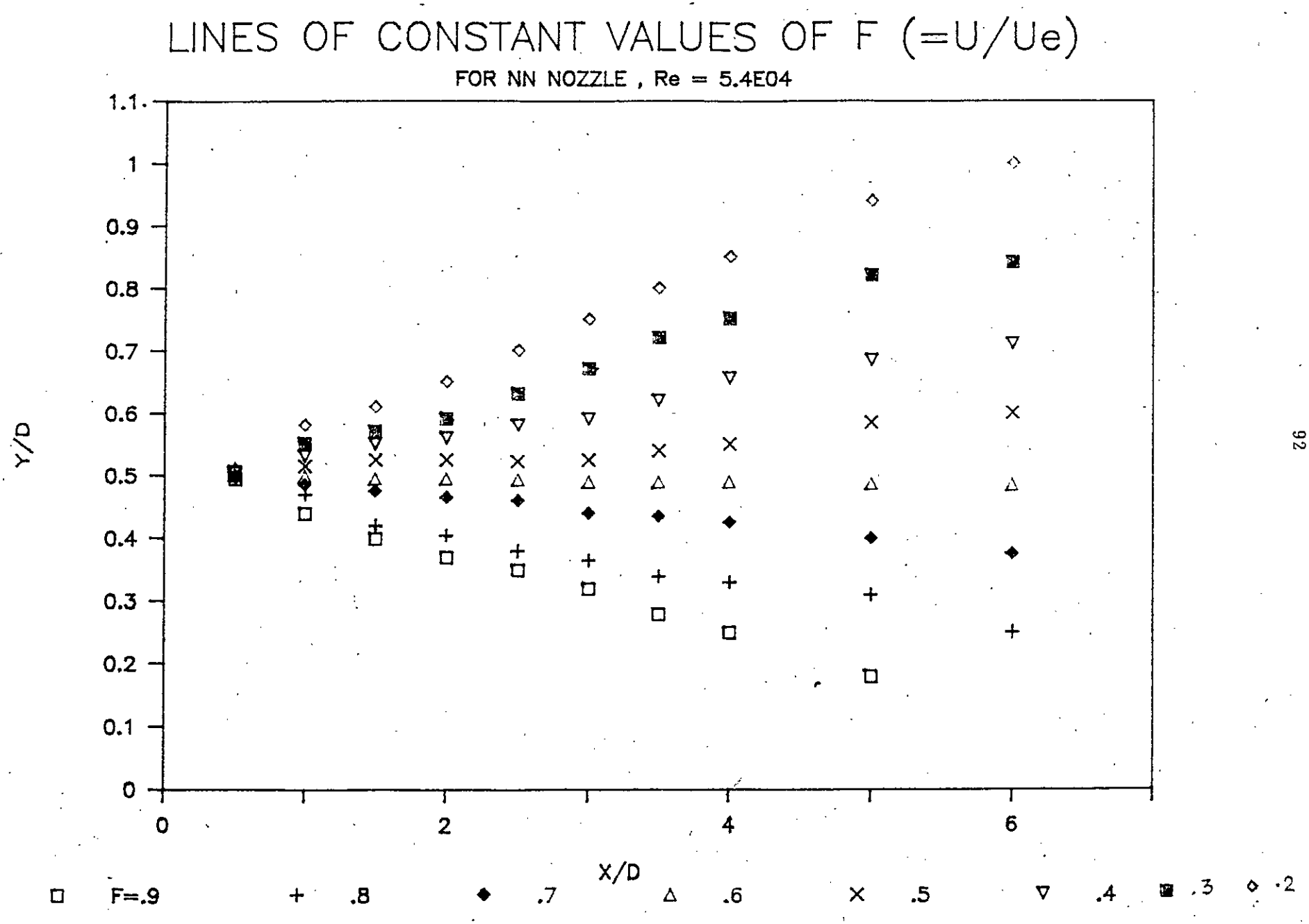

Fig. 5.2.9 : Constant mean velocity lines of NN nozzle for Re = 5.4 x 10^4.

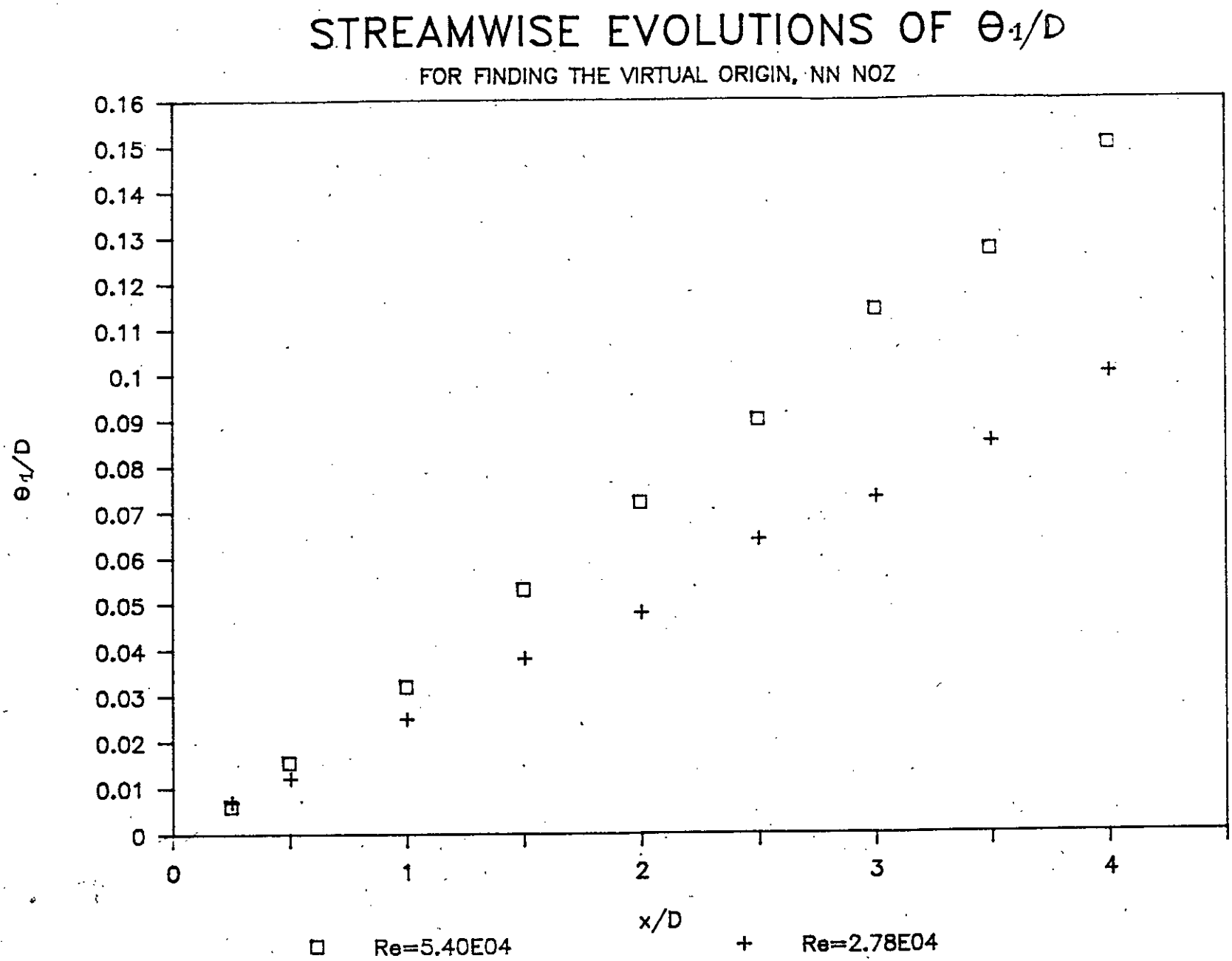

Fig. 5.2.10 : Variation of local momentum thickness in axial direction for finding the virtual origin.

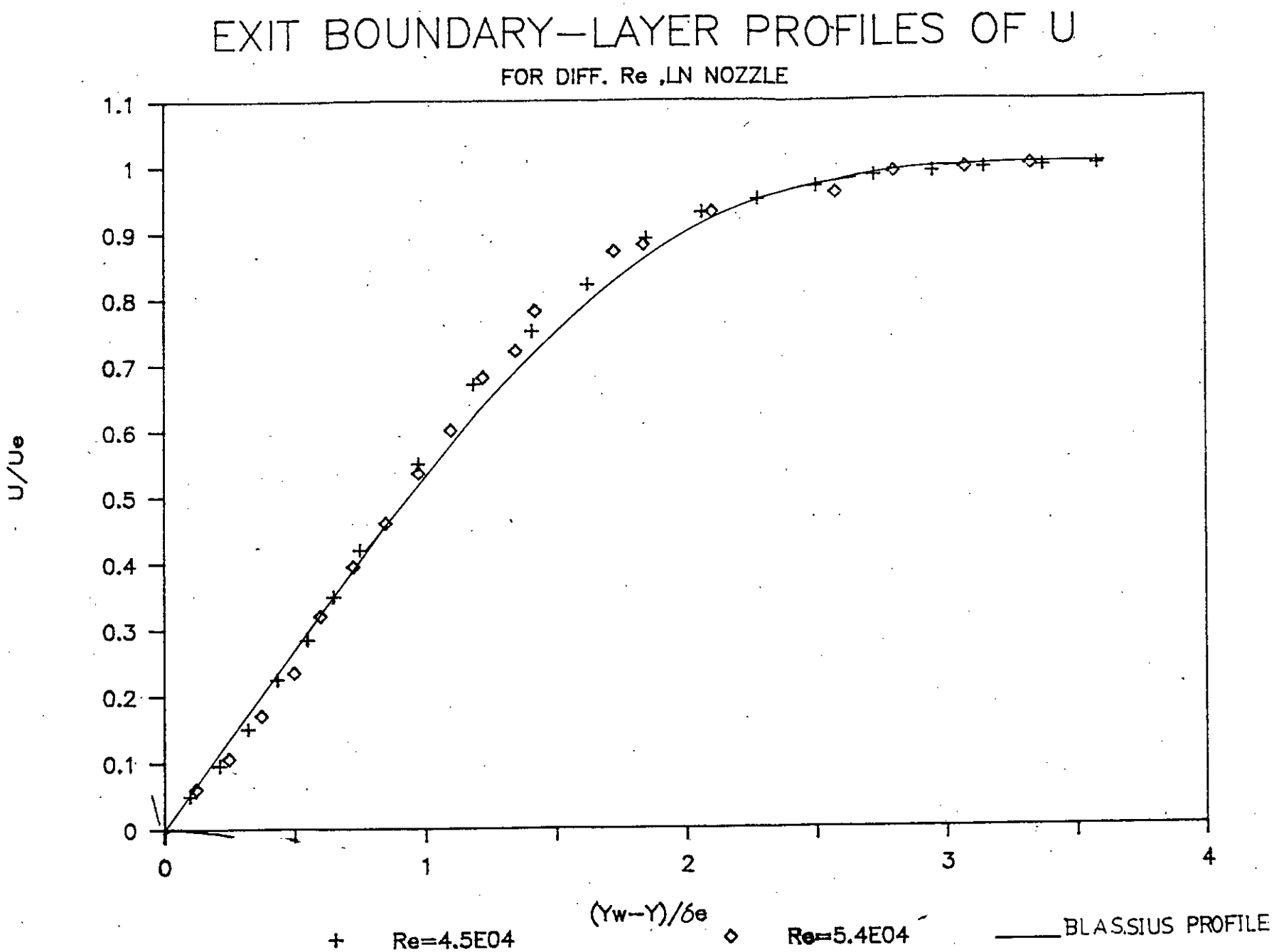

Fig. 5.3.1 : Exit boundary layer profiles of mean velocity (Ū) for different Reynolds number of LN nozzle.

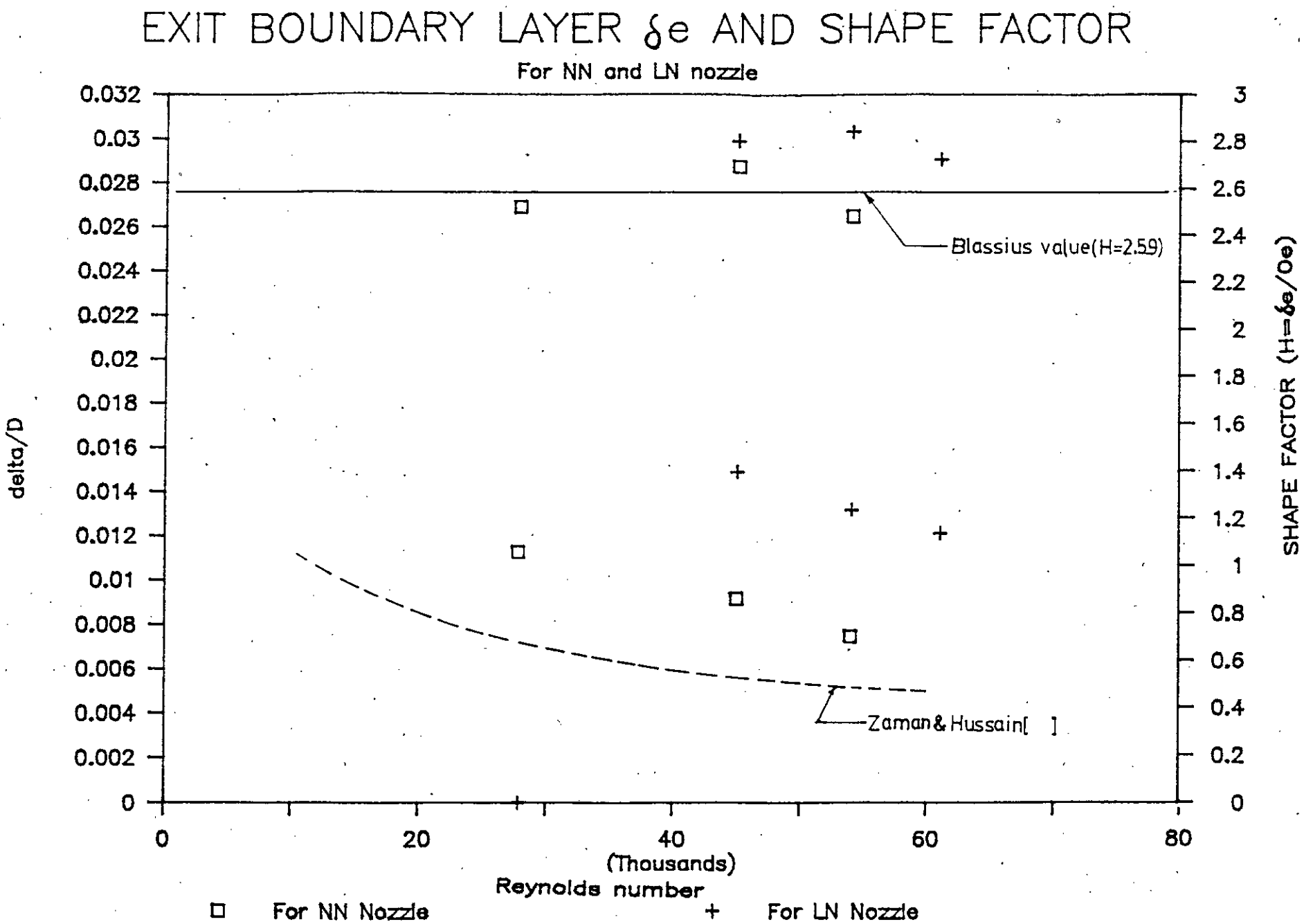

Fig. 5.3.2 : Exit boundary layer displacement thickness and shape factor distribution over the Re no. range of NN & LN nozzle.

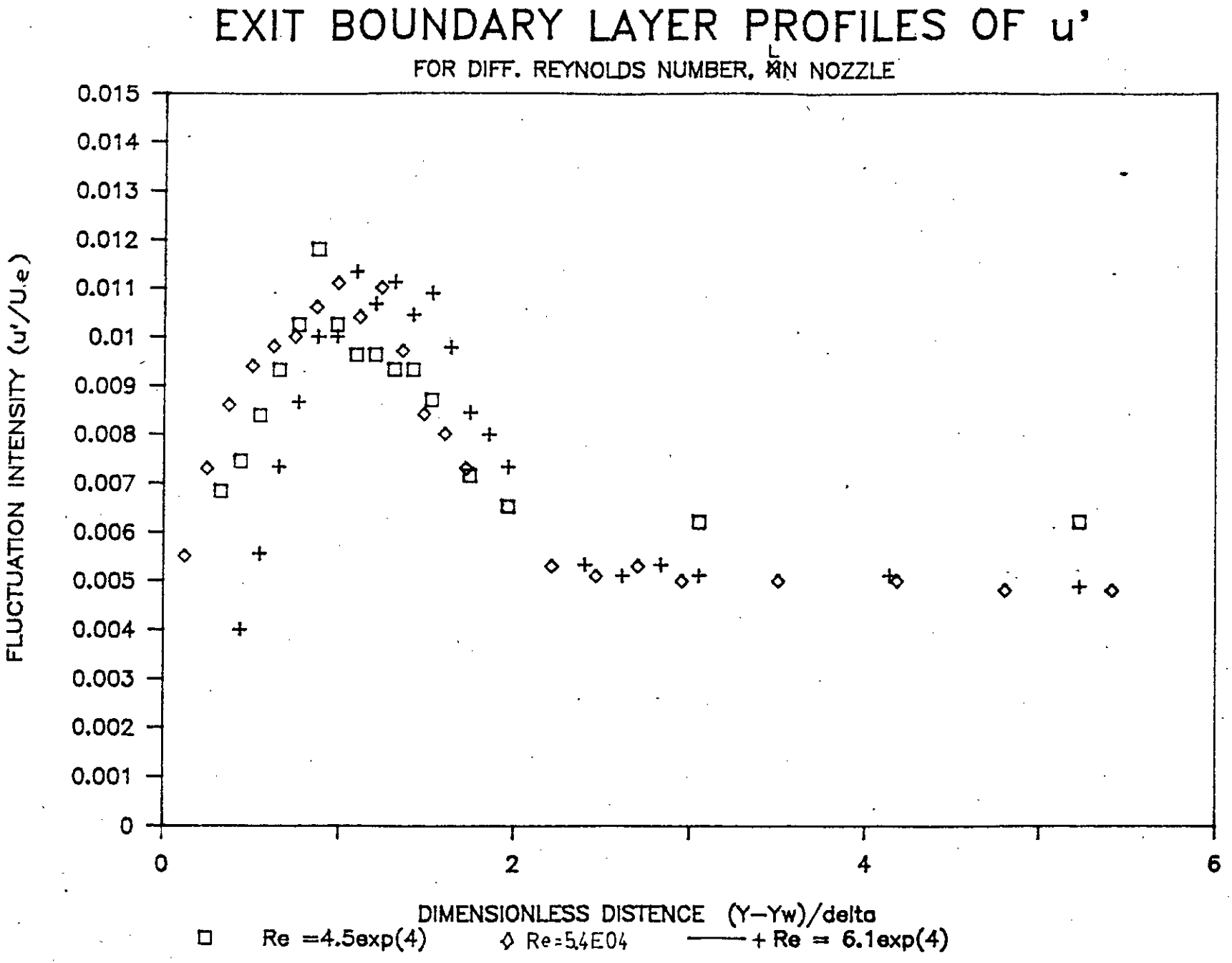

Fig. 5.3.3 : Exit boundary layer profiles of longitudinal turbulence intencity for Re = 4.5×10^4, 6.1×10^4 of LN nozzle.

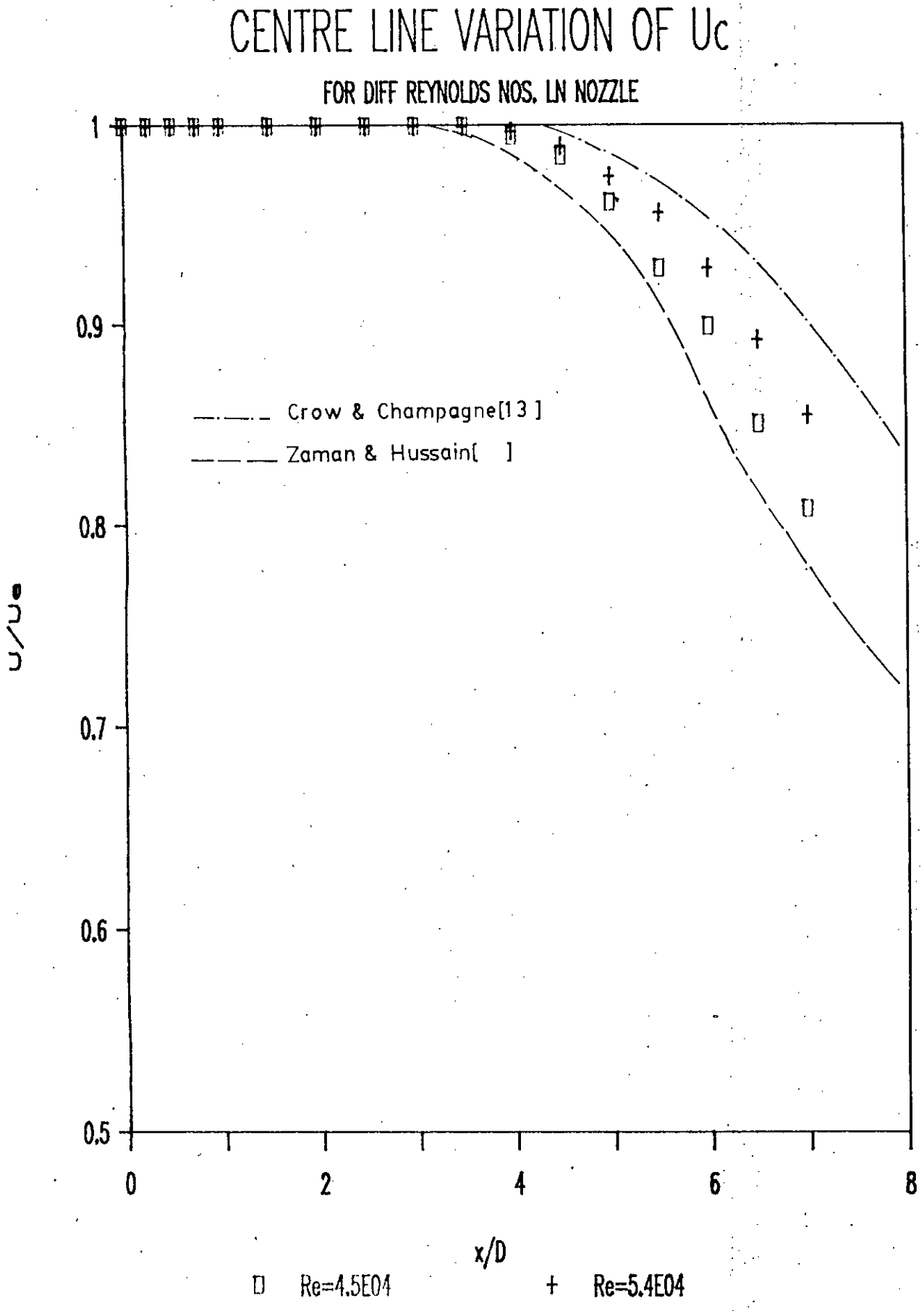

Fig. 5.3.4 : Centre line variation of mean velocity profiles for different Re of LN nozzle.

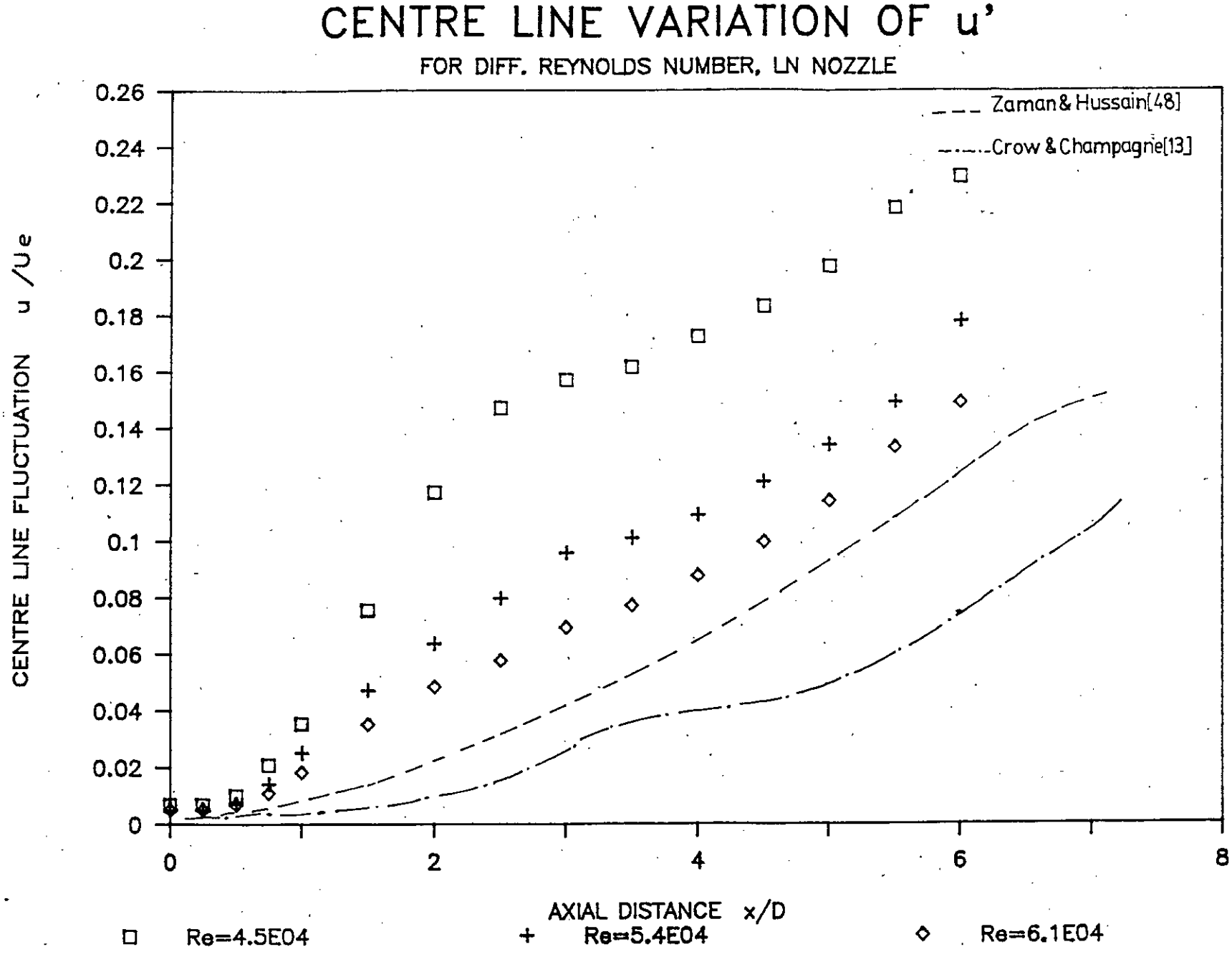

Fig. 5.3.5 : Centre line variation of longitudinal turbulence intensity (u') profiles for different Reynolds number of LN nozzle.

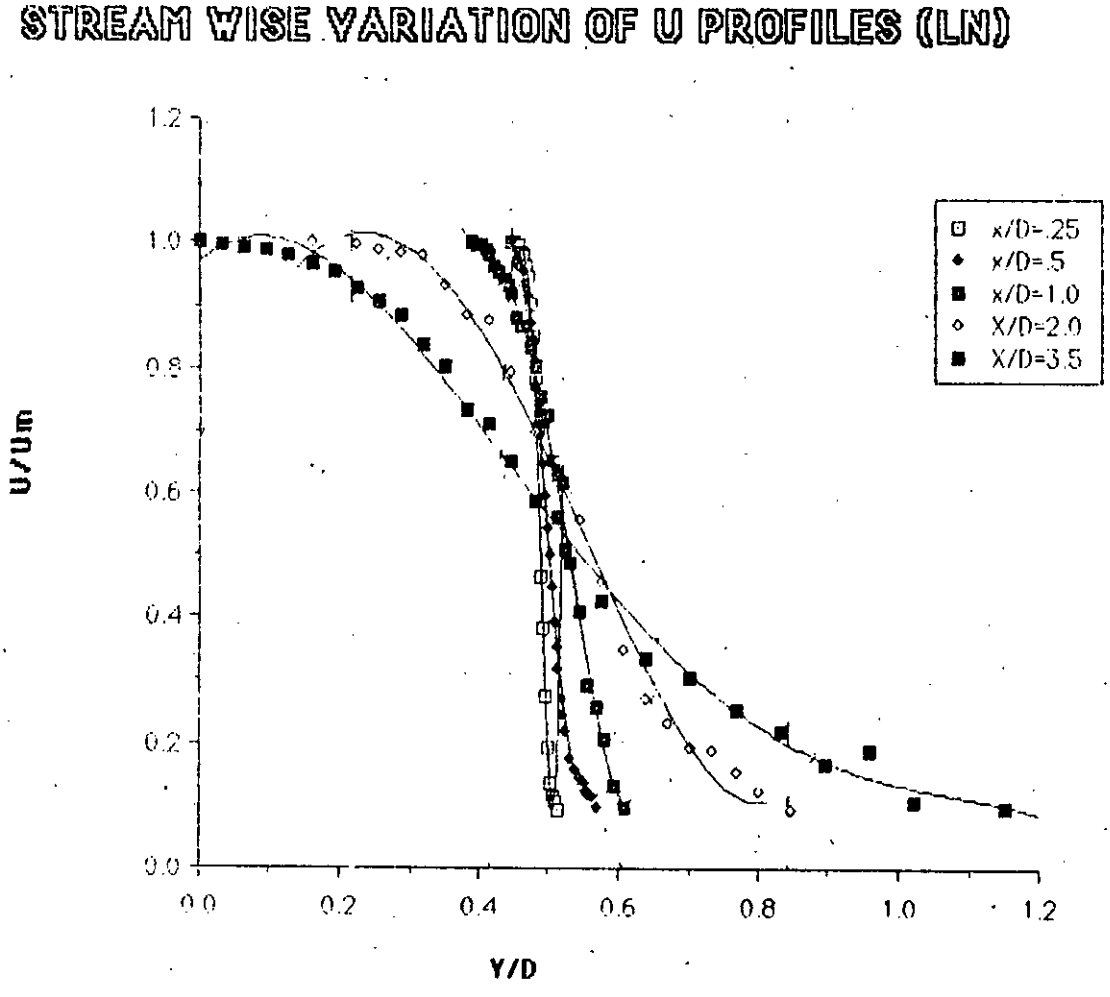

Fig. 5.3.6 : Stream-wise evolution of mean velocity (U) profiles for Re = 4.5×10^4 of LN nozzle.

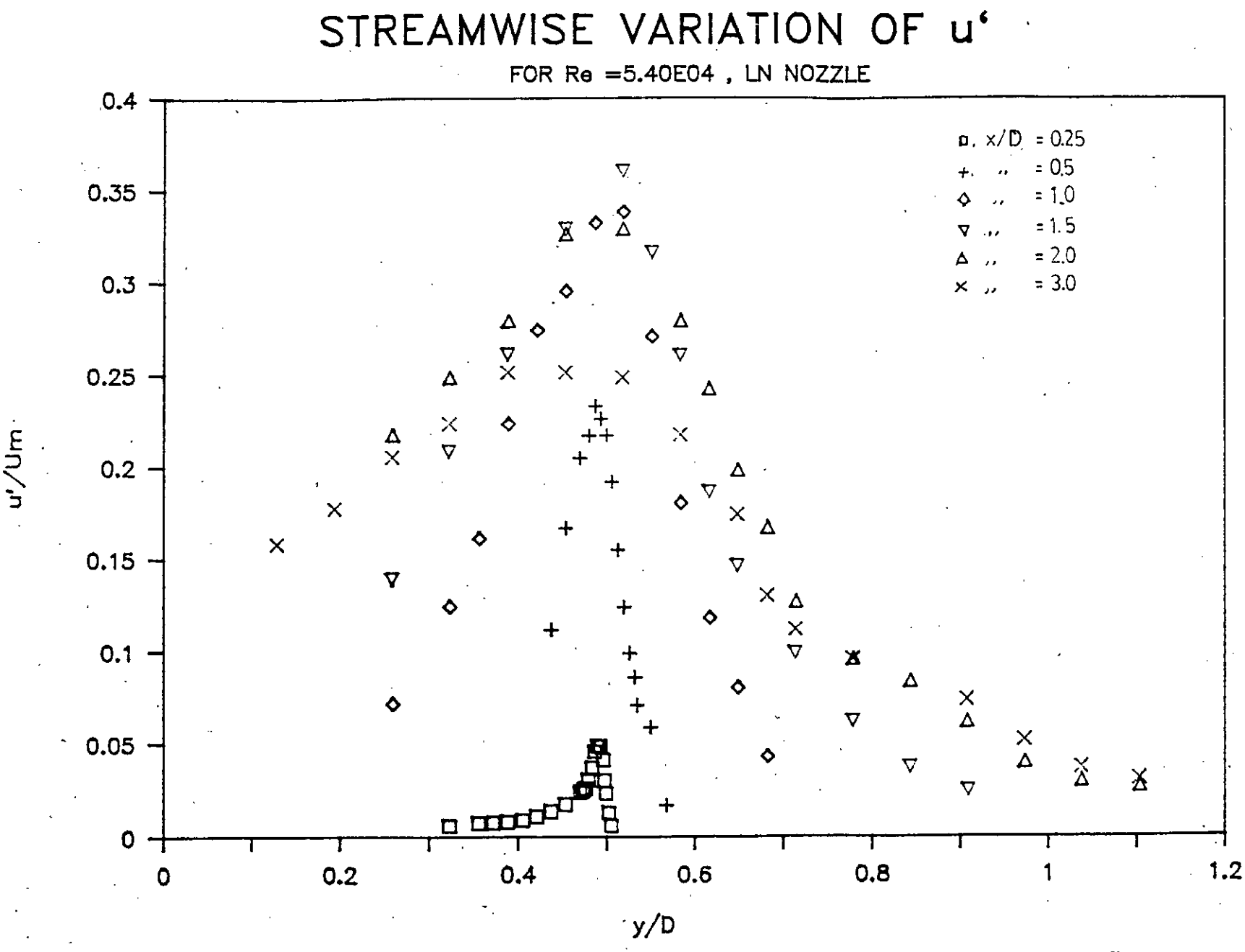

Fig. 5.3.7 : Stream-wise evolution of longitudinal turbulence intensity (u') profiles for Re = 4.5 x 10^4 of LN nozzle.

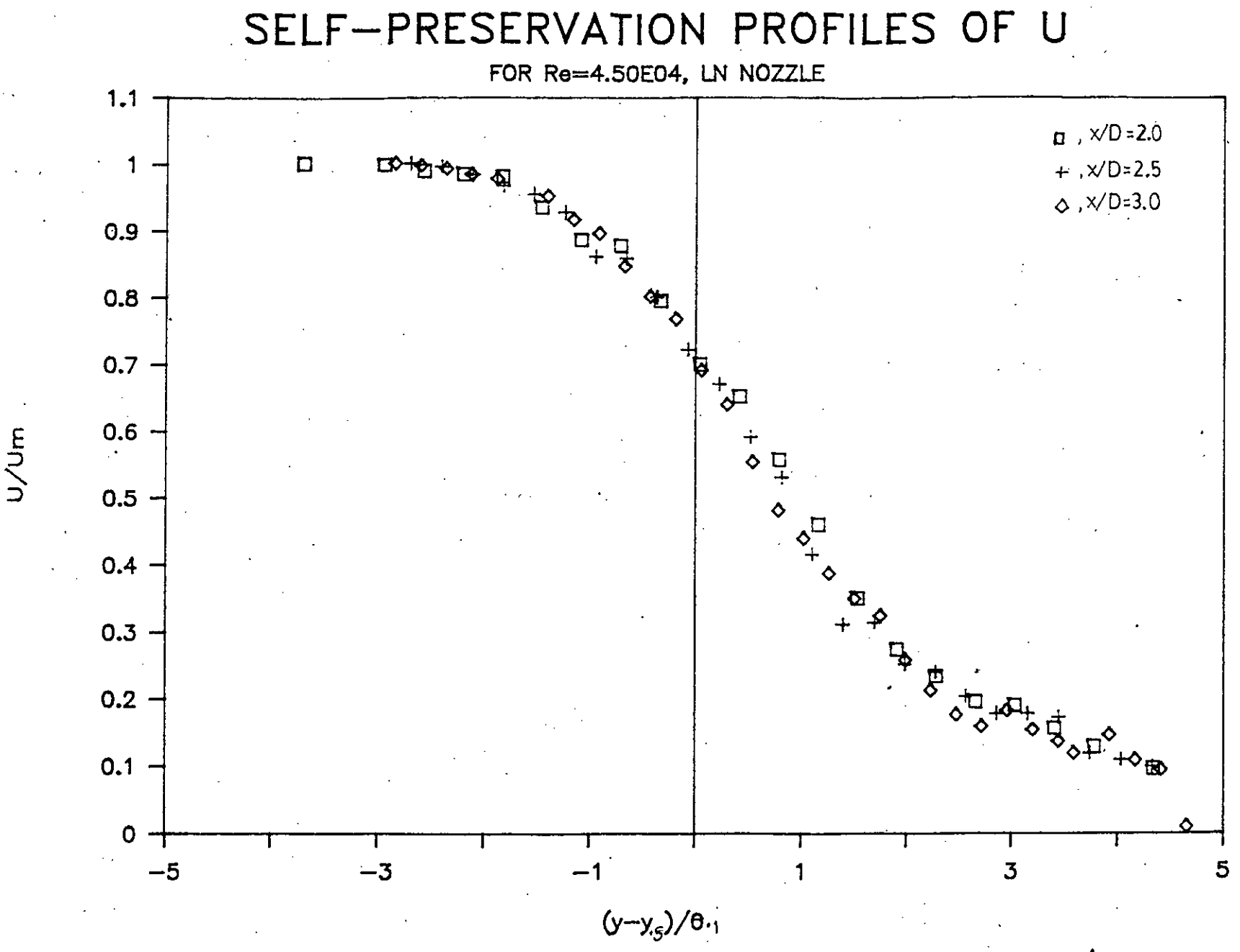

Fig. 5.3.8 : Self-preservation profiles of mean velocity (U) for Re = 5.4 x 10^4 of LN nozzle.

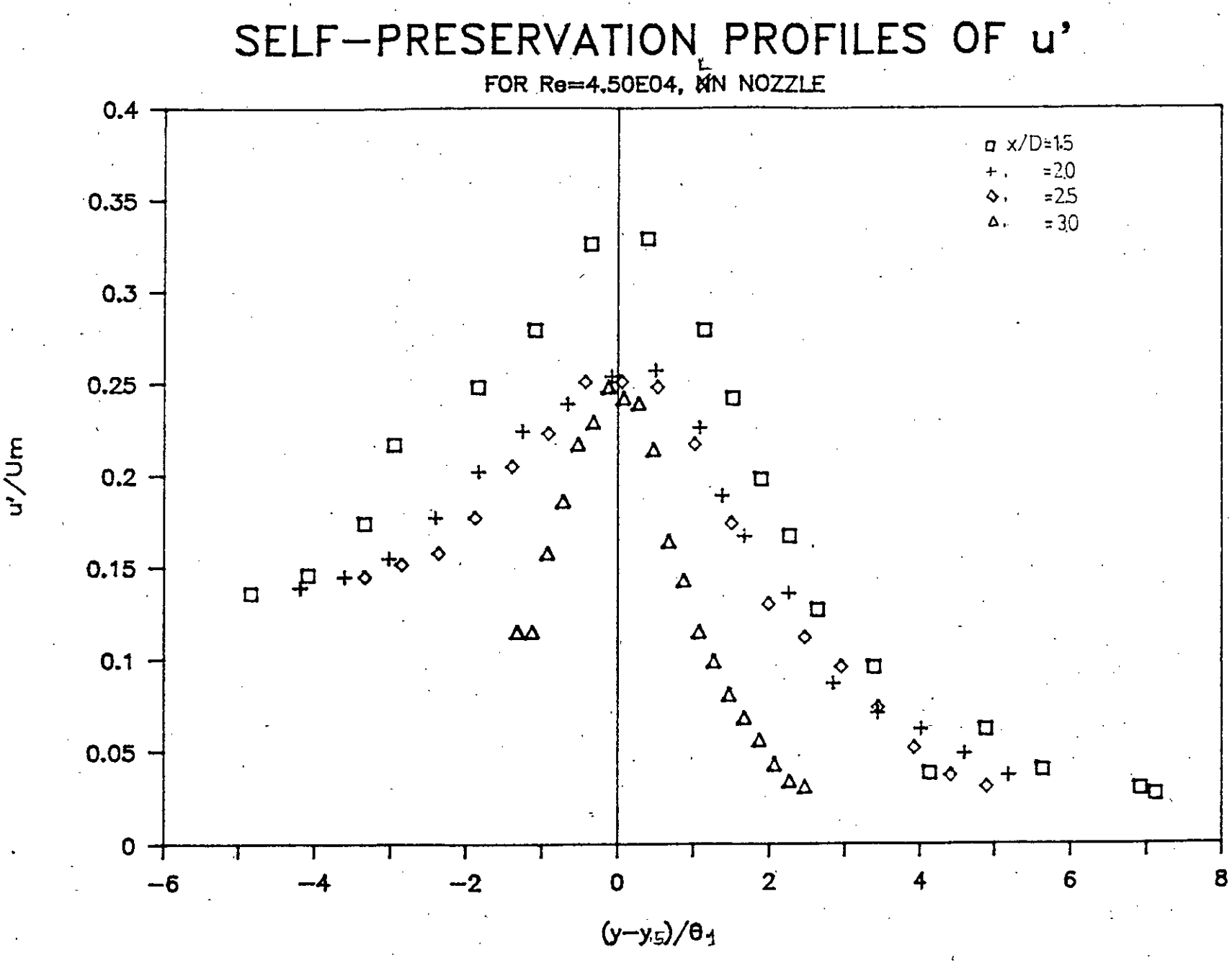

Fig. 5.3.9 : Self-preservation profiles of longitudinal turbulence intensity (u') profiles for Re = 4.5 x 10^4 of LN nozzle.

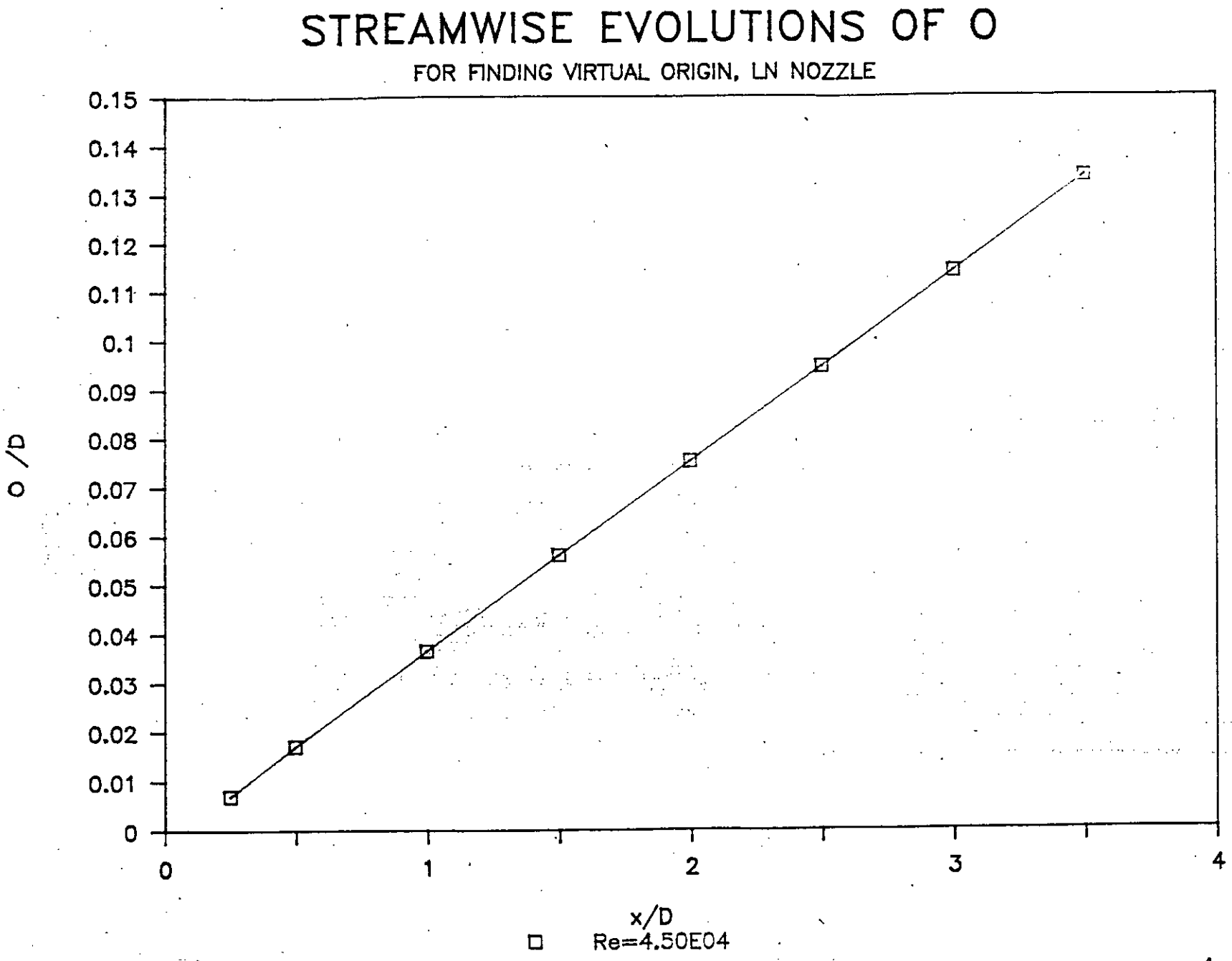

Fig. 5.3.10 : Stream-wise evolution of local momentum thickness ($\theta_{.1}$) for Re = 4.5 x 10^4 of LN nozzle.

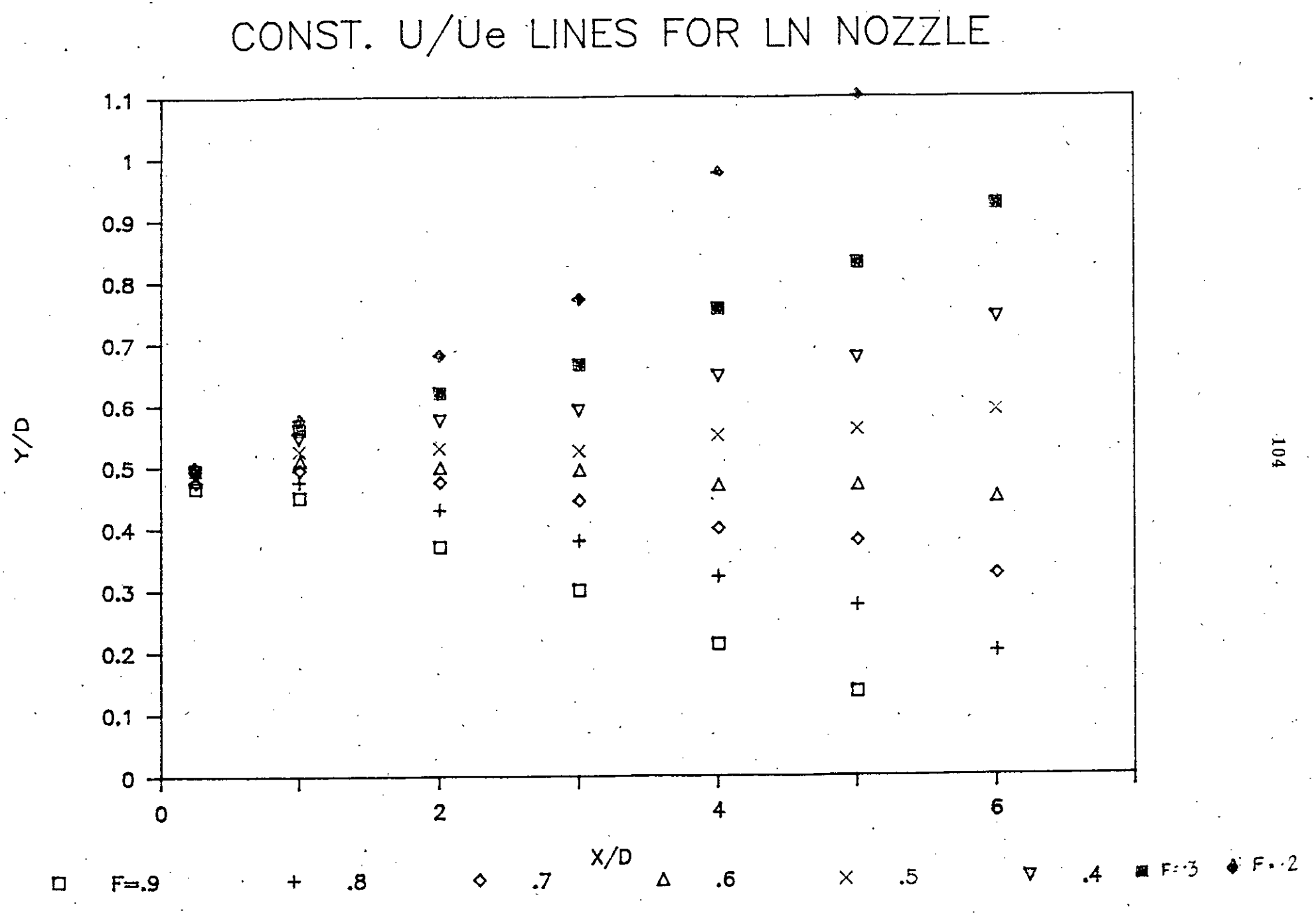

Fig. 5.3.11 : constant mean velocity lines of LN nozzle for Re = 4.5×10^4.

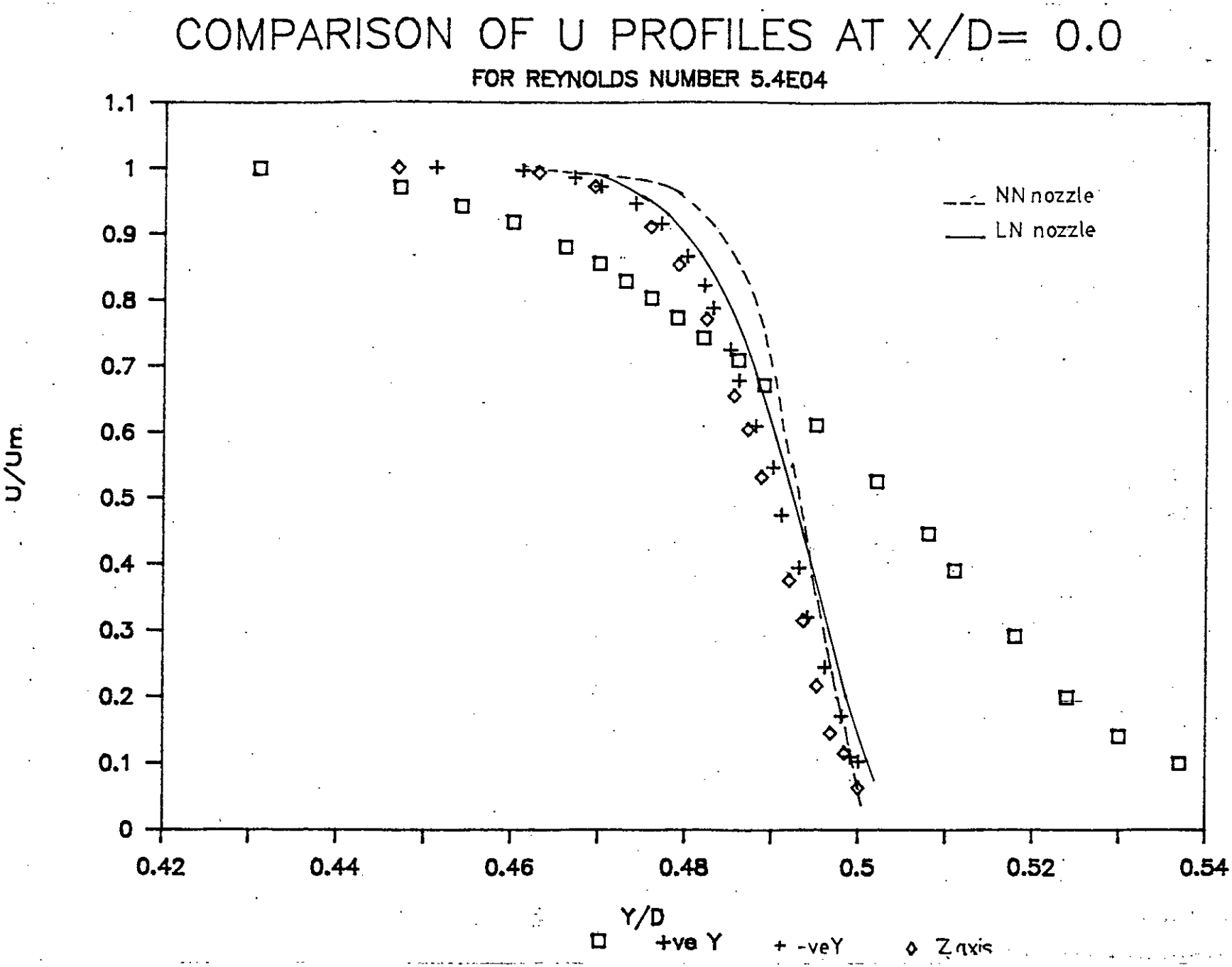

Fig. 5.4.1 : Mean velocity (U) profiles at the exit (x/D=0) of three axes (+ Y, -Y and Z axis), NN and LN nozzle for Re = 5.4×10^4.

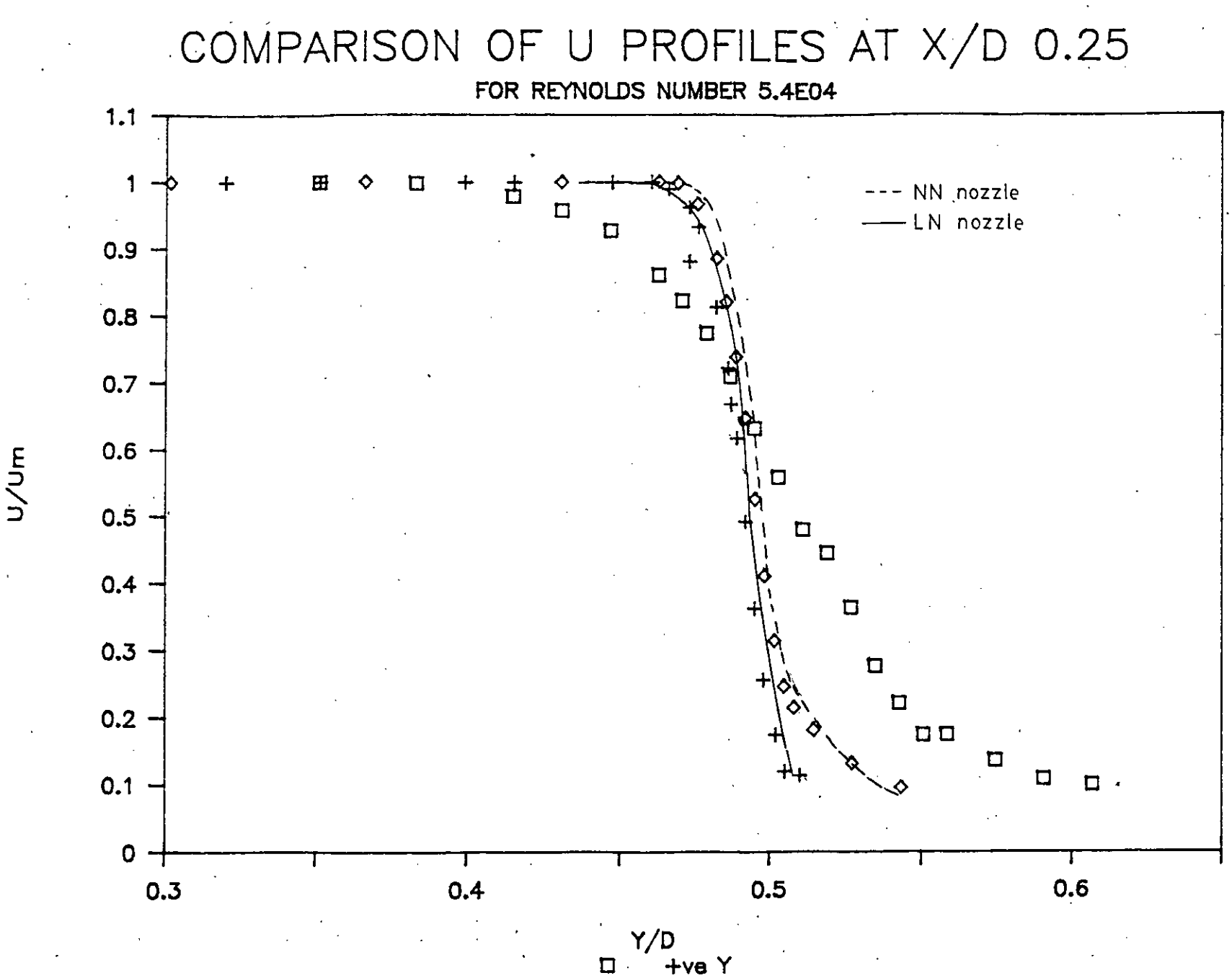

Fig. 5.4.2 : Mean velocity (U) profiles at x/D=0.25 of three axes (+ Y, -Y & Z axis) of WS nozzle, NN nozzle and LN nozzle.

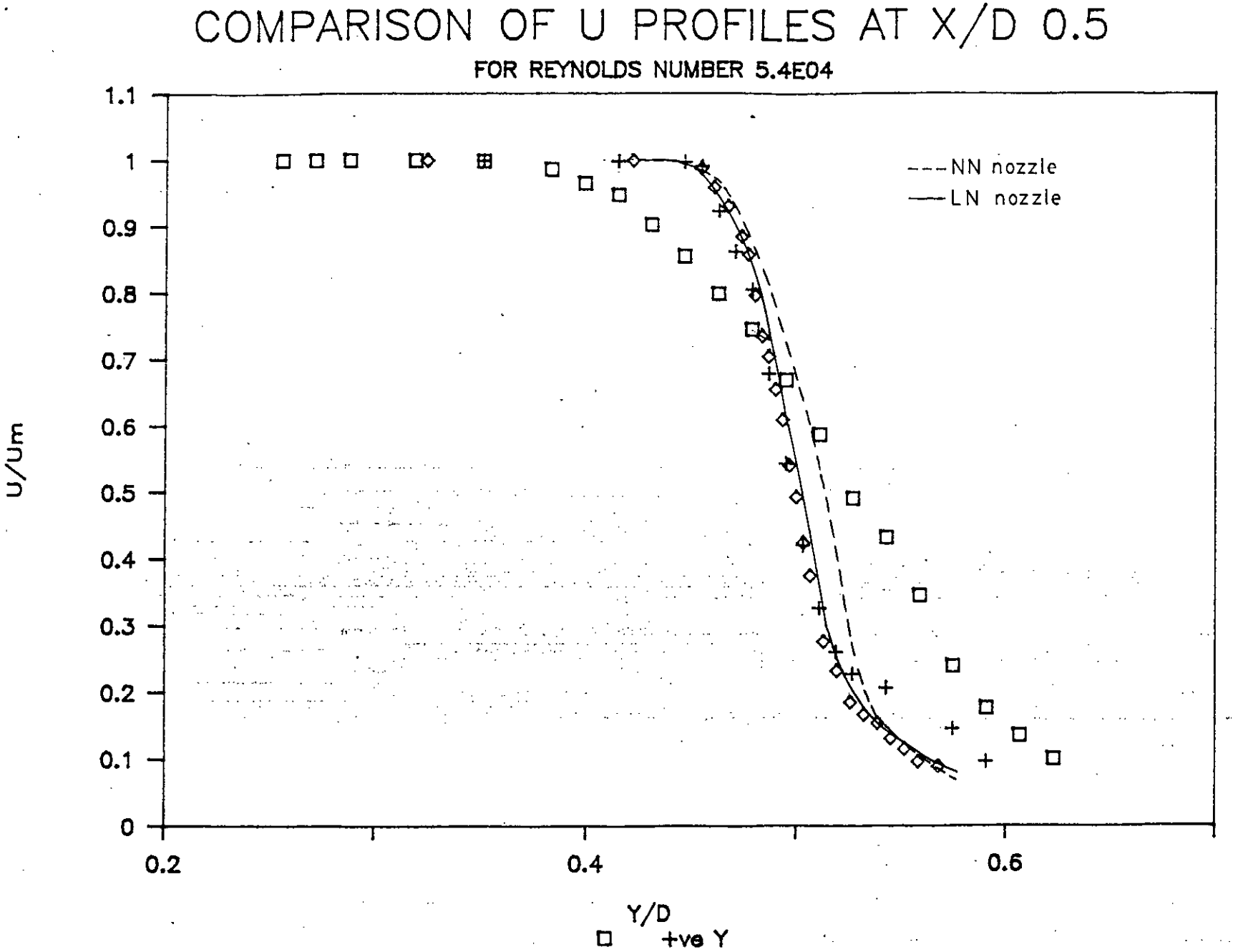

Fig. 5.4. 3 : Mean velocity profiles at x/D = 0.5 of three axes of WS nozzle, NN nozzle and LN nozzle for Re = 5.4 x 10^4 .

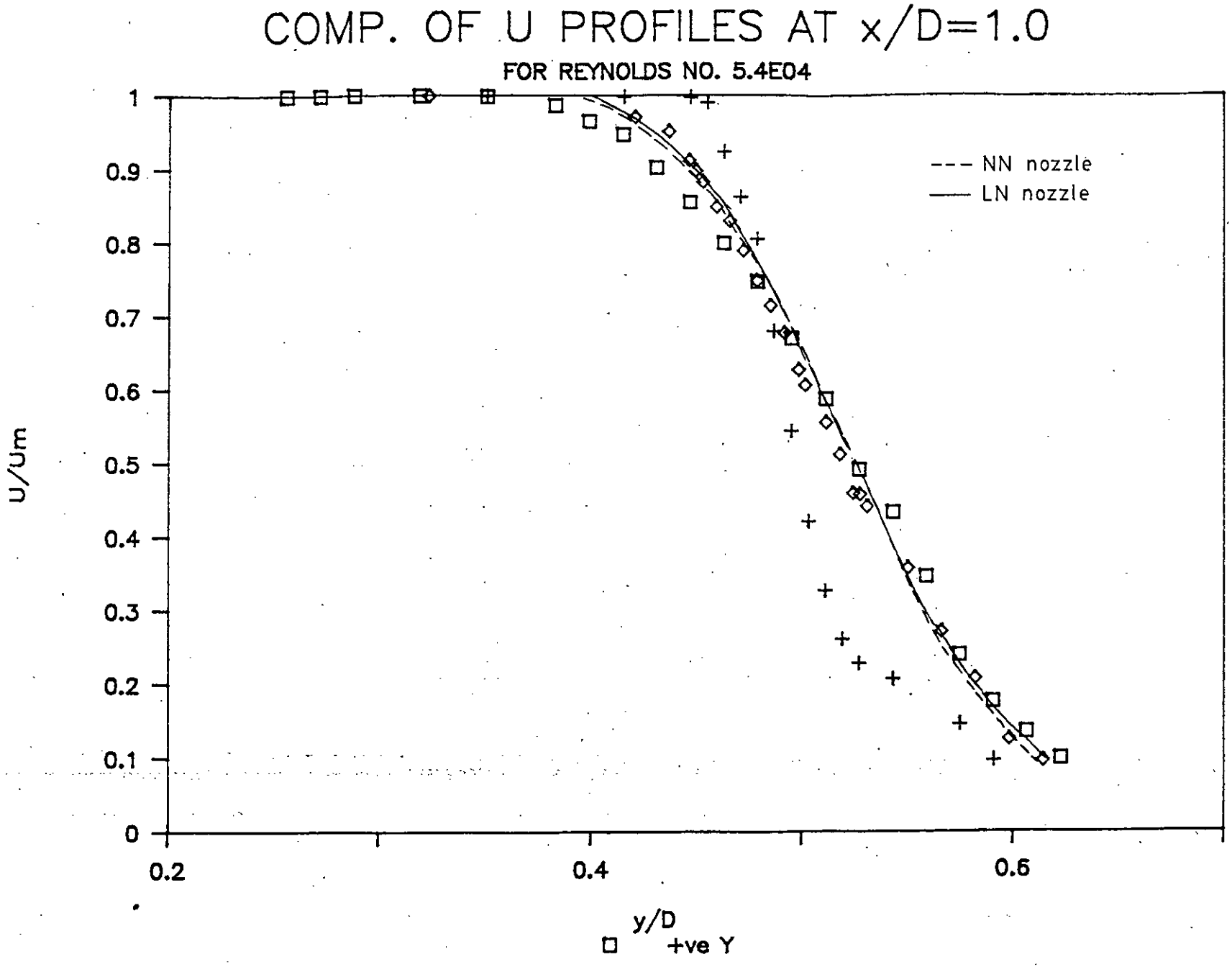

Fig. 5.4. 4 : Mean velocity profiles at x/D = 1.0 of three axes of WS nozzle, NN nozzle and LN nozzle for Re = 5.4 x 10^4 .

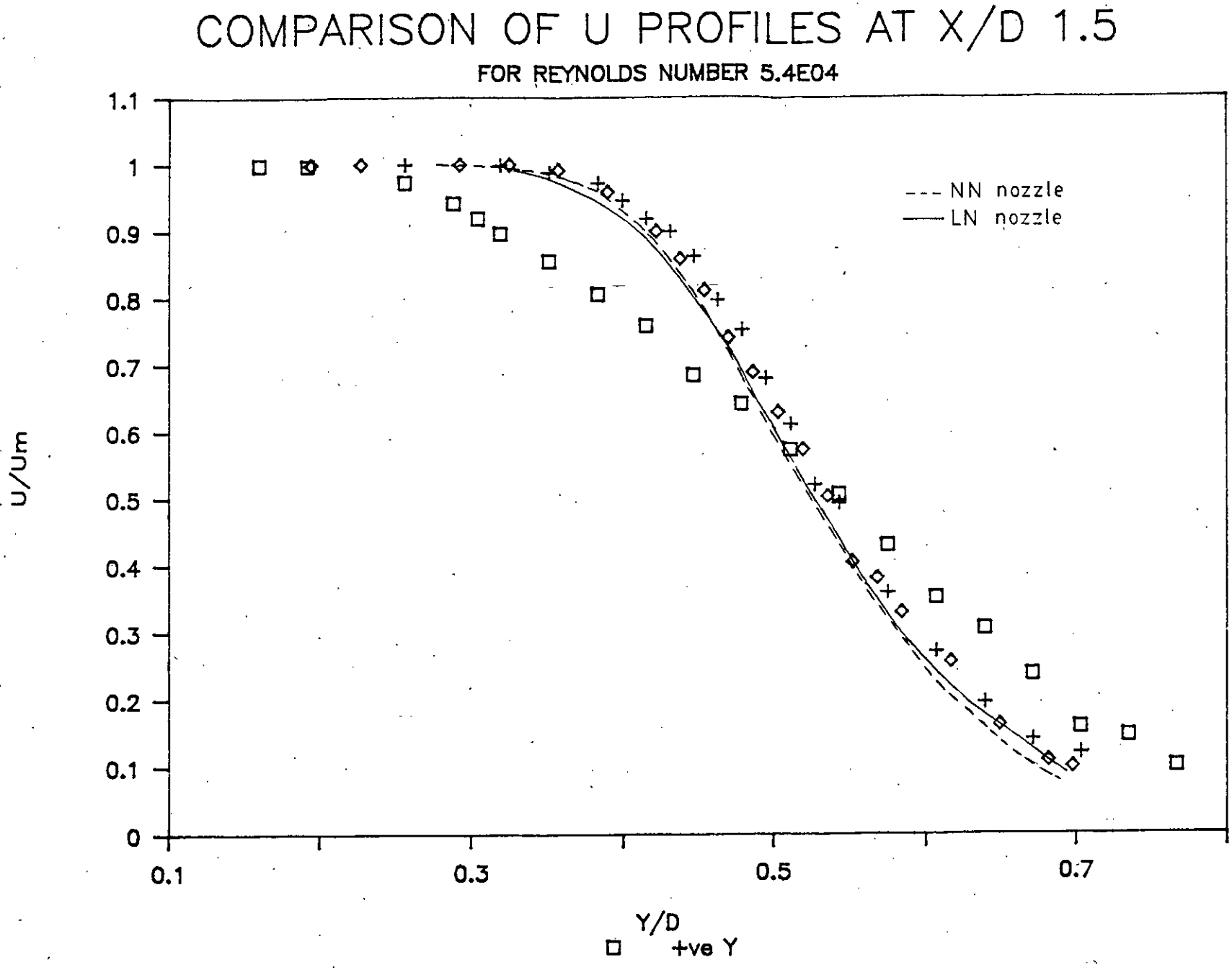

Fig. 5.4. 5 : Mean velocity profiles at x/D = 1.5 of three axes of WS nozzle, NN nozzle and LN nozzle for Re = 5.4 x 10^4 .

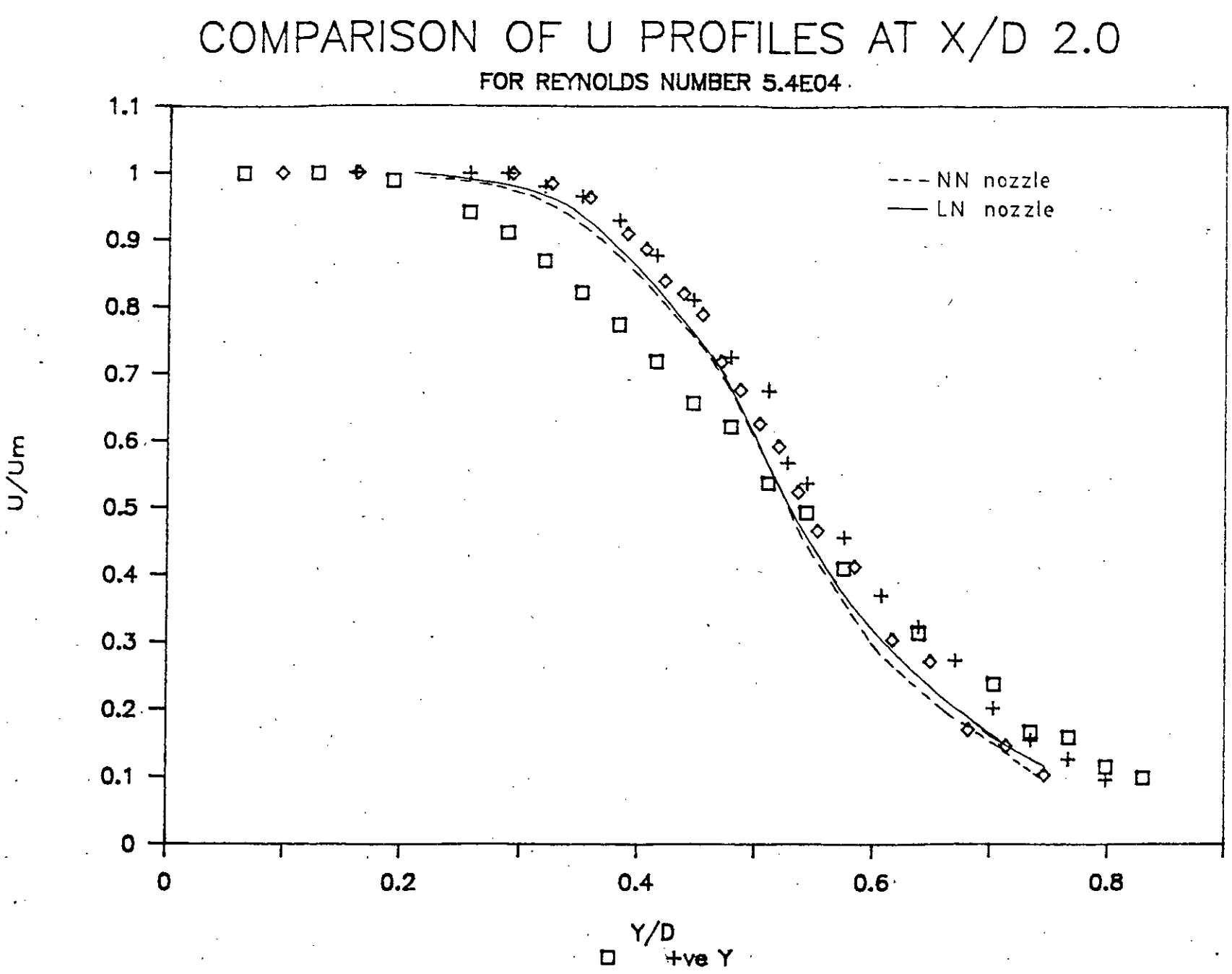

Fig. 5.4. 6 : Mean velocity (U) profiles at x/D= 2.0 of NN, LN and Three axes of WS nozzle for Re = 5.4 x 10^4 .

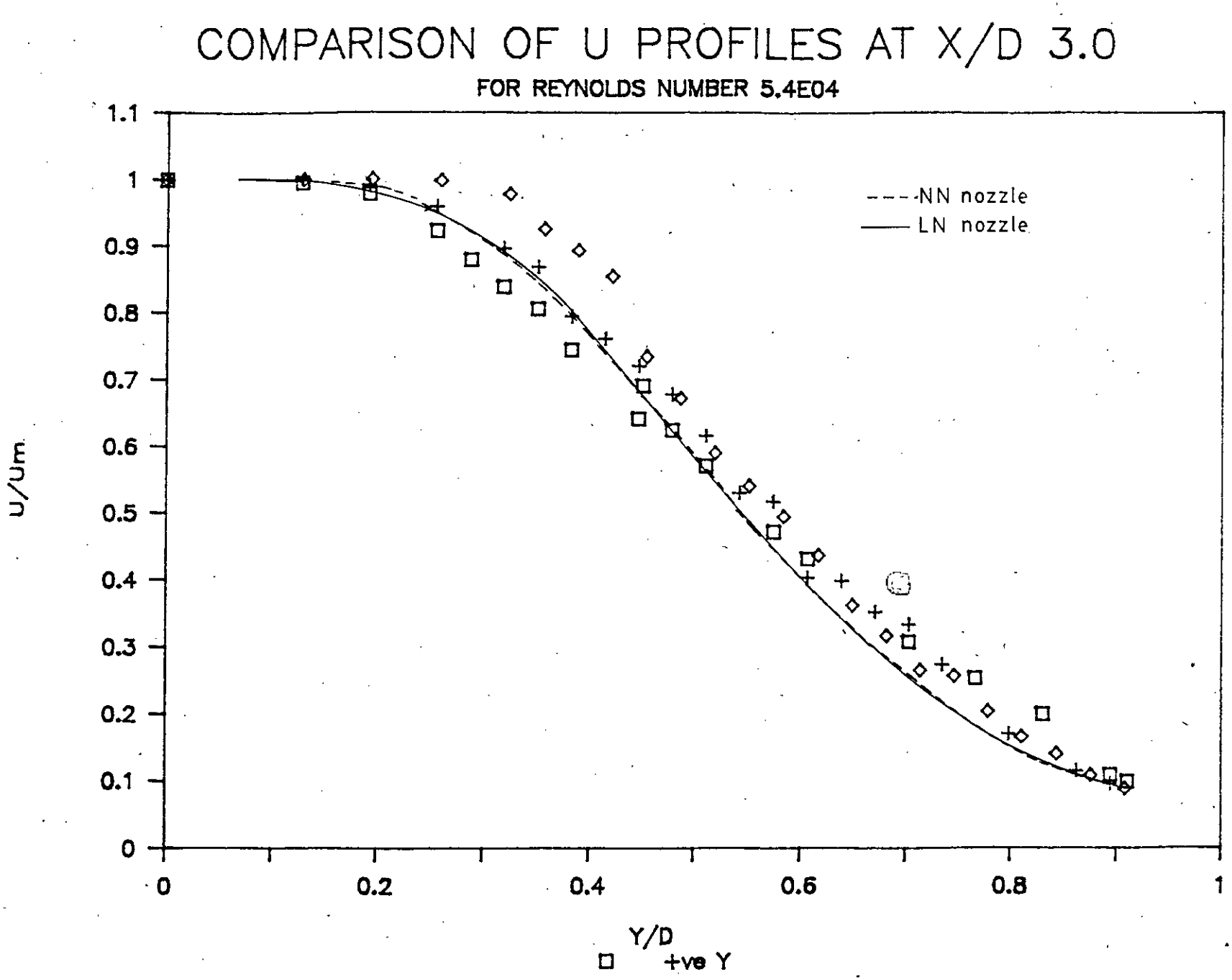

Fig. 5.4. 7 : Mean velocity (U) profiles at x/D= 3.0 of NN, LN and Three axes of WS nozzle for Re = 5.4 x 10^4 .

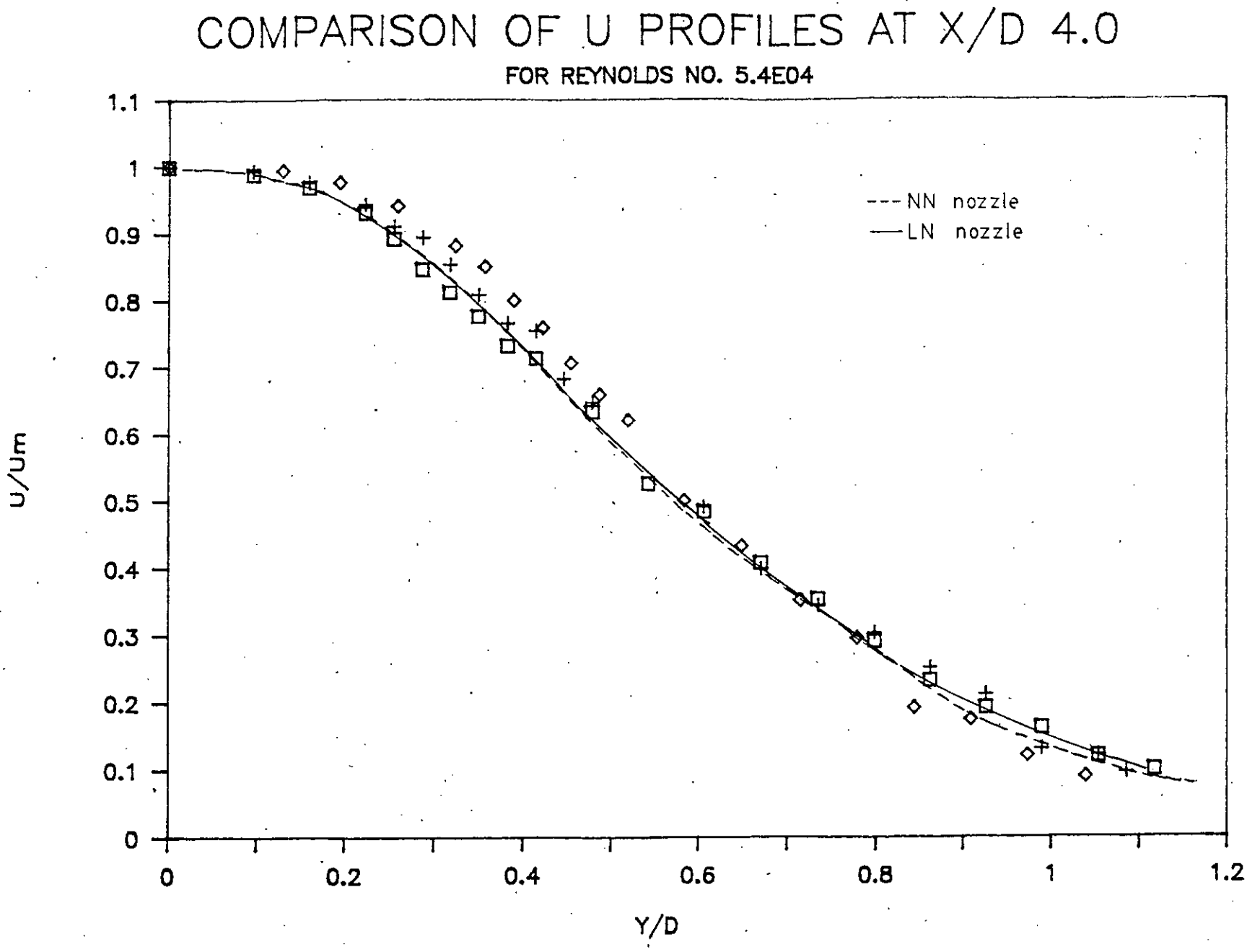

Fig. 5.4. 8 : Mean velocity (U) profiles at x/D= 4.0 of NN, LN and Three axes of WS nozzle for Re = 5.4 x 10^4 .

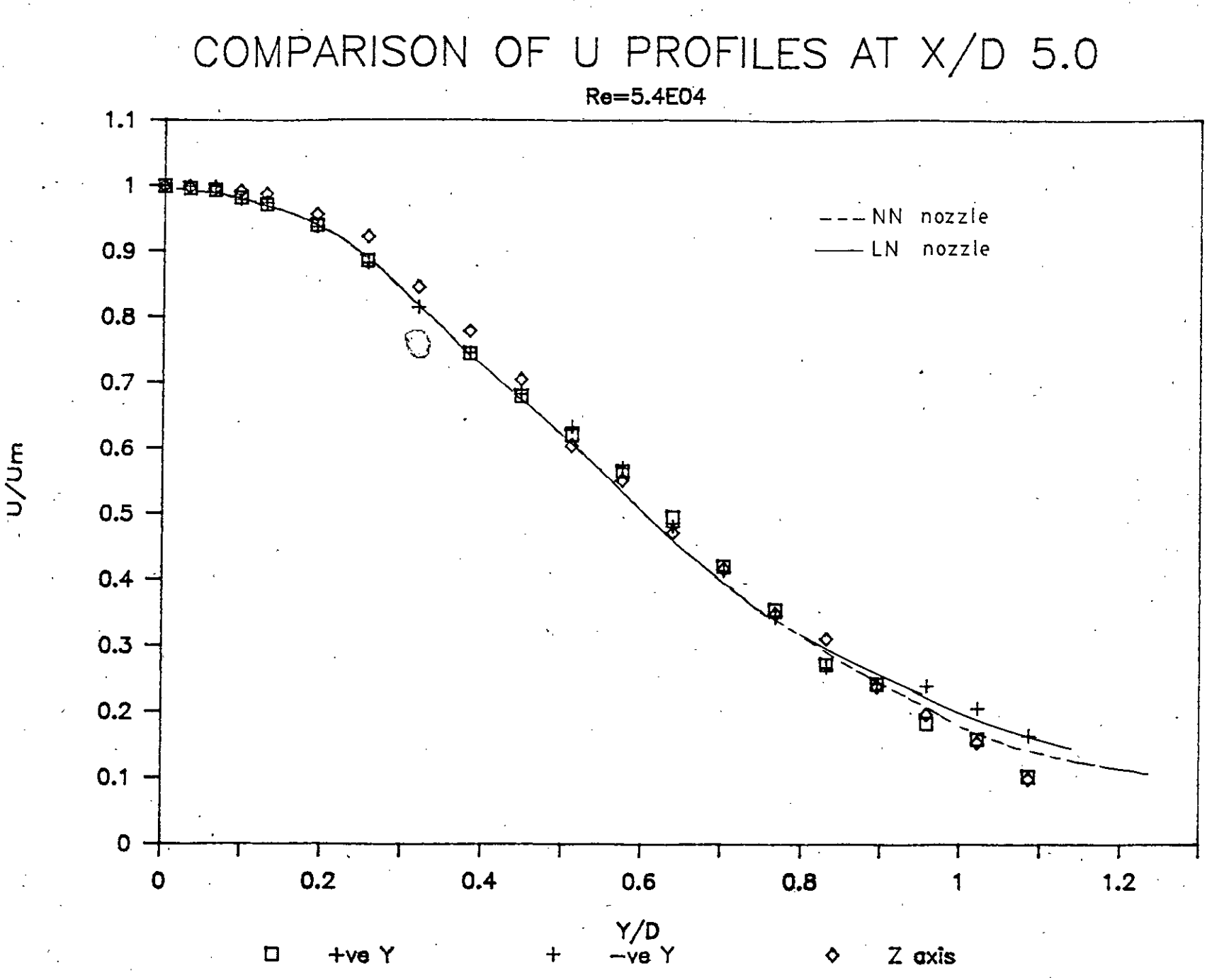

Fig. 5.4. 9 : Mean velocity (U) profiles at x/D= 5.0 of NN, LN and Three axes of WS nozzle for Re = 5.4 x 10^4 .

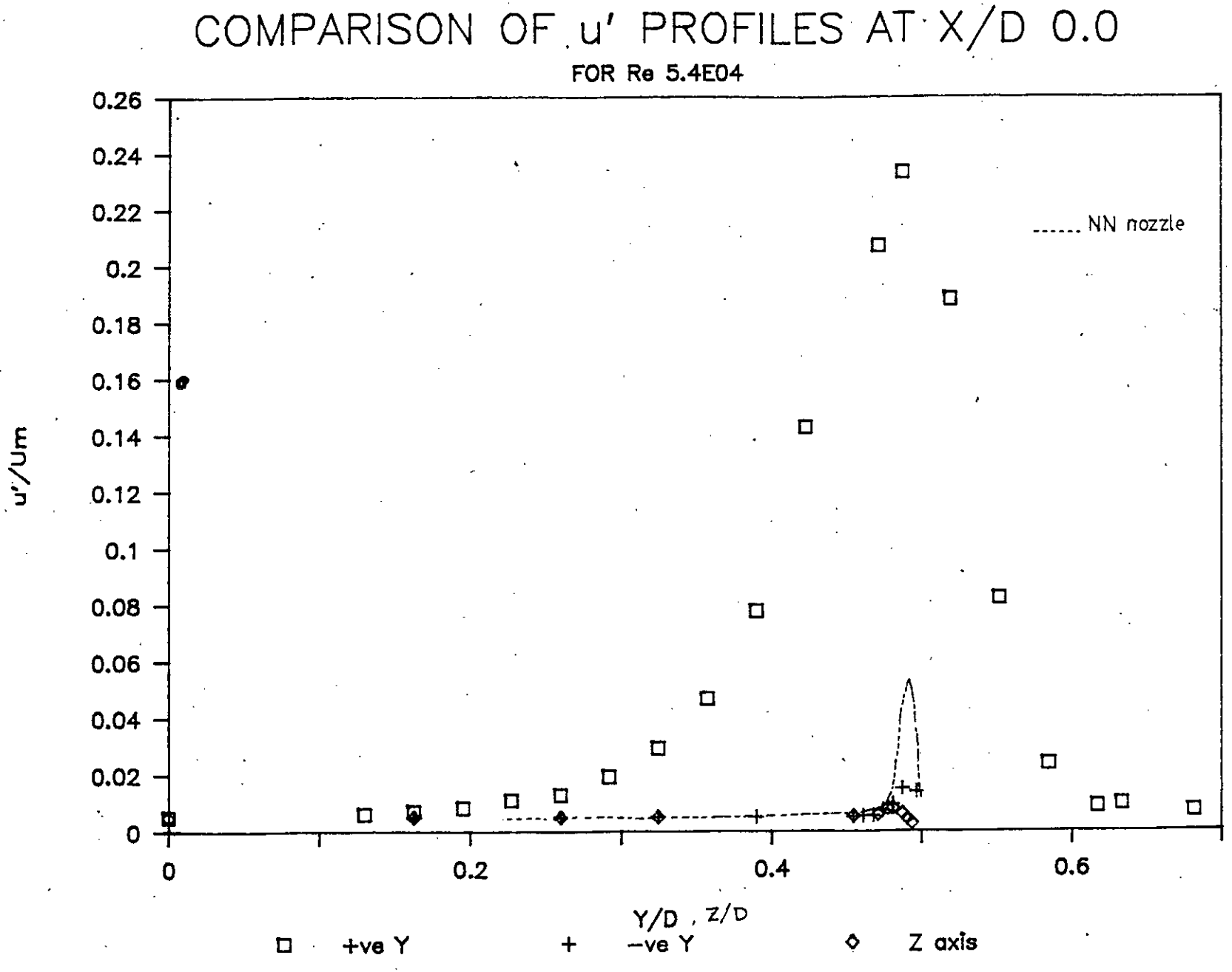

Fig. 5.4.10 : Longitudinal turbulence intensity (u') profiles at the exit (x/D=0) of NN nozzle and three axes of WS nozzle for Re = 5.4 x 10^4.

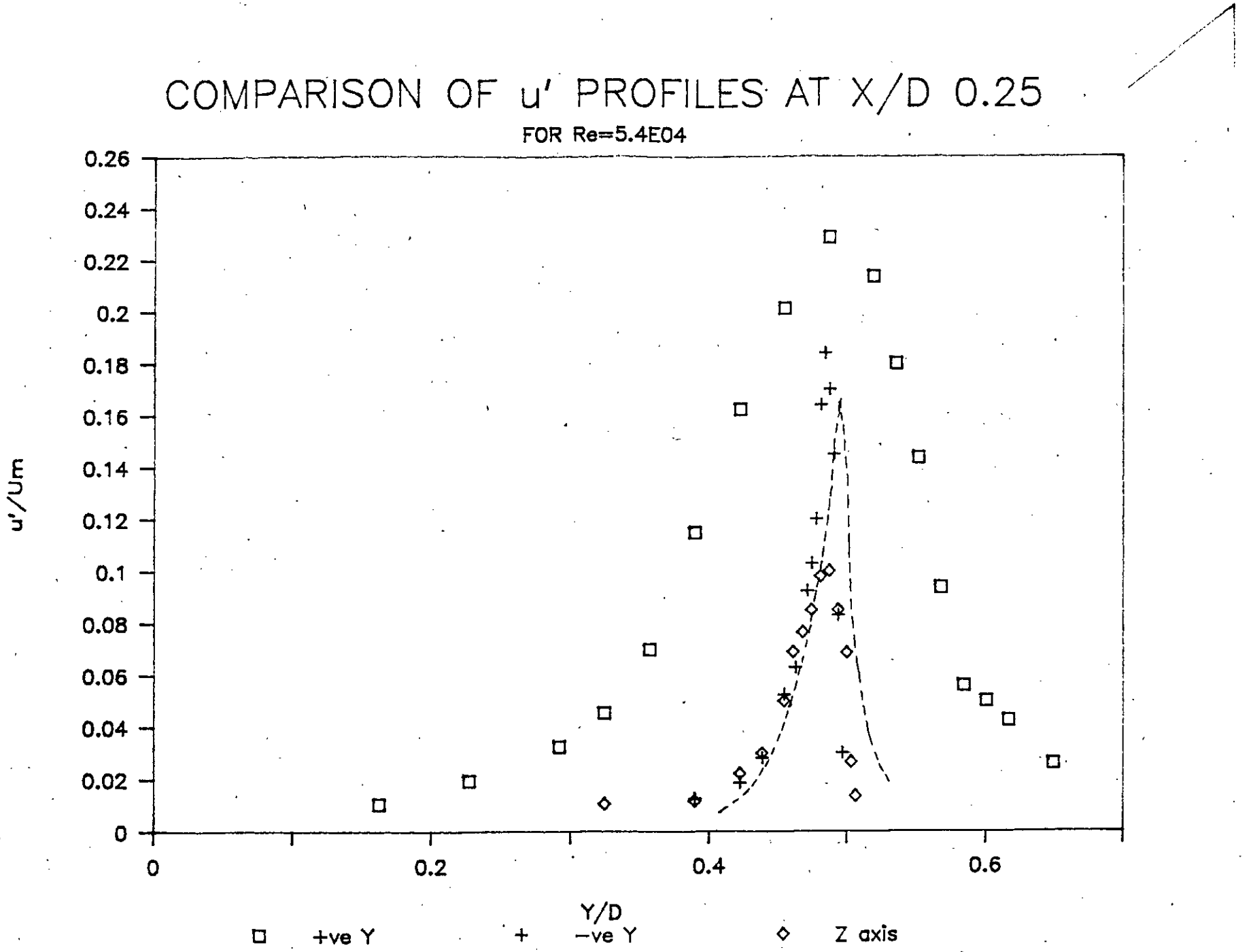

Fig. 5.4.11 : Longitudinal turbulence intensity profiles at x/D = .25 of NN and three axes of WS nozzle for Re = 5.4 x 10^4.

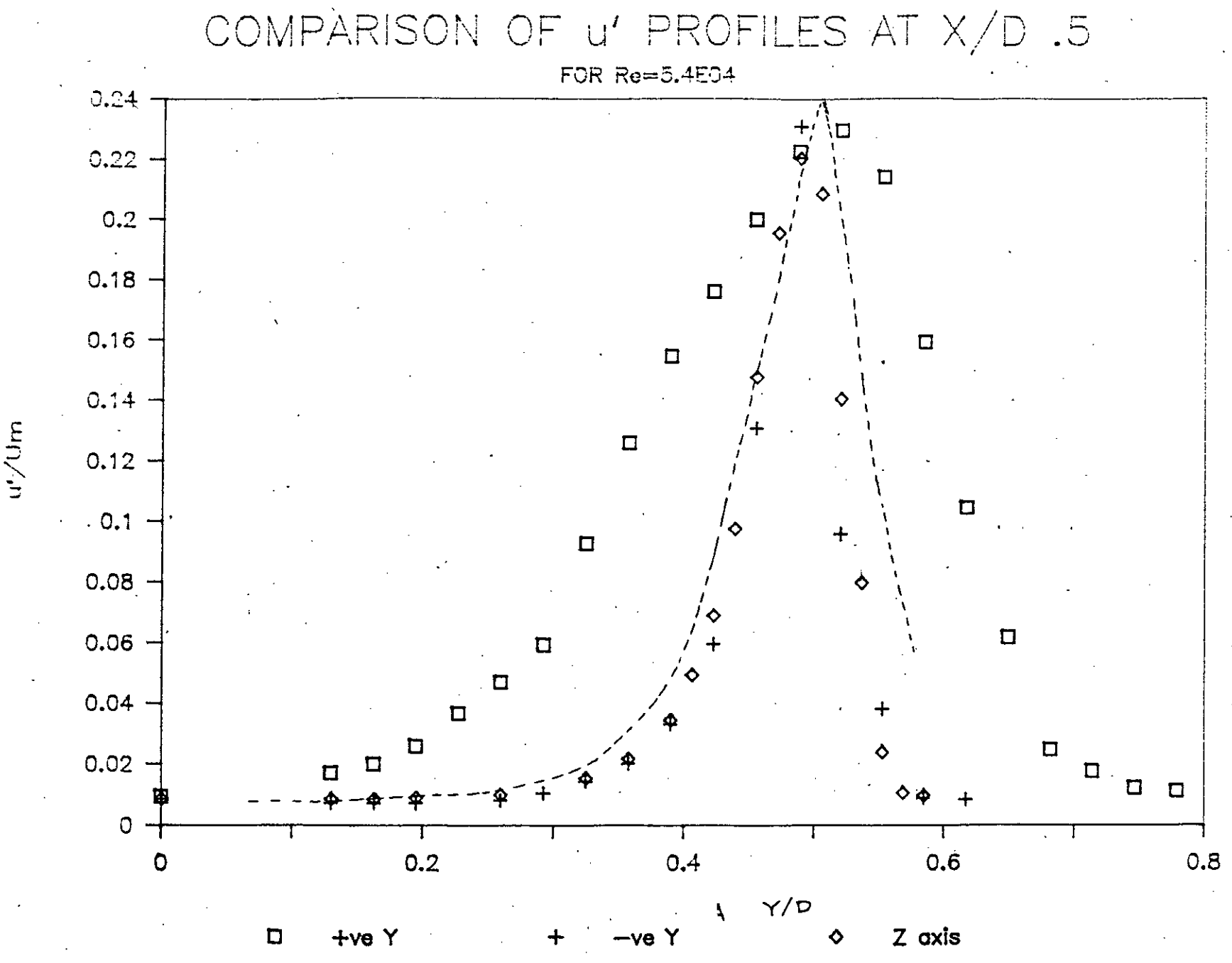

Fig. 5.4.12 : Longitudinal turbulence intensity profiles at x/D = .5 of NN and three axes of WS nozzle for Re = 5.4 x 10^4.

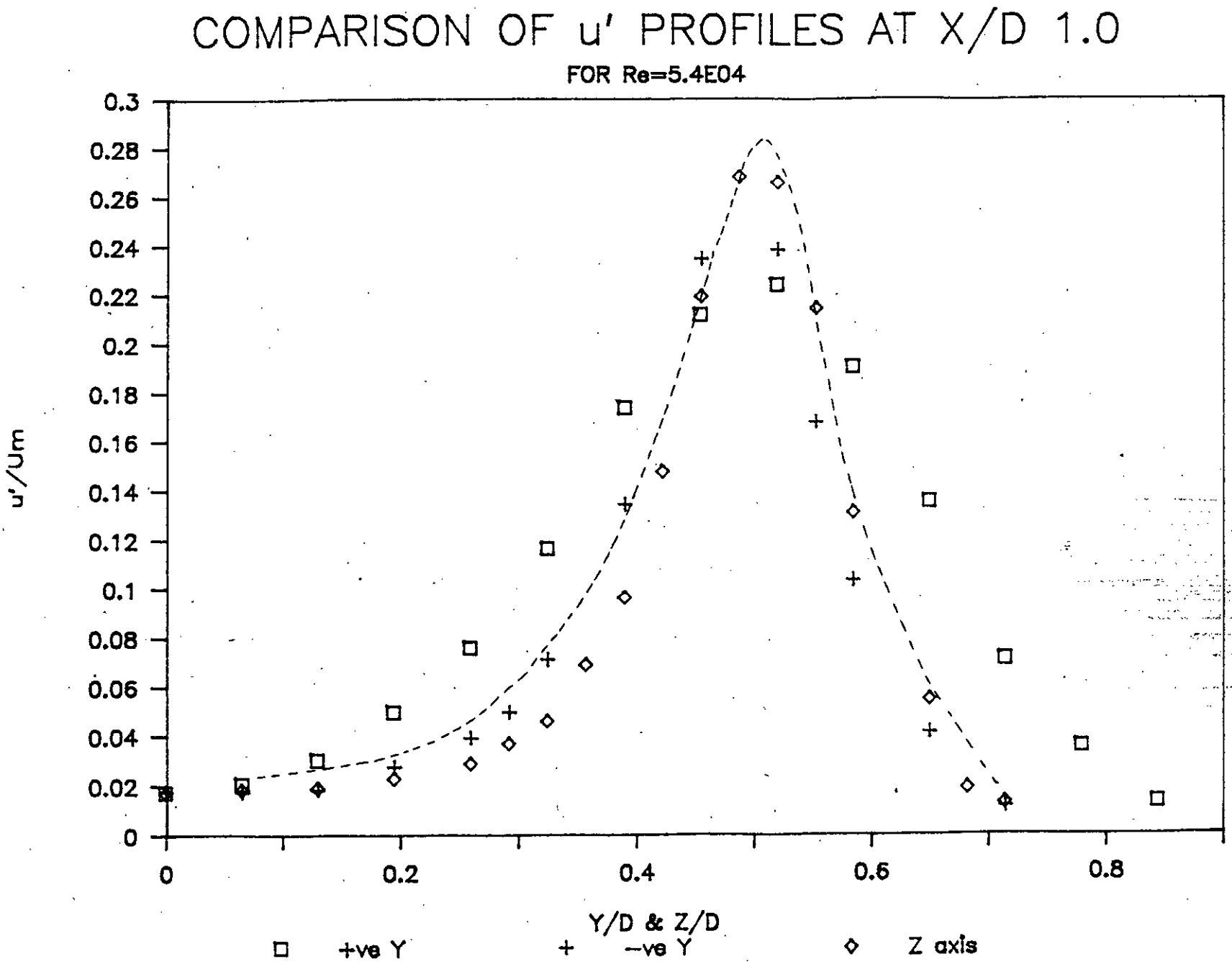

Fig. 5.4. 13: Longitudinal turbulence intesnity (u') profiles at x/D = 1.0 of NN and three axes of WS nozzle for Re = 5.4 x 10^4.

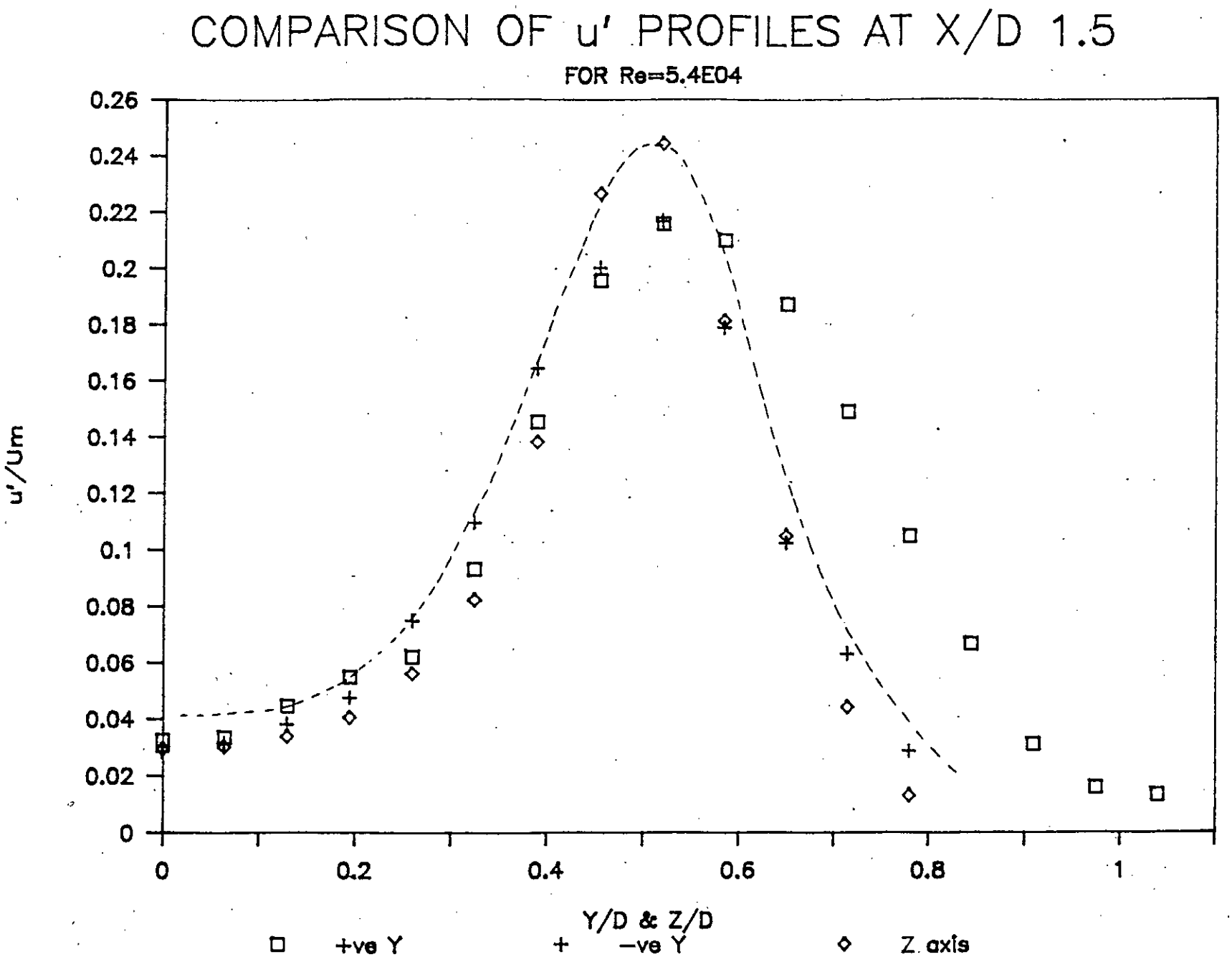

Fig. 5.4. 14: Longitudinal turbulence intesnity (u') profiles at x/D = 1.5 of NN and three axes of WS nozzle for Re = 5.4 x 10^4.

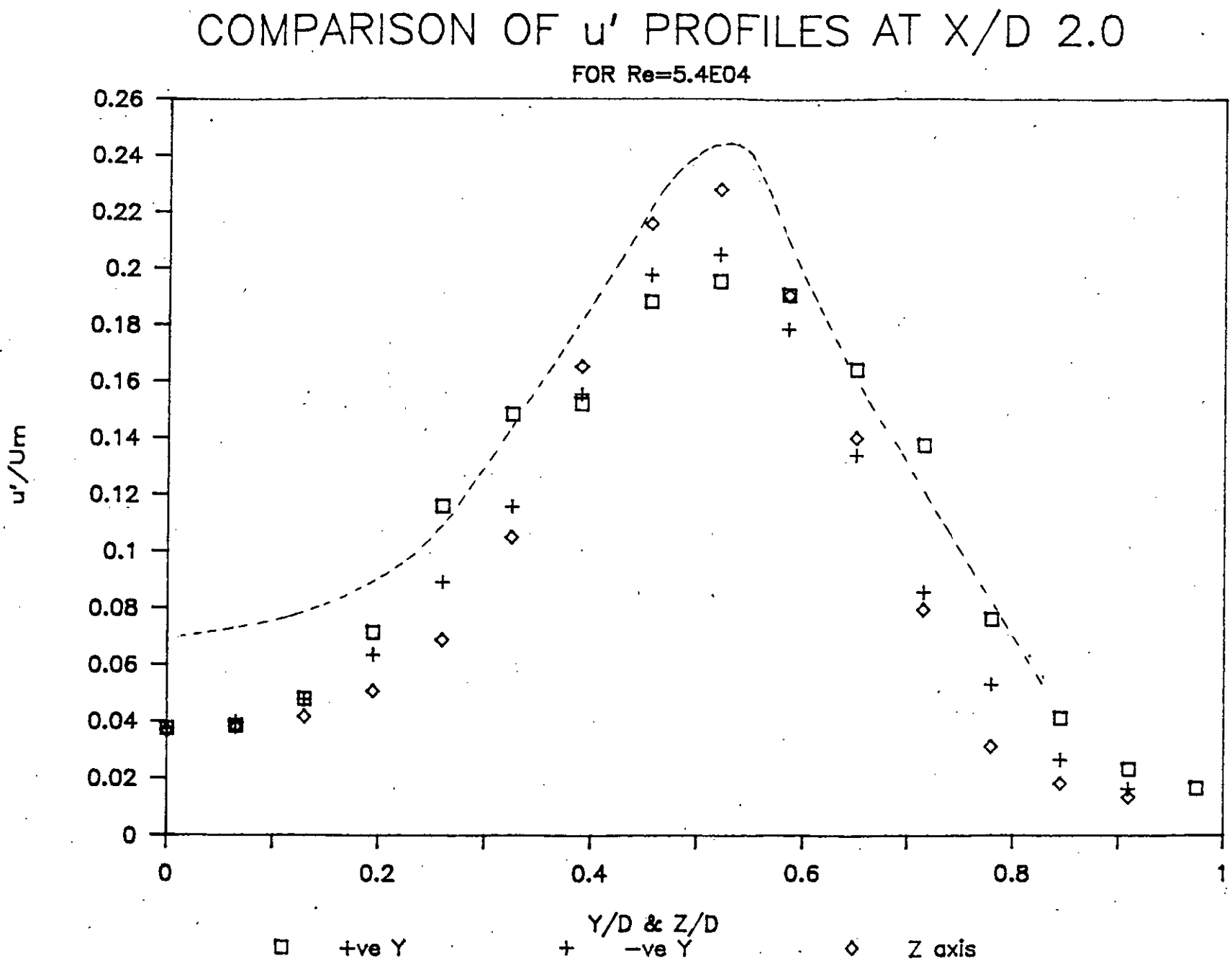

Fig. 5.4.15 : Longitudinal turbulence intesnity (u') profiles at x/D =2.0 of NN and three axes of WS nozzle for Re = 5.4 x 10^4.

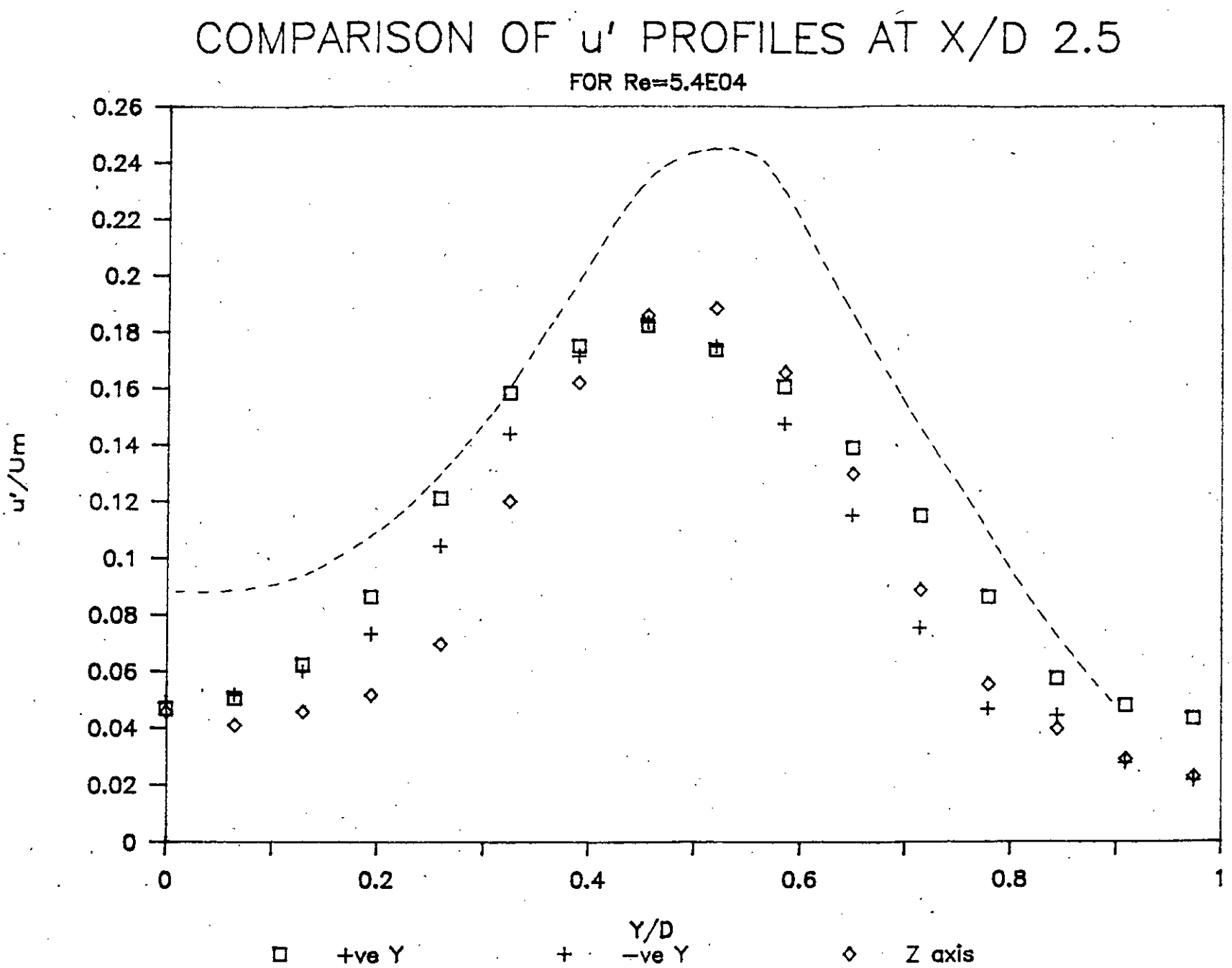

Fig. 5.4.16 : Longitudinal turbulence intesnity (u') profiles at x/D = 2.5 of NN and three axes of WS nozzle for Re = 5.4 x 10^4.

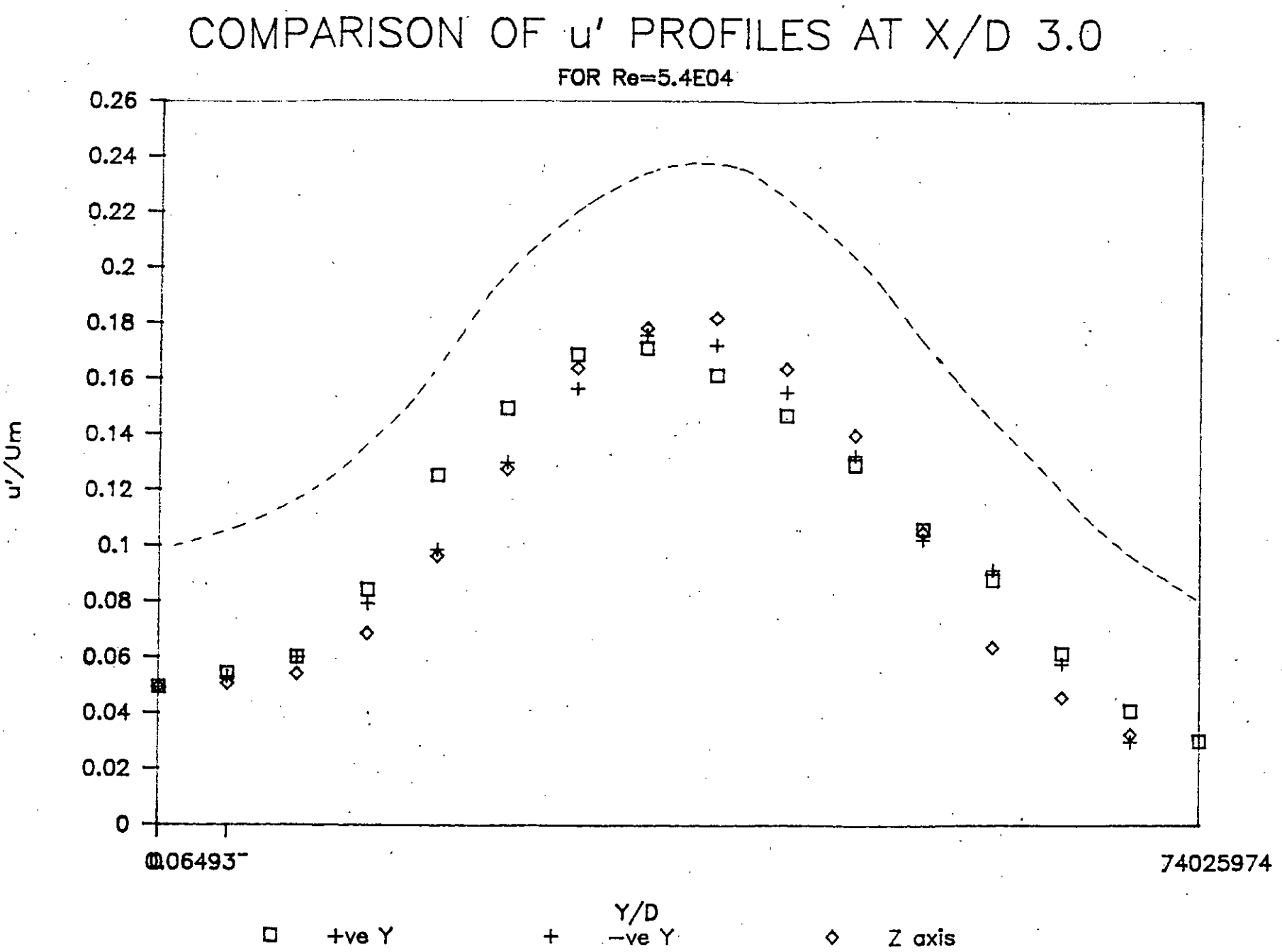

Fig. 5.4.17 Longitudinal turbulence intensity (u') profiles at x/D = 3.0 of NN and three axes of WS nozzle for Re=5.4×10^4.

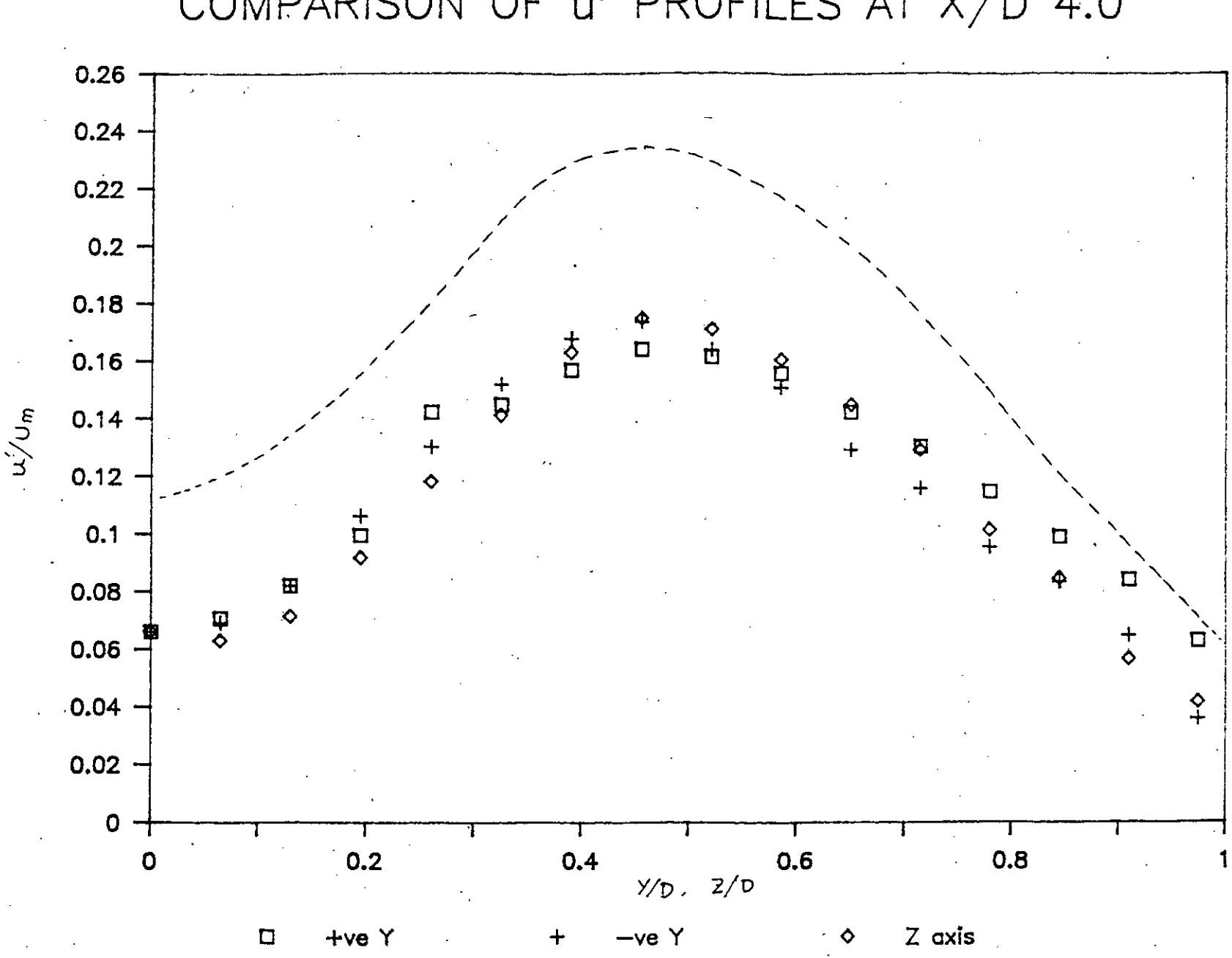

Fig. 5.4.18 : Longitudinal turbulence intesnity (u') profiles at x/D = 4.0 of NN and three axes of WS nozzle for Re = 5.4 x 10^4.

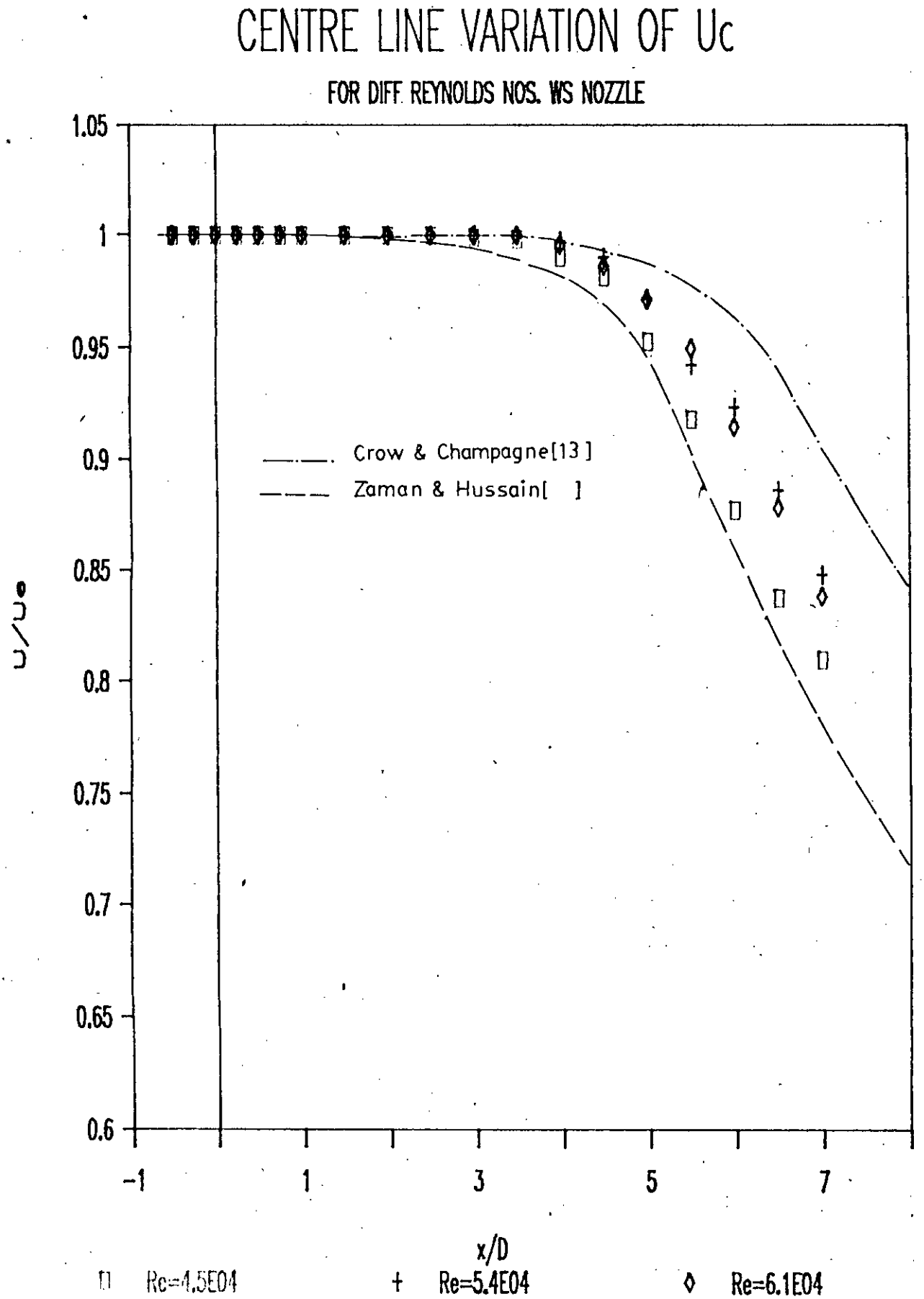

Fig. 5.4.19 : Centre line mean velocity profile of WS nozzle for different Reynolds number.

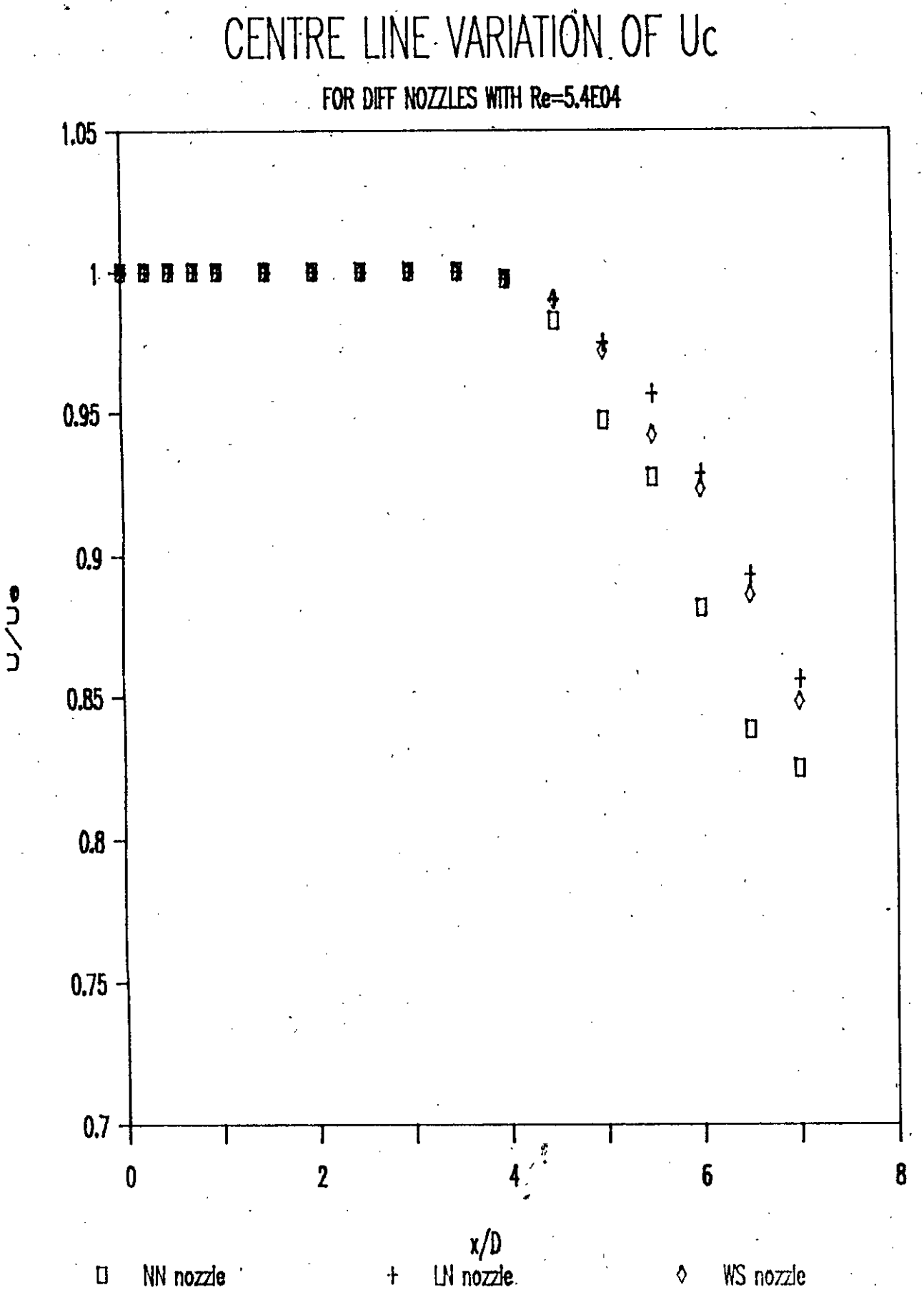

Fig. 5.4.20 : Centre line mean velocity profiles of NN, LN and WS nozzle for Re = 5.4 x 10^4.

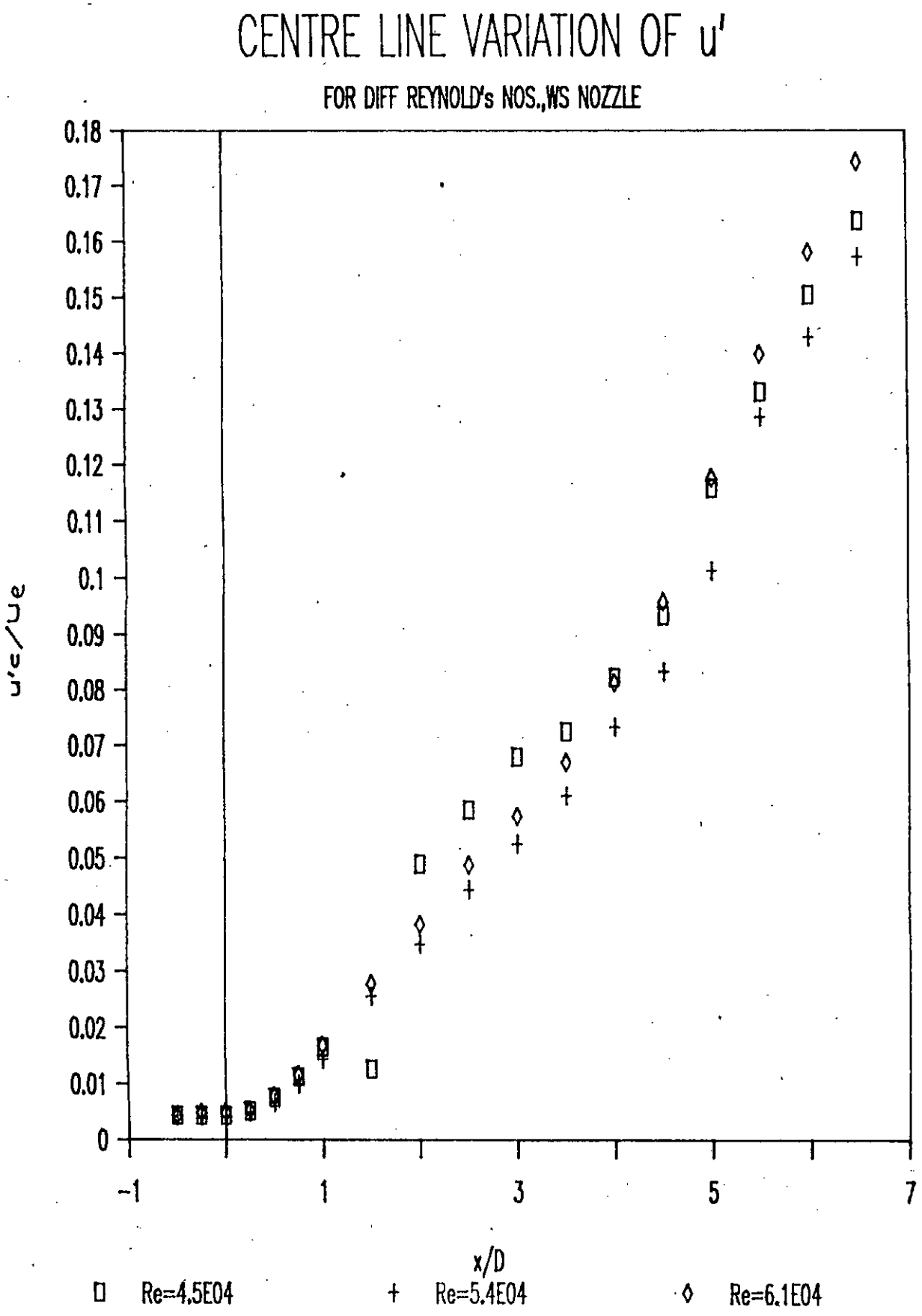

Fig. 5.4.21 : Centre line longitudinal turbulence intensity profiles of WS nozzle for different Re.

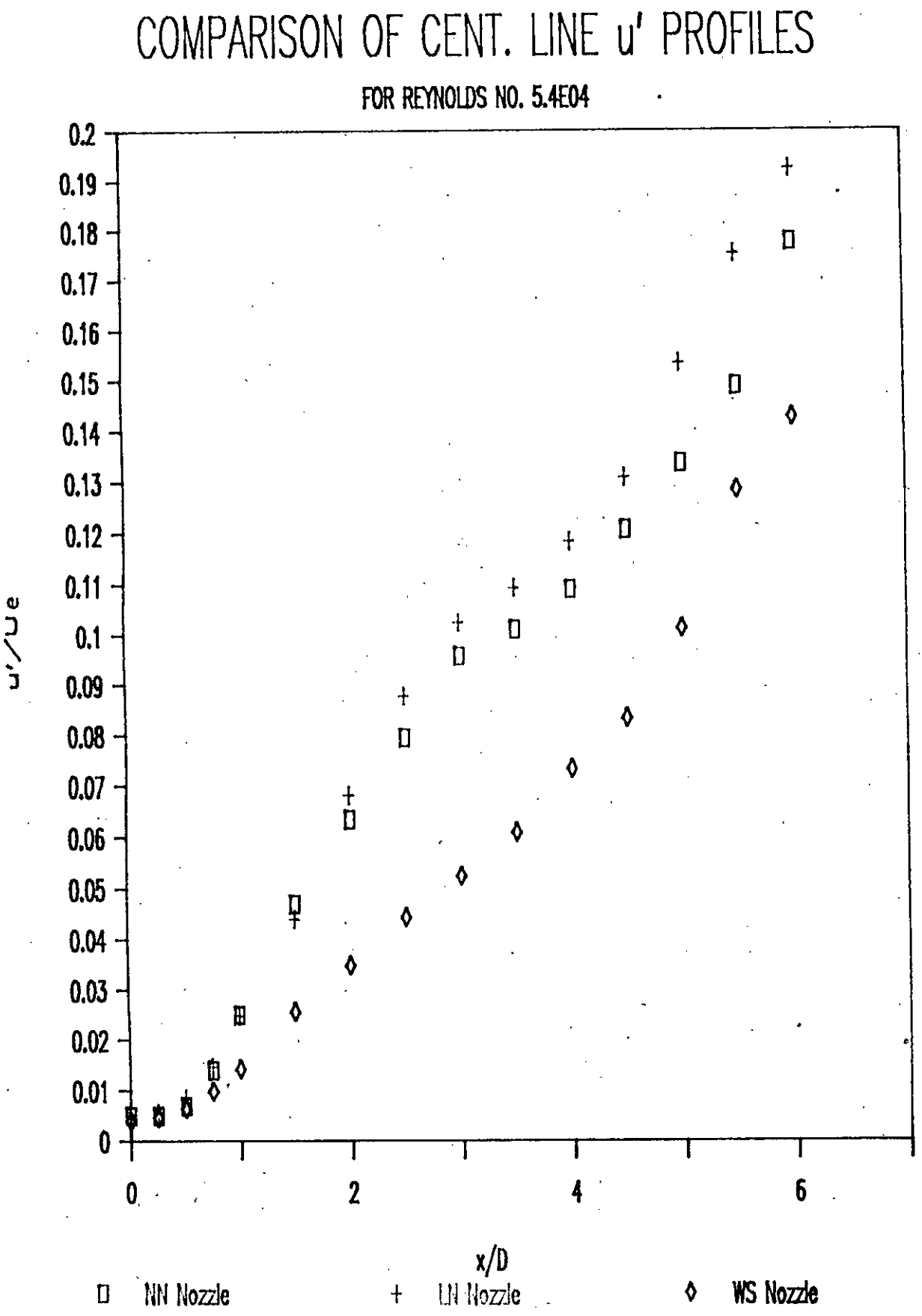

Fig. 5.4.22 : Comparison of centre line longitudinal fluctuating intensity (u') of three nozzle for Re = 5.4E04.

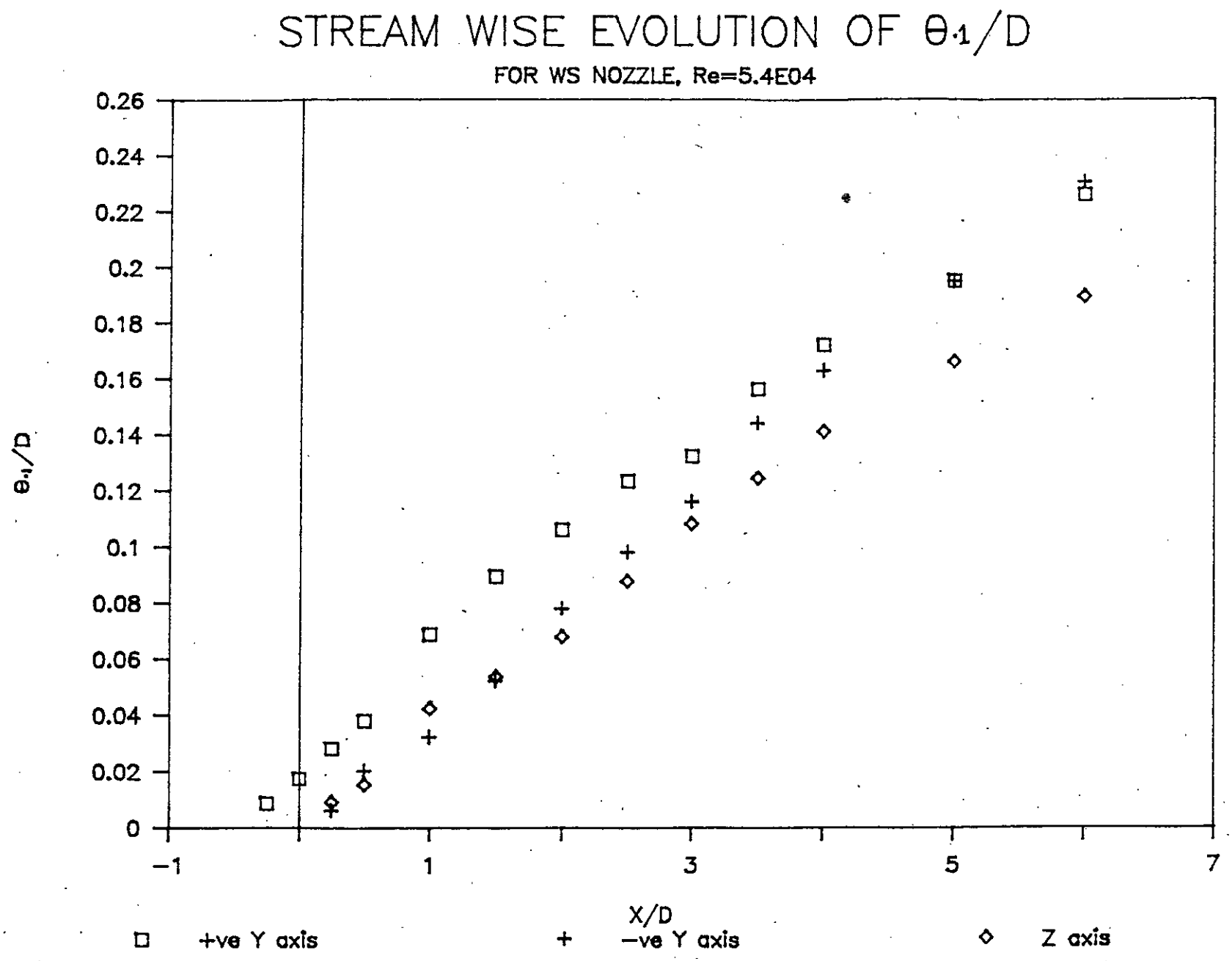

Fig. 5.4.23 : Stream-wise evolution of local momentum thickness of three axes of WS nozzle for Re = 5.4 x 10^4.

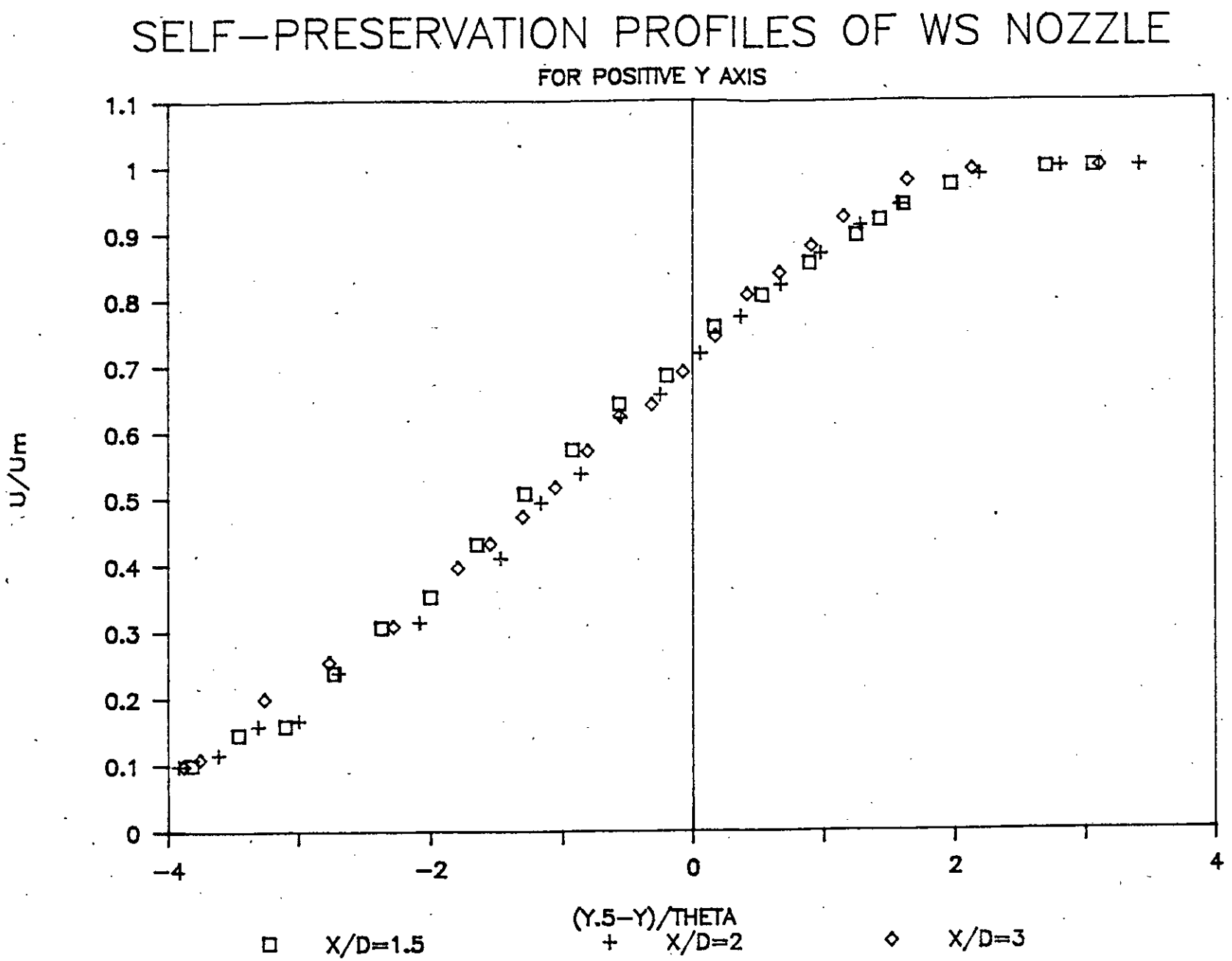

Fig. 5.4.24 : Self-preservation profiles of Ws nozzle for +ve Y axis with Re = 5.4 x 10^4.

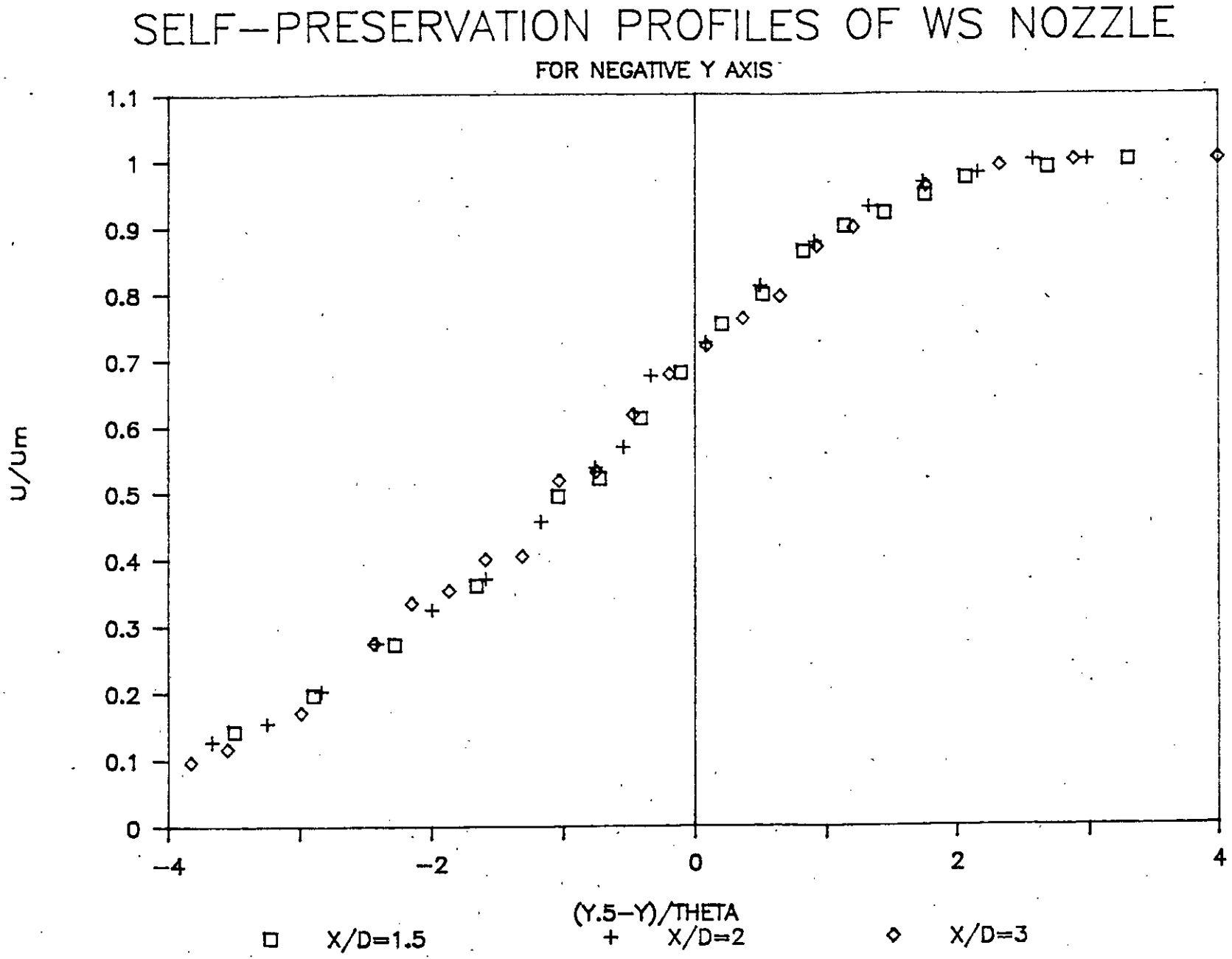

Fig. 5.4.25 : Self-preservation profiles of mean velocity (U) in -ve Y axis of WS nozzle for Re = 5.4×10^4.

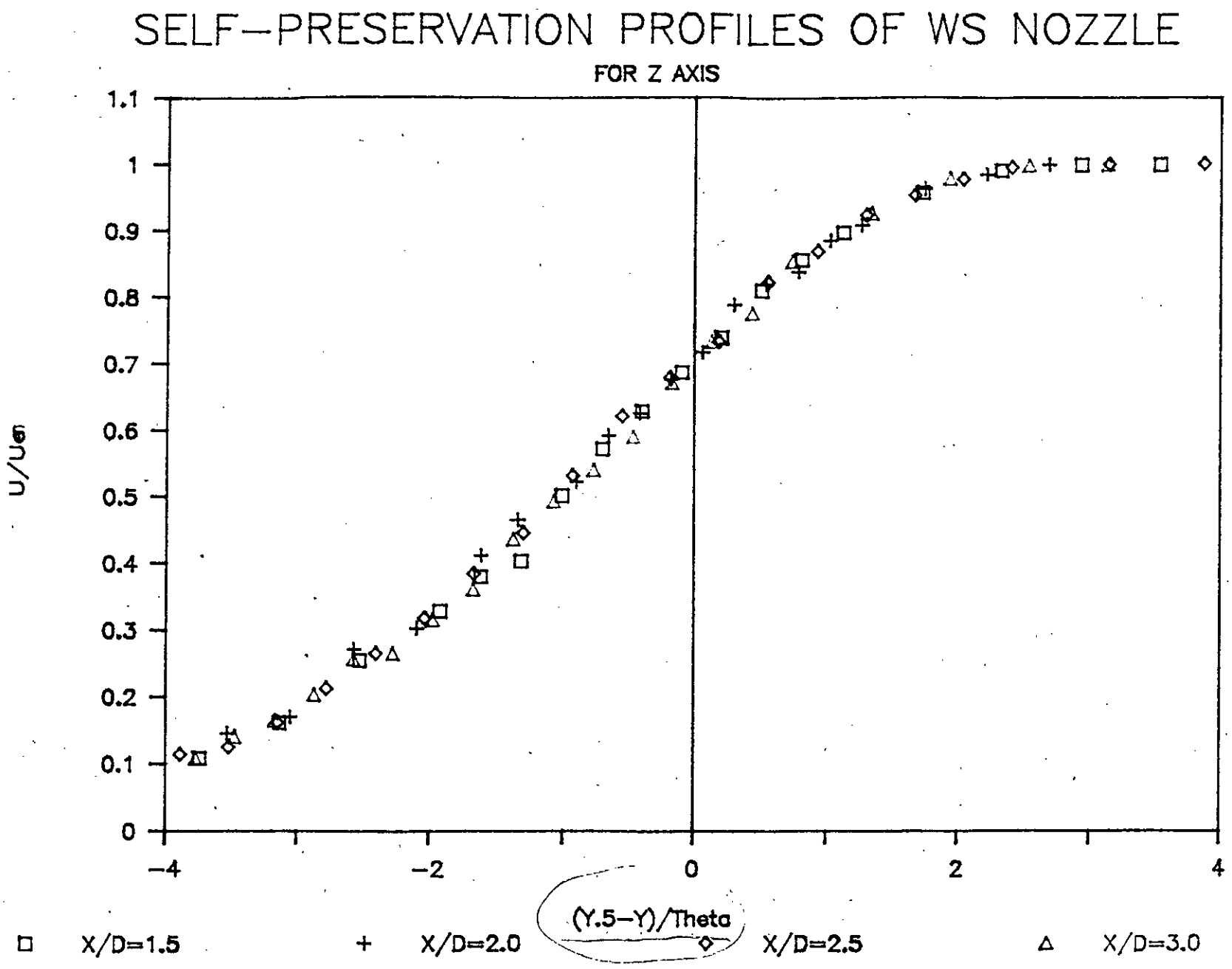

Fig. 5.4.26 : Self-preservation profiles of mean velocity (U) in Z exis of WS nozzle for Re = 5.4 x 10^4.

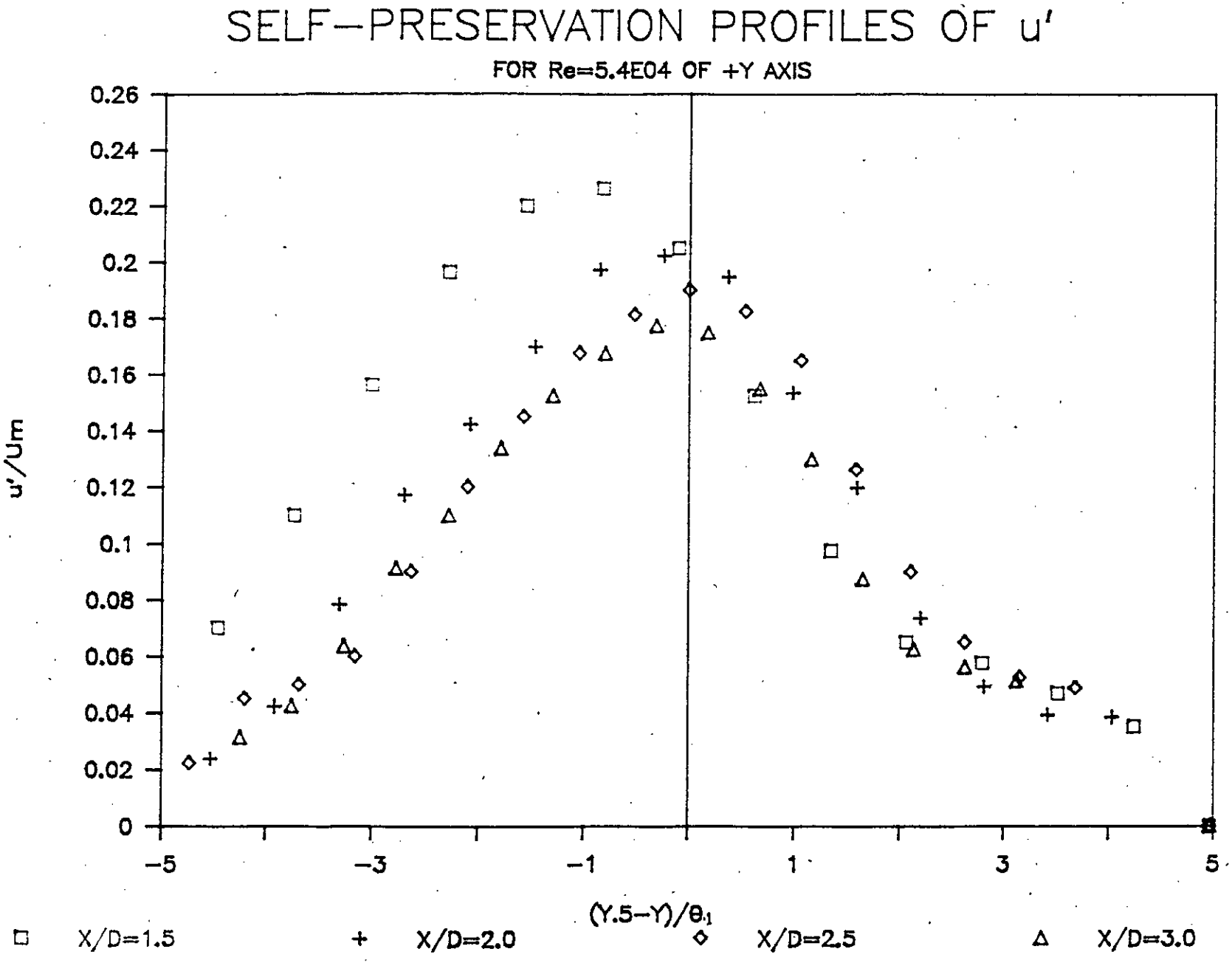

Fig. 5.4.27 : Self-preservation of longitudinal turbulence intensity (u') in +veY axis of WS nozzle for Re = 5.4 x 10^4.

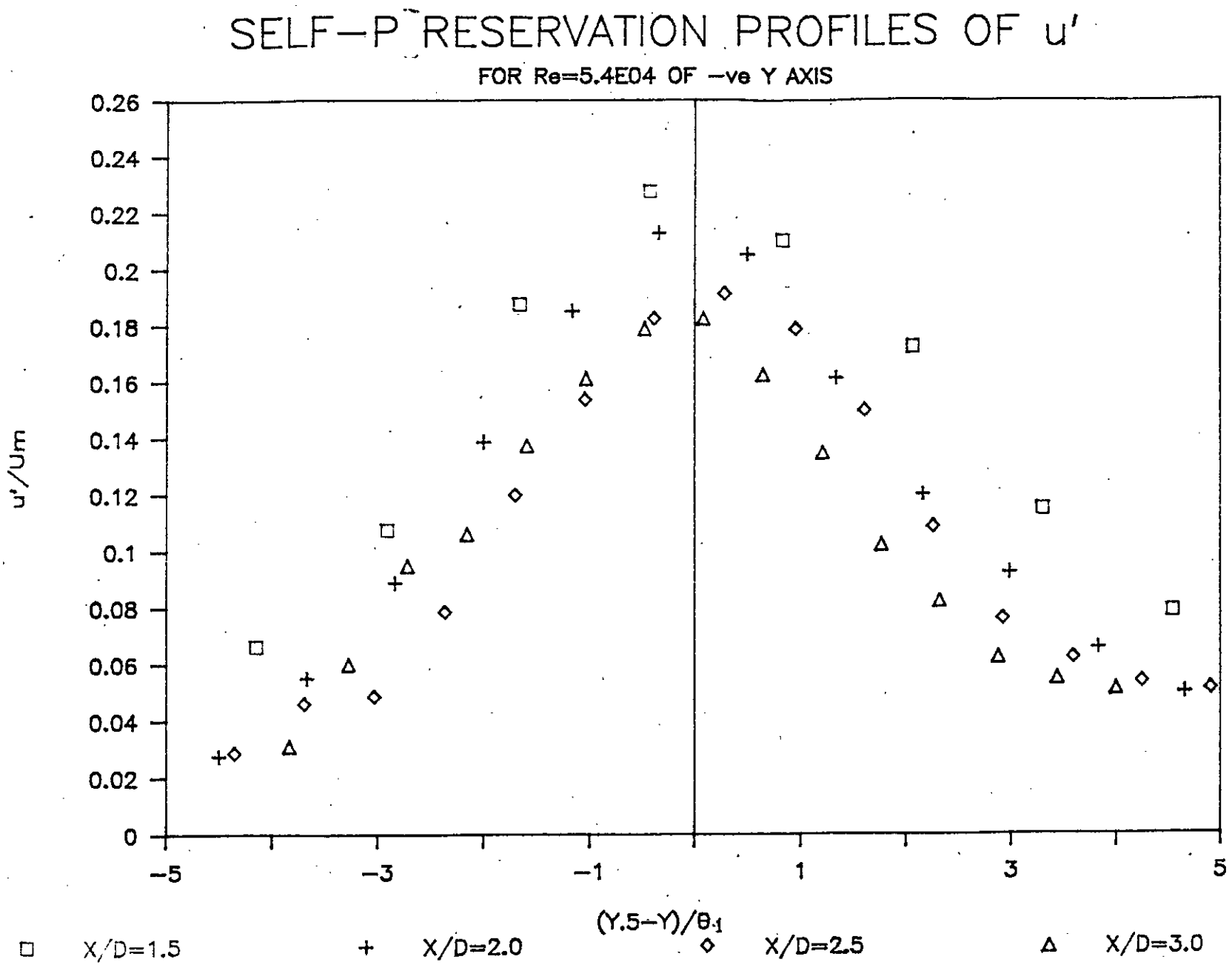

Fig. 5.4.28 : Self-preservation profiles of longitudinal turbulence intensity in -ve Y axis of WS nozzle for Re = 5.4 x 10^4.

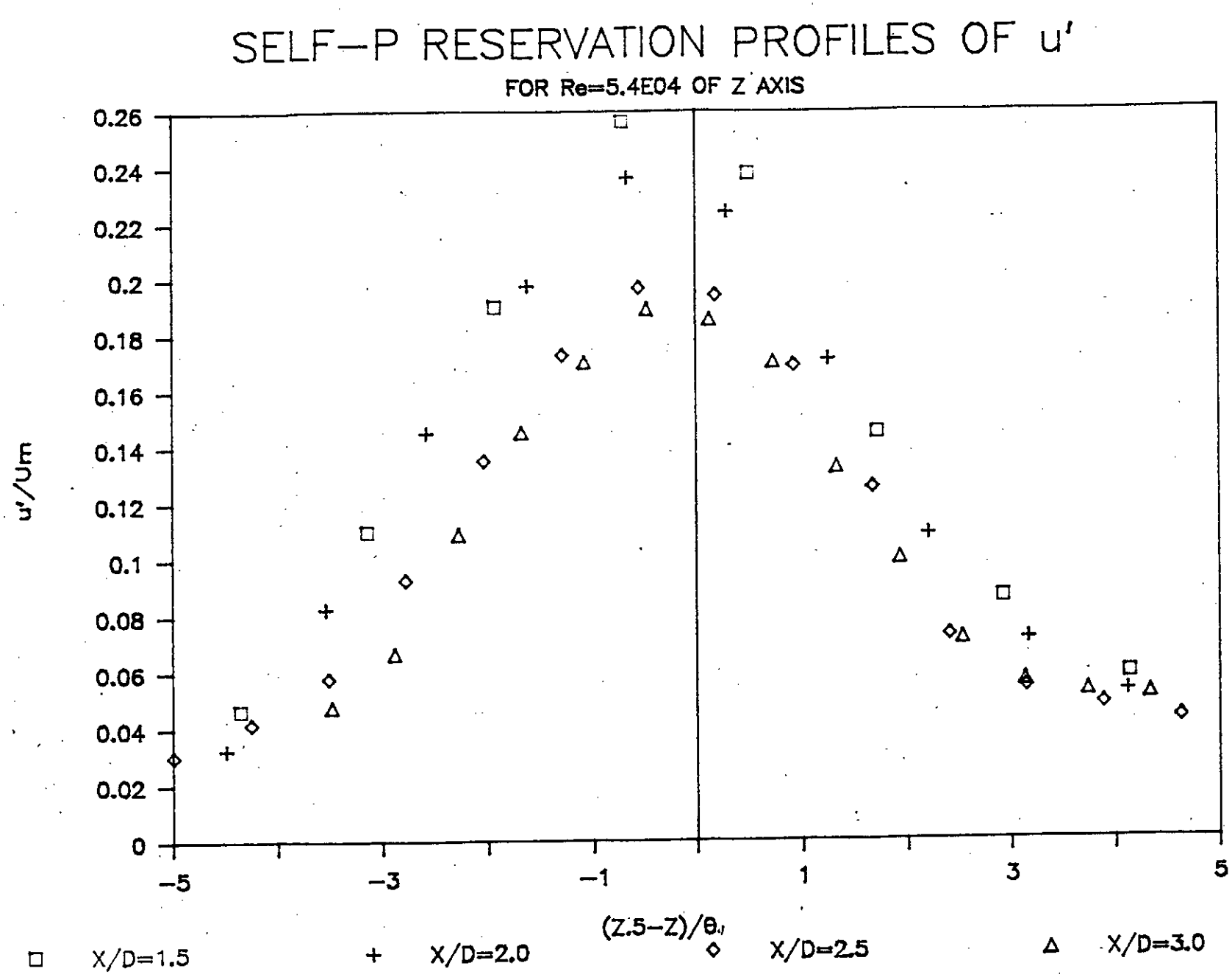

Fig. 5.4.29 : Self-preservation profiles of longitudinal fluctuating intensity (u') in Z axix of WS nozzle for Re = 5.4 x 10^4.

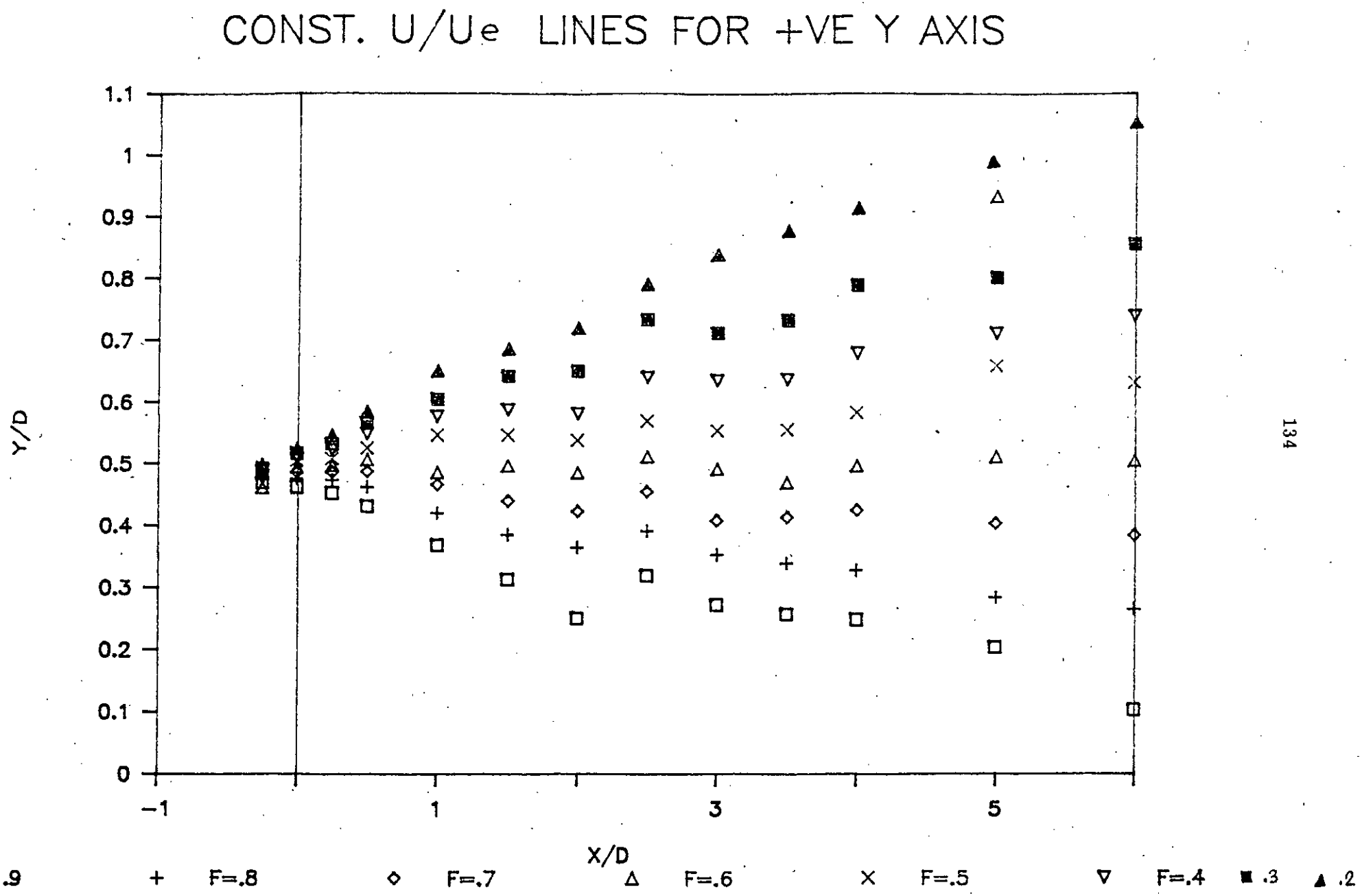

Fig. 5.4.30 : Constant mean velocity lines in +ve XY plane of WS nozzle for Re = 5.4 x10^4.

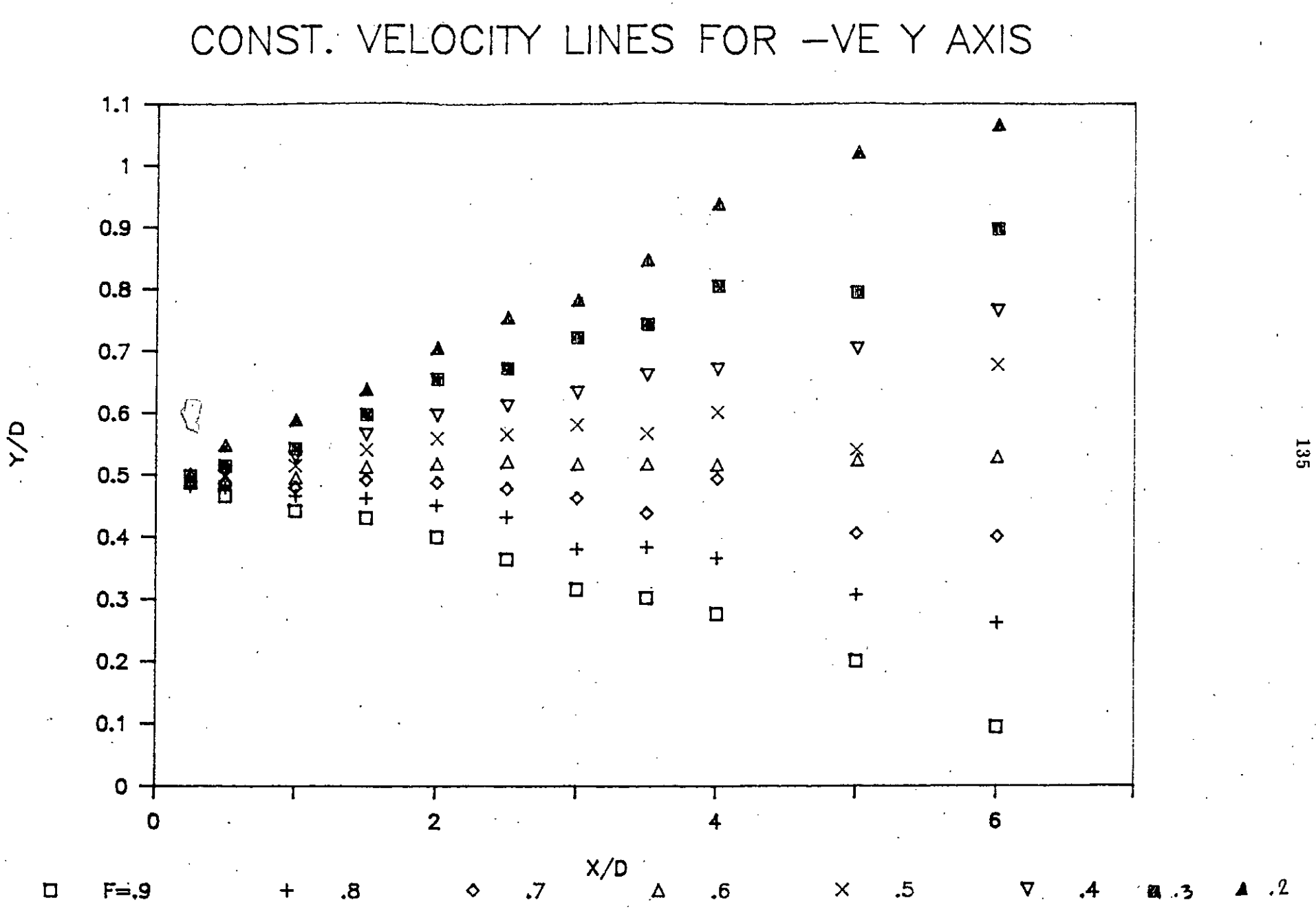

Fig. 5.4.31 : Constant mean velocity(U) lines in -ve XY plane of WS nozzle for Re =5.4 x 10^4.

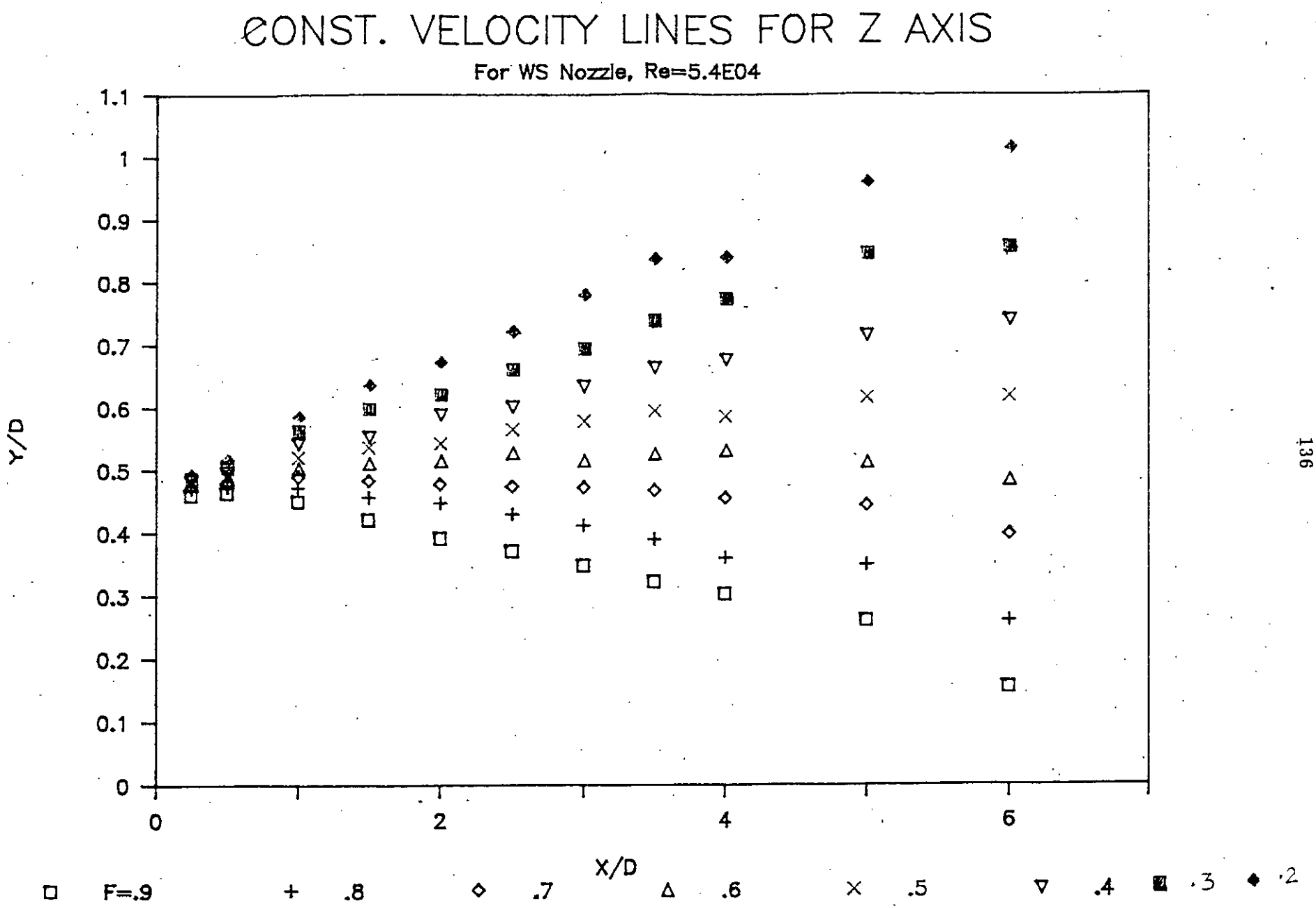

Fig. 5.4.32 : Constant mean velocity(U) lines in XZ plane of WS nozzle for Re =5.4 x 10^4.

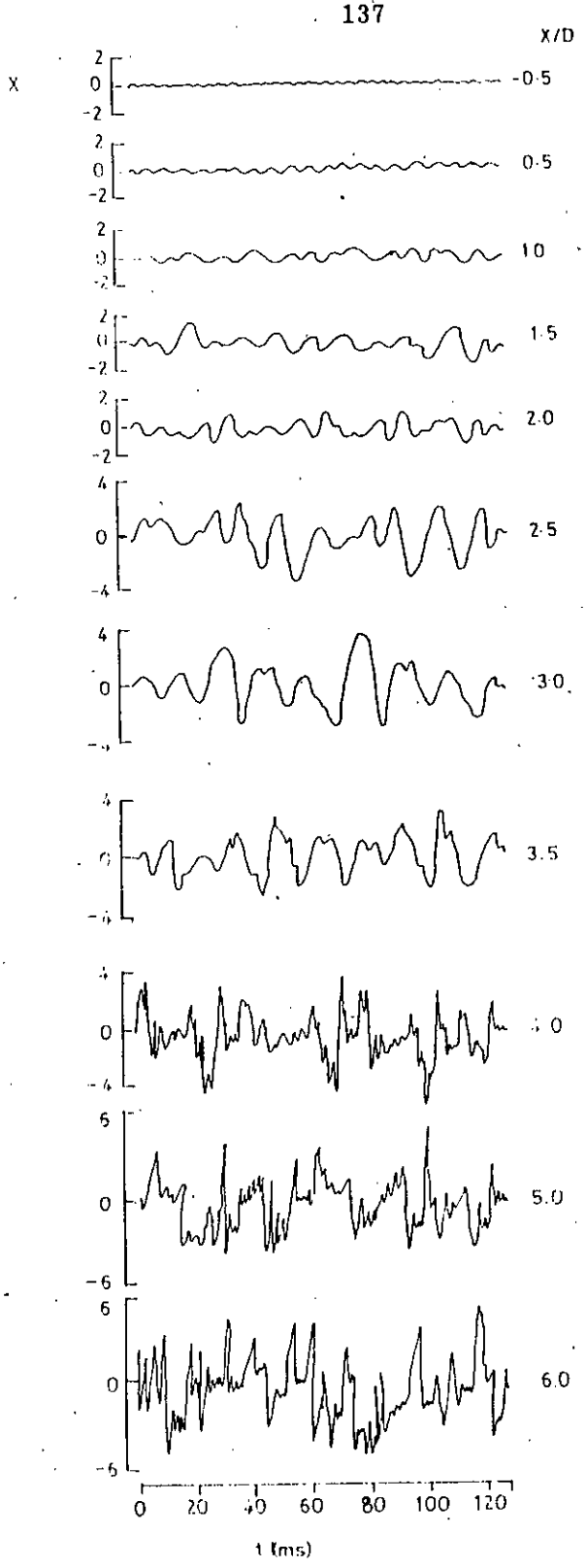

Fig. 5.4.33 : Oscilloscope traces u' signals on the centre line of WS at diff. x/D locations with Re = 5.4 x 10^4, Gain = 10.

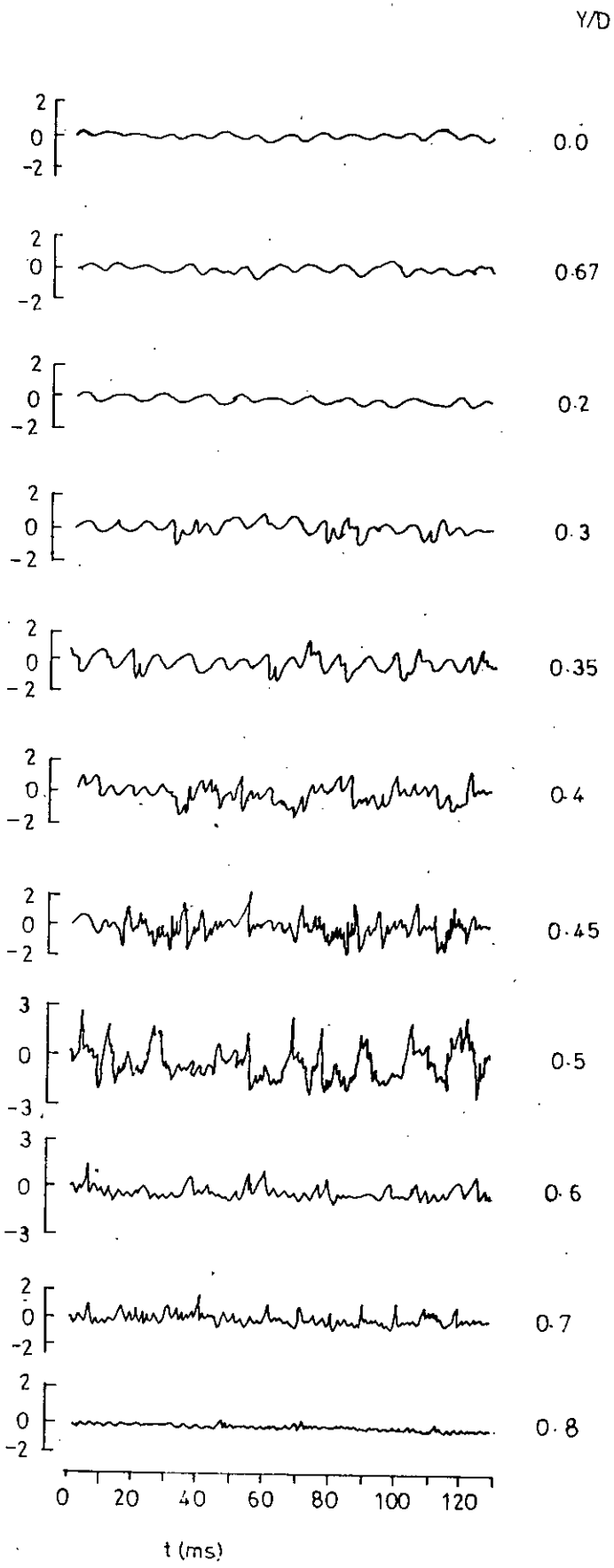

Fig. 5.4.34 : Oscilloscope traces of u' signals of WS jet at diff. y/D locations in the +Y direction with x/D = 1.0 and Re = 5.4×10^4 (Gain = 5).

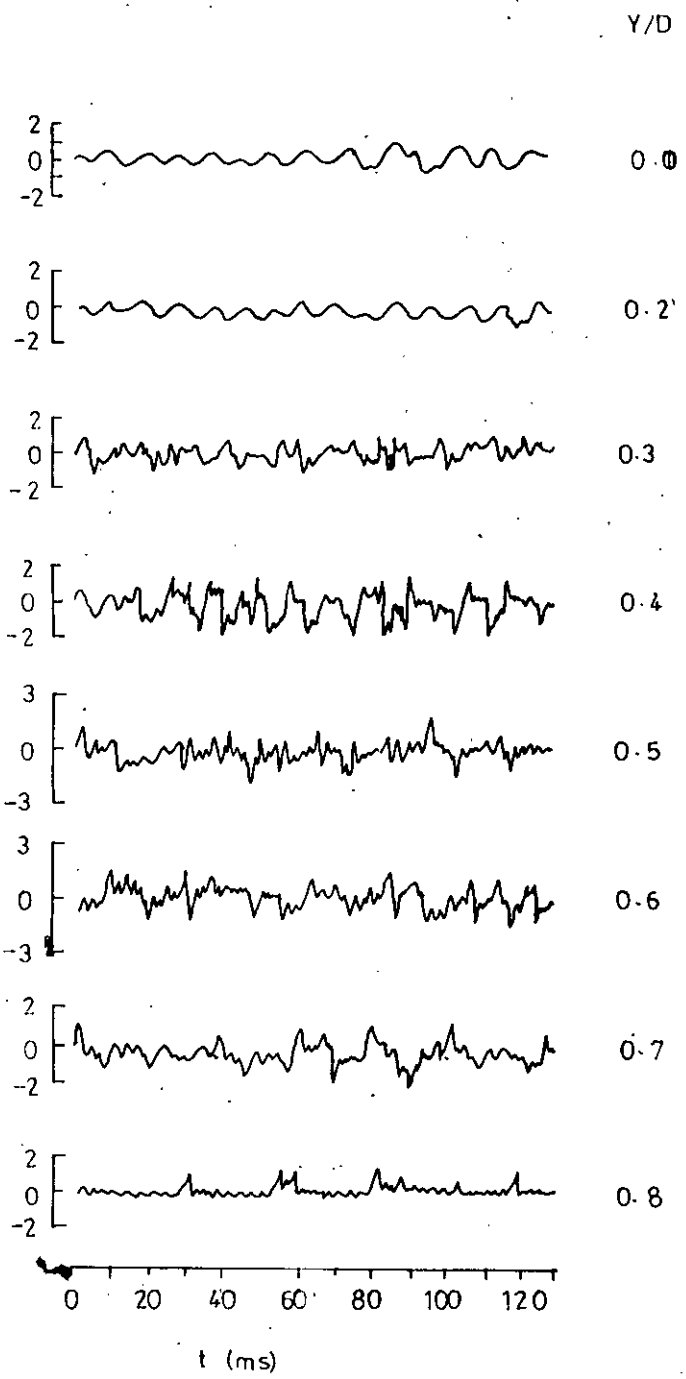

Fig. 5.4.35 : Oscilloscope traces of u' signals of WS jet at diff. y/D locations in the +Y direction with x/D = 1.5, Re = 5.4 x 10^4 and Gain = 10.

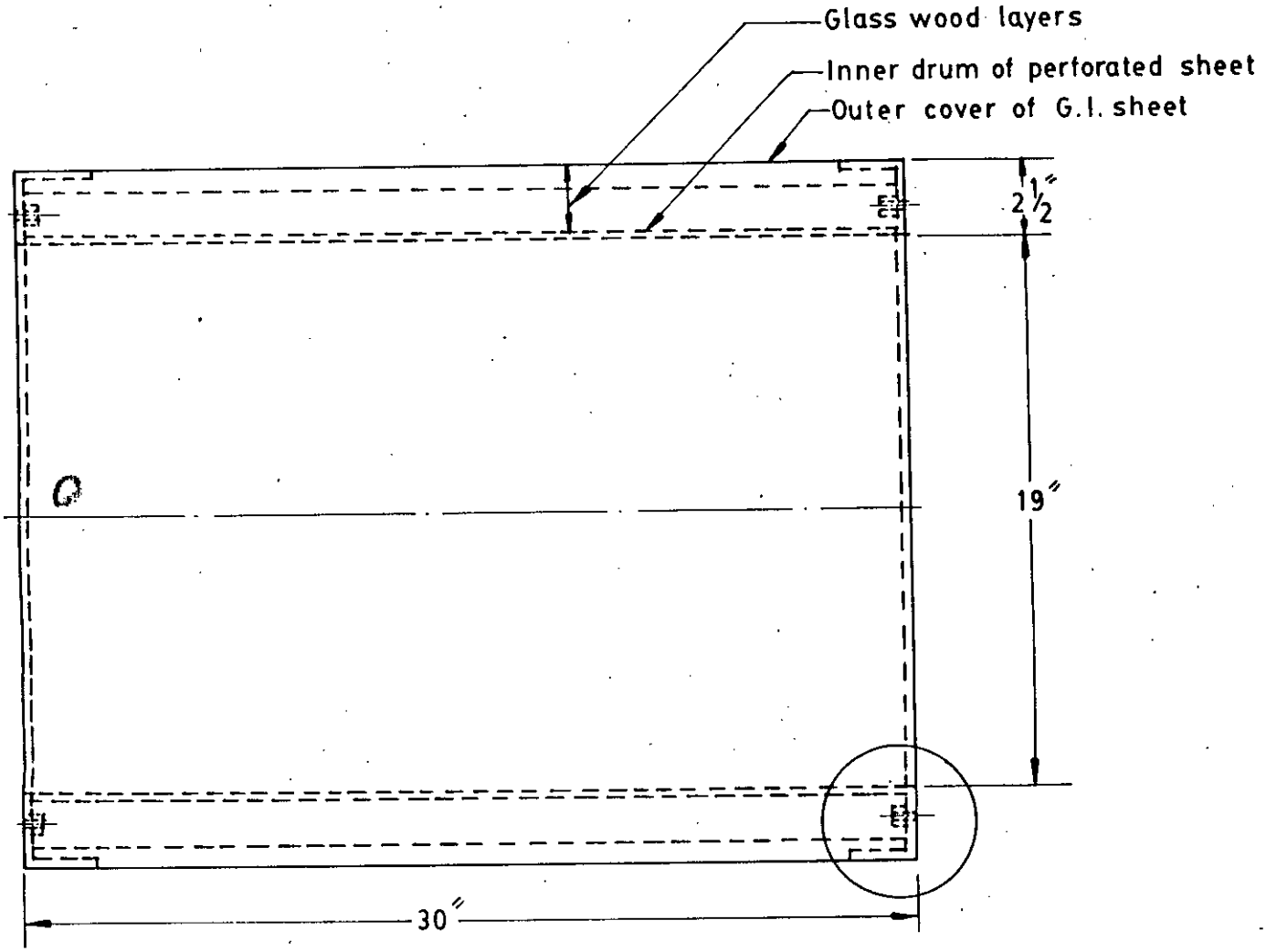

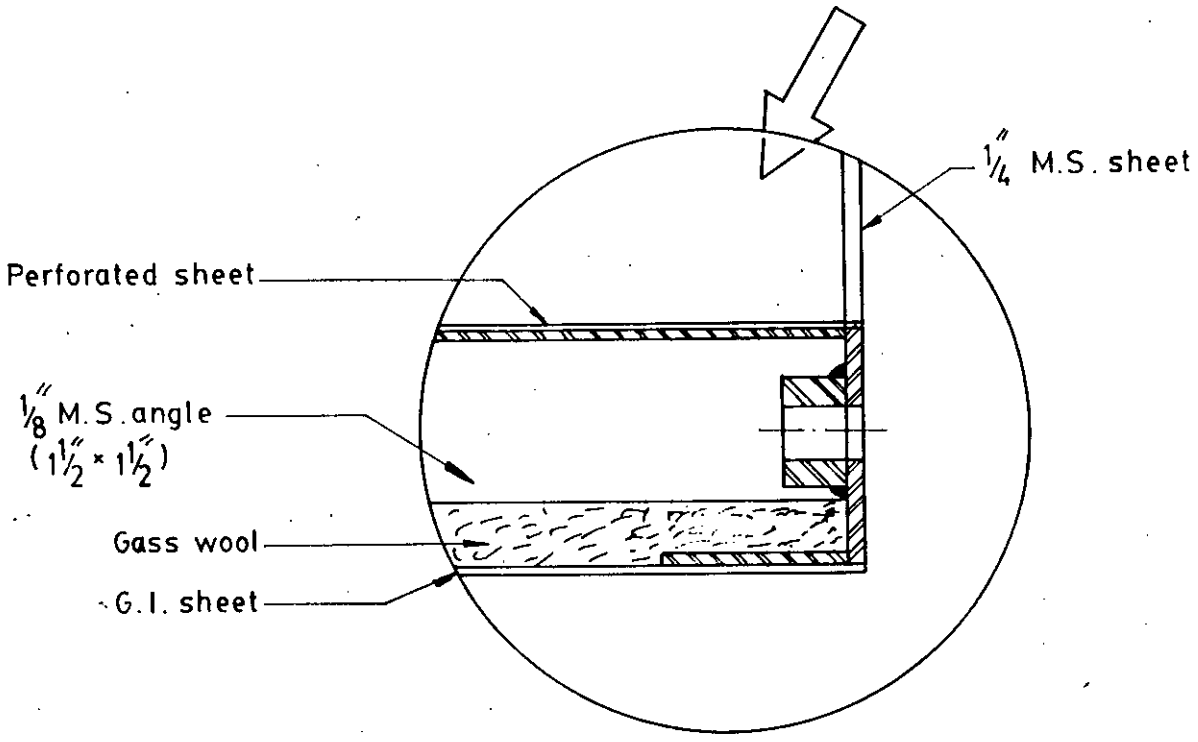

FIG. A.1 SILENCER

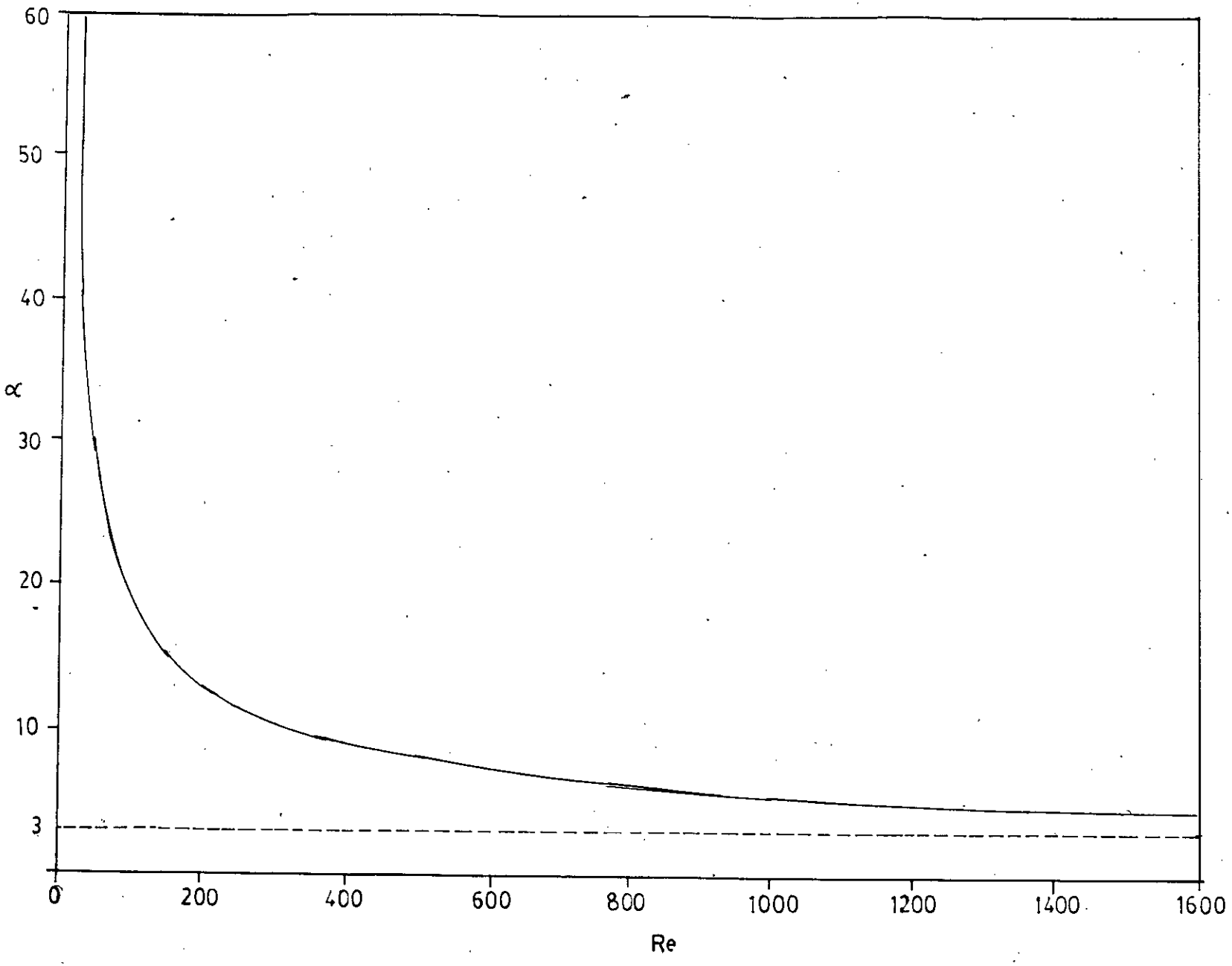

Fig. B.1 : Reynolds number vs. angle of divergence for flow through a diffuser.

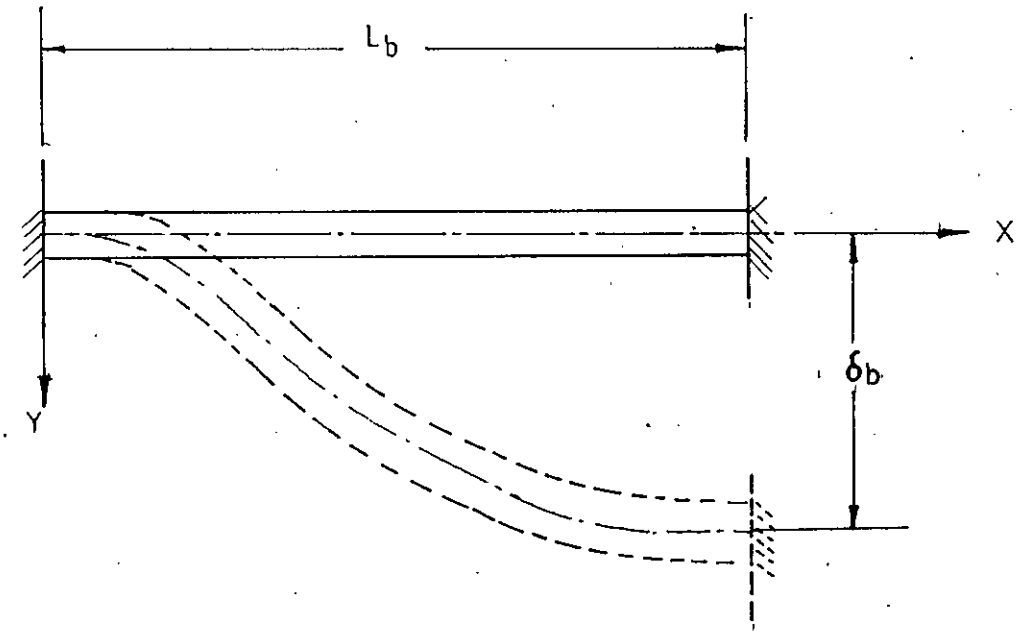

Fig. C.1 Beam deflection without load.

PLATES

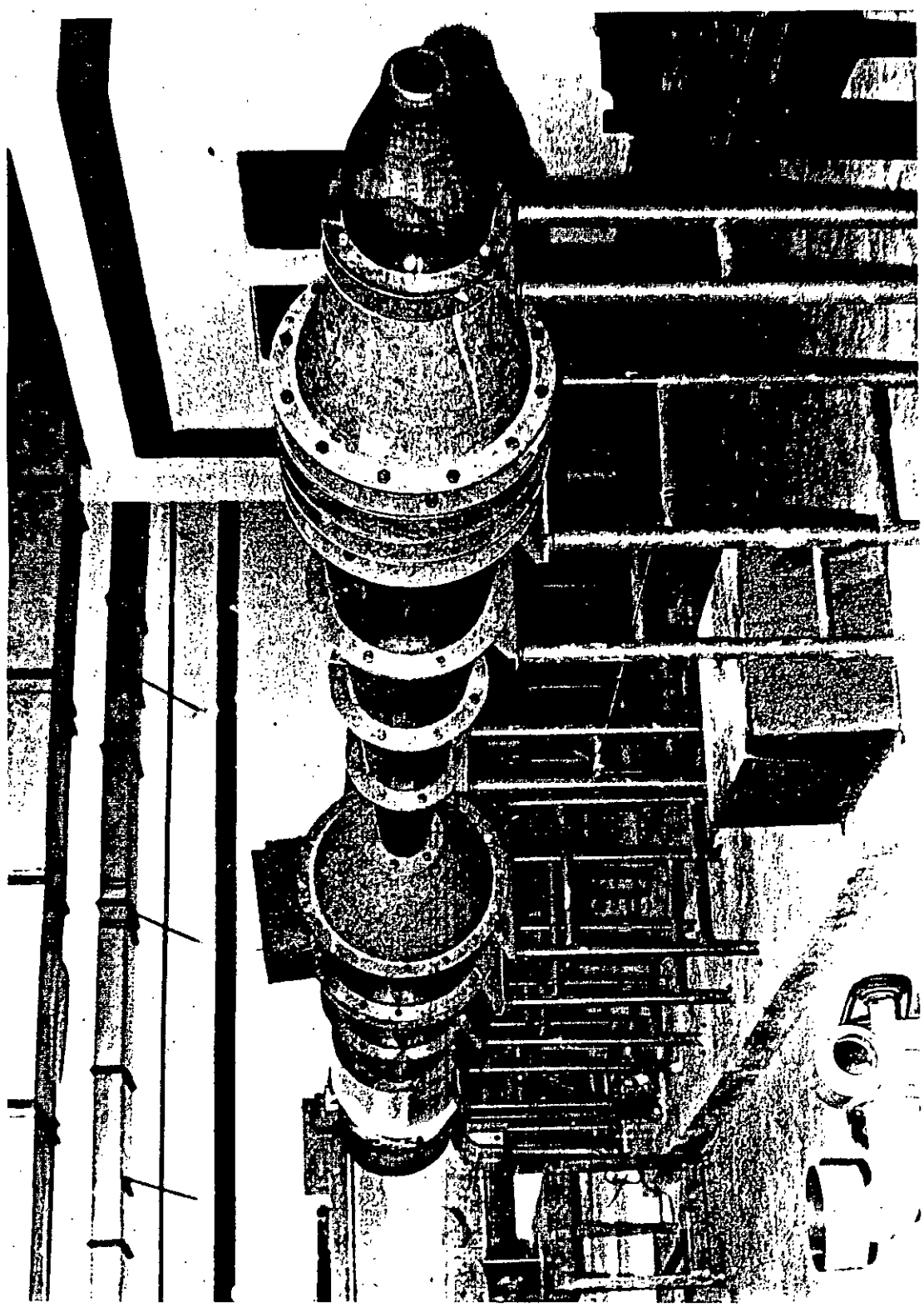

Plate 4.1.1 : The circular air jet facility fitted with NN nozzle.

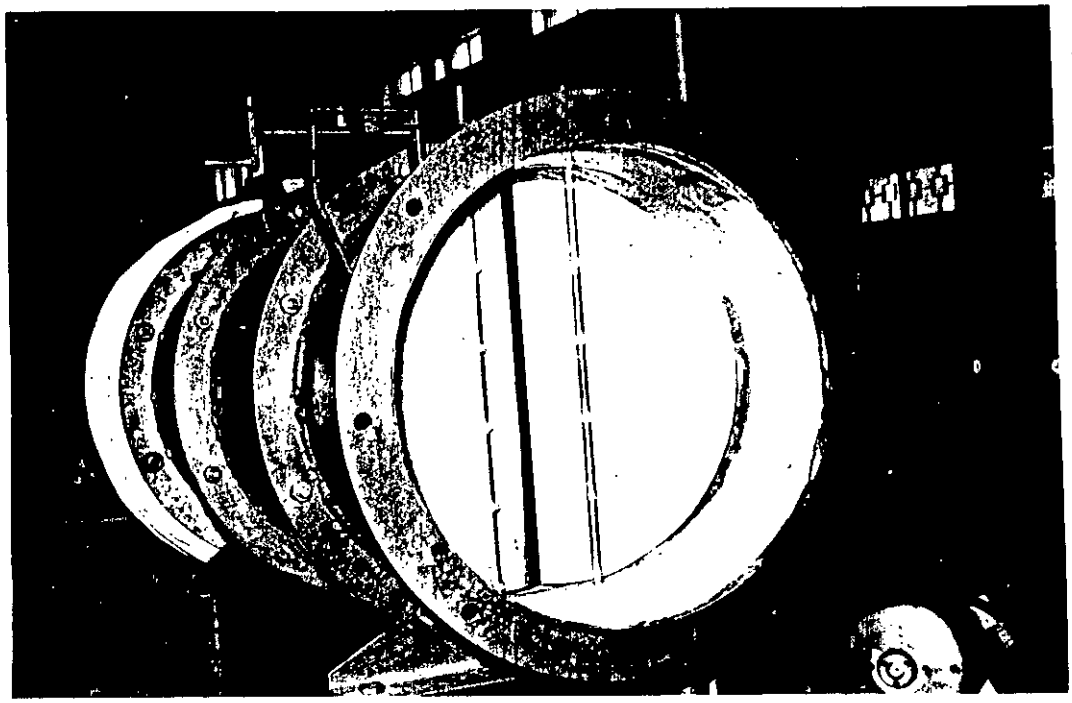

Plate 4.1.2 : The butterfly valve.

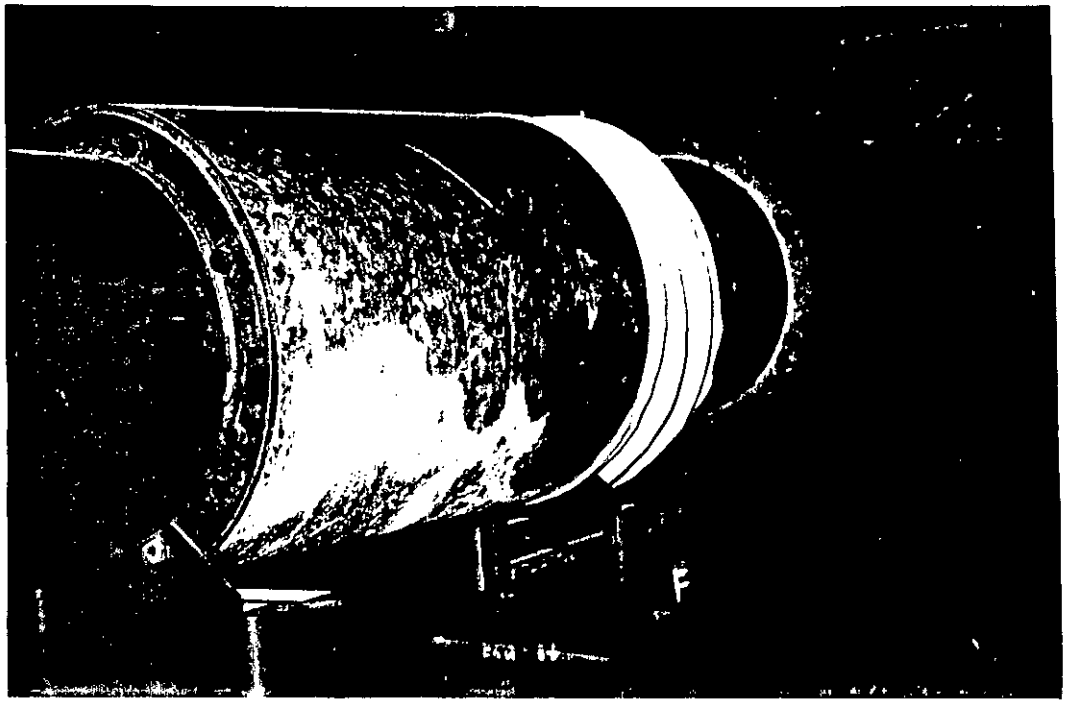

Plate 4.1.3 : Silencer and Below .

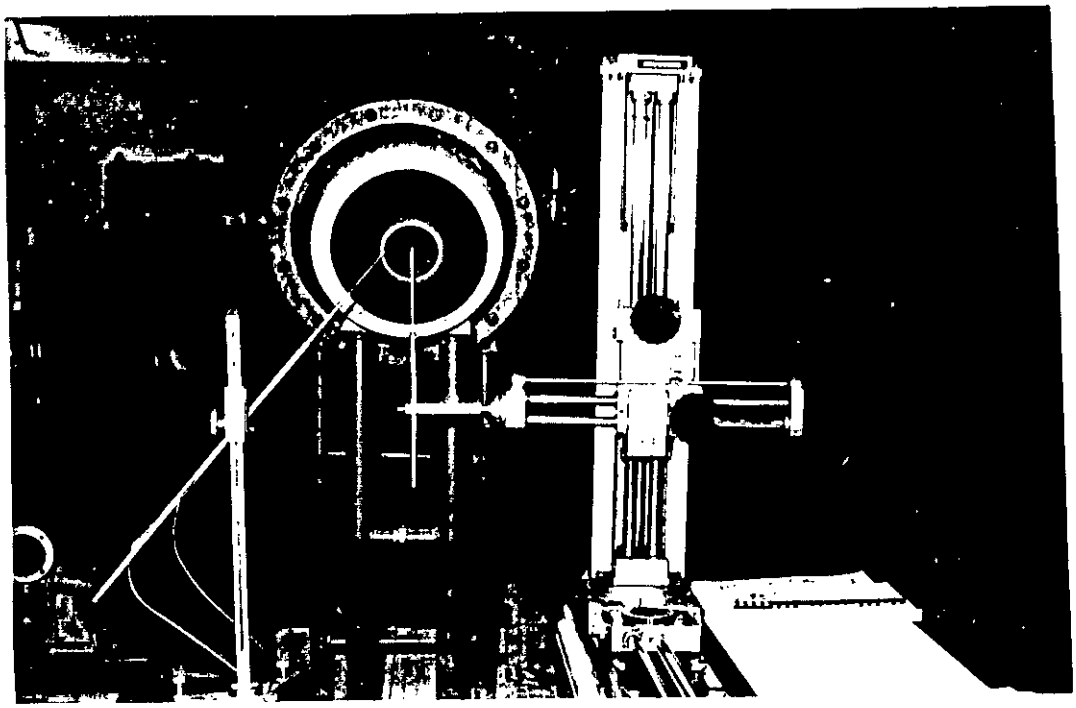

Plate 4.5.1 : The Traversing mechanism and probe setting

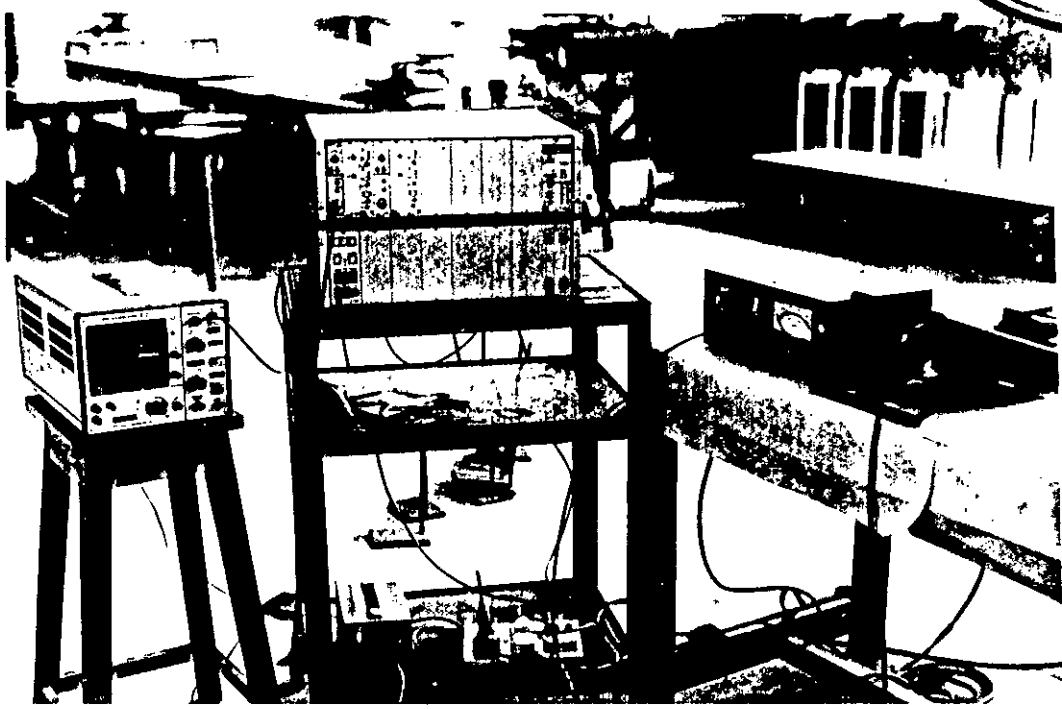

Plate 4.7.1 : The DISA 56C00 CTA system.